2011

# Physically Meaningful Harmonization of Tire/Pavement Friction Measurement Devices

Madhura Priyanga Nishshanke Rajapakshe
*University of South Florida*, mrajapak@mail.usf.edu

## Scholar Commons Citation

Rajapakshe, Madhura Priyanga Nishshanke, "Physically Meaningful Harmonization of Tire/Pavement Friction Measurement Devices" (2011). *Graduate Theses and Dissertations.*
http://scholarcommons.usf.edu/etd/3303

# Physically Meaningful Harmonization of Tire/Pavement Friction Measurement Devices

by

Madhura P.N. Rajapakshe

A dissertation submitted in partial fulfillment
of the requirements for the degree of
Doctor of Philosophy
Department of Civil and Environmental Engineering
College of Engineering
University of South Florida

Co-Major Professor: Manjriker Gunaratne, Ph.D.
Co-Major Professor: Autar K. Kaw, Ph.D.
Rajiv V. Dubey, Ph.D.
Daniel P. Hess, Ph.D.
Kandethody Ramachandran, Ph.D.
Marion Pottinger, Ph.D.

Date of Approval:
October 19, 2011

Keywords: tire-pavement interaction, LuGre model, semi-empirical parameterization,
standardization, tire property measurement

# DEDICATION

To my father, Mr. Ananda N. Rajapakshe, and

my grandfather, Mr. Sarathchandra Wijayasiri

for teaching me the value of education and scientific thinking.

# ACKNOWLEDGEMENTS

The funding provided by NASA for this research is gratefully appreciated. The exceptional guidance and advising of Dr. M. Gunaratne is greatly appreciated. I would like to take this opportunity to recognize Dr. Gunaratne's advising approach that suits students with different educational, social and mental backgrounds. I am proud to have Dr. A. Kaw, an excellent model for the present-world educator, as a co-major professor. Dr. Kaw's invaluable advice for the research and for building a successful professional career is greatly acknowledged. Dr. R. Dubey's advice and support at certain critical stages of my career is especially appreciated. I appreciate Dr. D. Hess's input with his research background in frictional dynamics. Dr. K. Ramachandran's kind consideration to become a committee member on short notice and his input from his background in statistics is highly appreciated. Dr. P. Lin's perfect job as the committee chair is also appreciated. I would like to specially thank Dr. M. Pottinger for his remarkable input as a pioneer in tire/pavement interaction research with decades of related experience. The invaluable support given by Dr. J. Popio, Mr. J. McIntyre and all the other great people at Smithers Scientific Services, Akron, Ohio, for the experimentation, data analysis and finalization of this dissertation is gratefully appreciated.

I would like to acknowledge my family, especially my mother for her boundless love and exceptional mental strength. Last and not least, I thank my wife for supporting me throughout this endeavour and giving me invaluable thoughts for research and life.

## TABLE OF CONTENTS

# LIST OF TABLES

LIST OF FIGURES

# ABSTRACT

Accurate characterization and evaluation of tire/pavement friction is critical in assuring runway and highway safety. Historically, Pavement Friction Measurement Devices (PFMDs) employing different measuring mechanisms have been used to evaluate tire/pavement friction. They yield significantly disparate friction coefficients under the same contact conditions. Currently, an empirically developed data harmonization method based on a reference device (Dynamic Friction Tester (DFT)) is used in an attempt to overcome the disparities between the measurements using various different PFMDs. However, this method, which has been standardized by the American Society for Testing and Materials (ASTM E1960), has been criticized for its inconsistency by researchers and runway/highway operations personnel.

The objective of this dissertation research was to develop a systematic and physically intuitive harmonization method for PFMDs that will improve the comparability of their data. As a foundation for such a harmonization, the LuGre tire model that employs physically meaningful parameters to represent the main attributes of tire/pavement friction was evaluated and validated. Measurements of tire/pavement friction by three widely used PFMDs; Locked Wheel Skid Trailer (LWST), Runway Friction Tester (RFT) and DFT, were accurately predicted using nonlinear optimization of LuGre model parameters. The LuGre model was found to be superior compared to the model used in the current ASTM E1960 standardization procedure for predicting PFMD measurements.

A sensitivity analysis was performed to identify the relative significance of the LuGre model parameters in characterizing tire/pavement friction, and to study the effects of variation of those parameters on predicted frictional behavior. A set of laboratory tire experiments was designed and performed to validate the physical significance of LuGre tire model parameters and to study how they behave under typical load, inflation pressure, excitation frequency, and amplitude conditions. An empirical method was developed to accommodate the effects of water film thickness on tire/pavement friction in the LuGre model. The results of the sensitivity analysis and the experiments to directly estimate the model parameters were used to identify and quantify appropriate modifications to the measurement mechanisms of PFMDs that can be introduced to improve the comparability of their results. Friction experiments performed after introducing such modifications to the LWST showed an average reduction of 20% in the deviations between the results of LWST and RFT measurements.

The research carried out in this dissertation is significant because it: (i) identified the deficiencies in the current method for harmonizing PFMD measurements and the underlying reasons for these deficiencies, (ii) emphasized the importance of a standardization approach that regulates the physical condition of PFMDs, in order to achieve universal comparability of tire/pavement friction measurements, (iii) validated that the LuGre tire model is a tire/pavement friction model capable of facilitating a better standardization approach, and, (iv) initialized the development of a physically meaningful harmonization procedure for PFMDs.

# CHAPTER 1

# INTRODUCTION

Accidents due to insufficient traction force are quite common in ground transportation. Water on the pavement is responsible for many accidents due to the significantly reduced tire/pavement friction under wet conditions. Although many prudent drivers take necessary precautions, wet pavement related accidents occur constantly due to the variability of related conditions and the difficulty in identifying the remedial actions. Susceptibility of aircraft to accidents is also relatively high during takeoff and landing under inclement weather. The overrunning of an Air France A-340 on August 2nd 2005 in Toronto, Canada, the landing veer-off accident of a DC-9 on October 6th 2000 in Reynosa, Mexico, and the skidding of a British Aerospace BAE 146-200 on February 20th 1991 in Port Williams, Chile are some examples of such crashes (Ranganathan, 2005, Yager et al, 2002 and Wikipedia, 2009). One common reason for many such air crashes is inadequate contact between the landing-gear tires and the runway pavement surface to provide the traction forces required to decelerate, accelerate or maneuver within the available time or runway stretch. Due to the above reasons, evaluation of the capacity of the tire/pavement interface to produce required traction has been a well-attended research and technical topic throughout the years. It has been a major responsibility of transportation safety personnel to maintain highway and runway pavements at acceptable friction levels to prevent possible hazards.

## 1.1 Measurement of Pavement Friction

According to basic mechanics, the ratio of shear force to normal force at the contact of two given surfaces can be identified as the coefficient of friction ($\mu$) between the two surfaces. Therefore, the shear force at the tire/pavement contact is referred to as the frictional force. The common practice to evaluate tire/pavement friction has been based on calculating $\mu$ as the ratio between measured frictional force and normal force when the tire is run on the pavement under specific conditions. The basic assumption is that a higher $\mu$ produces higher frictional force at a given normal force.

Most of the accidents due to loss of traction between the pavement and tire occur in situations where the pavement is wet or covered with snow or ice. In aviation terminology, a runway is considered to be 'wet' if the water film thickness is less than 3 mm. On the other hand, a water film above 3 mm thickness is considered to be 'slippery' or 'contaminated'. An aircraft requires 40% more runway length to stop in 'wet' conditions, whereas on 'contaminated' runways, the percentage increases by 300% (Ranganathan, 2005). However, the above definitions of 'wet' and 'contaminated' will not be used in this dissertation; wet conditions will not imply any water film thickness unless specifically mentioned. Naturally, in consideration of the worst scenario, tire/pavement $\mu$ is always measured under wet conditions.

There are numerous devices that use different mechanisms to measure $\mu$ on runway and highway pavements. Most of them measure $\mu$ by collecting data using a standard test wheel attached to a vehicle. Before introducing these devices some basic but essential concepts are described in section 1.2.

## 1.2 Basic Concepts of Tire/Pavement Friction Measurements

### 1.2.1 Mechanisms of Friction Development

When an elastomer (e.g. rubber) is pressed against a hard and rough pavement surface which is stiffer than it (e.g. pavement), the elastomer surface deflects at the rigid asperities of the rough surface. If a tangential force is then applied on one of the mating bodies, an equal and opposite friction force is experienced. As the tangential force exceeds the limiting friction force, sliding occurs at the interface.

The friction results mainly from two distinct mechanisms, namely, adhesion and hysteresis (Figure 1.1).

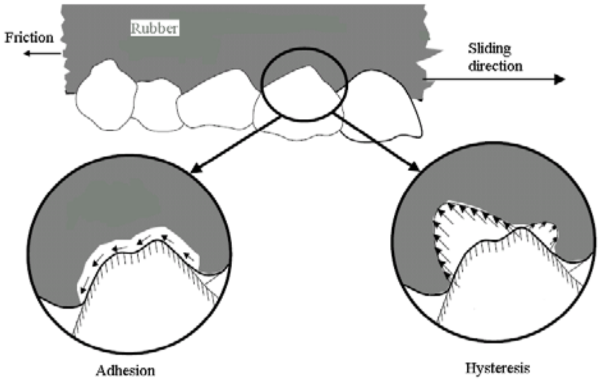

Figure 1.1: Basic mechanisms of friction

#### 1.2.1.1 Adhesion

Adhesion results from molecular bonding of the two materials in contact. Sliding of one material on the other causes these bonds to stretch, break and relax before new bonds are made. During the relaxation period, the elastomer molecules jump a molecular distance to a new equilibrium position. The cycle of bonding and breaking, or the phenomenon of stick-slip is repeated in sliding. As the sliding speed is increased, the adhesion component of friction is lowered due to lack of time for bond formation. Also, if the actual contact area between the surfaces is reduced due to lower normal pressure, higher roughness or a contaminant at the interface, the adhesion component of the frictional force is reduced.

#### 1.2.1.2 Hysteresis

Hysteresis friction occurs due to the imbalance of the pressure distribution in the elastomer at the surface asperities. The pressure imbalance is a result of the visco-elastic nature of the rubber. The pressure distribution in a stationary undisturbed elastomer is balanced with tangential and normal components of the pressure in equilibrium. In the case of sliding, the pressure distribution at asperities tends to be unbalanced producing a resultant tangential component in the direction opposite to the sliding direction. This resultant force is the hysteresis contribution of friction. Therefore, higher roughness and higher speeds increase the hysteresis effects, while any contamination (solid or fluid) which fills the asperities of the surface reduces hysteresis.

Shearing within an intact material in contact can also contribute to the development of friction. However, this contribution to friction is relatively insignificant compared to adhesion and hysteresis components, under normal operating conditions. Shearing effects become significant when one contact material assumes ‘sacrificial’ or being sheared off by the stresses developed at the contact. Tire sacrificial conditions are generally experienced at considerably high temperatures, speeds and normal forces. When the pavement surface is covered with a layer of solidified ice surface, sacrificial situations are experienced (Andresen et al, 1999). These special conditions are beyond the scope of the intended investigation.

### 1.2.2 Parameters Affecting Pavement Friction

The coefficient of friction depends on many parameters which can be categorized as, surface and geometric properties of the pavement and tire, material properties of the pavement and tire, loading and dynamics of the tire, and contamination at the tire/pavement interface.

Tire surface is characterized by the tread pattern geometry and the texture of rubber. The main function of treads is to provide drainage paths for water to squeeze out of the contact surface during wet pavement conditions, avoiding hydroplaning. Hydroplaning is the phenomenon where the direct contact between the tire and the pavement is fully or partially prevented due to a water film. The tradeoff associated with having treads on the tire surface is the reduction of available area for adhesion and higher stresses on the points of contact increasing the wear and tear of the treads (Moore, 1975).

The influence of texture on pavement friction is well identified (Rado, 1994). Every surface has a unique unevenness at some magnification level, and texture is the scientific term for these deviations from a perfectly smooth surface. A texture can constitute a wide spectrum of amplitudes and wavelengths. Specific levels of pavement texture can be defined by the arbitrary ranges of wavelength and peak-to-peak amplitude as given in Table 1.1 and Figure 1.2.

Table 1.1: Levels of pavement texture

| Type of texture | Wavelength range (mm) | Amplitude range (mm) |
|---|---|---|
| Micro-texture | less than 0.5 | less than 0.005 |
| Macro-texture | 0.5 to 50 | 0.1 to 20 |
| Mega-texture | 50 to 500 | 0.1 to 50 |
| Roughness | greater than 500 | Greater than 50 |

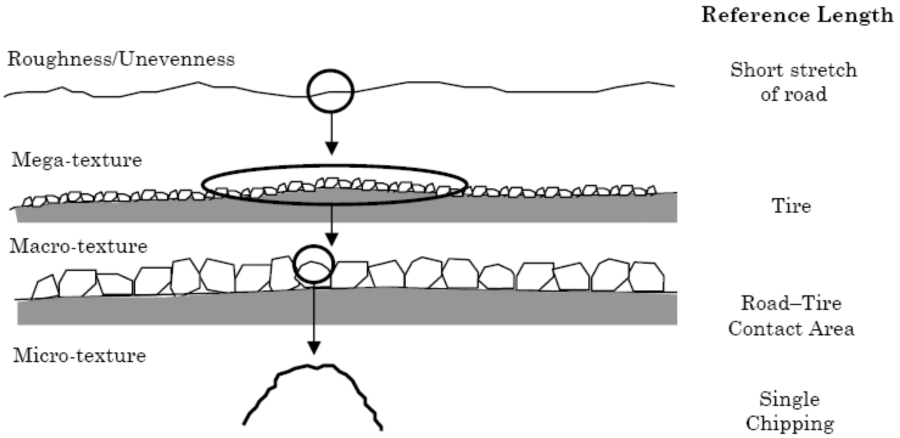

Figure 1.2: Spectrum of pavement texture

At times, the pavement surfaces are grooved to generate mega-texture that can facilitate drainage. Meanwhile, tire texture is generally of the order of magnitude of the pavement micro-texture. The geometry of the inflated tire cross-section determines the geometry and size of the contact area. This affects the frictional force by changing the adhesion and hysteresis contributions.

Tire/pavement contact is established along a footprint, the shape of which depends on geometry of the tire cross-section and the composite mechanical properties of the tire structure. The most important structural element of a pneumatic tire is the casing or the carcass made up of many high modulus but flexible cord, natural textile, synthetic polymer, glass fiber or fine hard drawn steel embedded in, and bonded to a low modulus polymer, a natural or synthetic rubber (Clark, 1981). A tire with very little tread rubber on the external shoulder (e.g. aircraft tires) produces an elliptical footprint. On the other hand, in the case of tires with heavy treads on the shoulder (e.g. automotive tires) longitudinal sides of the footprint are straight and parallel, and the shape is approximately rectangular. Normal force, rubber properties and inflation pressure are the major factors determining the magnitude of the contact area (Clark, 1981). However, the actual contact area between the tire surface and the pavement is only a fraction of the apparent contact area.

Physical properties of the tire material play a dominant role in determining the frictional output. The modulus of elasticity of tire rubber controls the deflection of the tire segment in contact with the pavement, which is one important input to footprint. Hardness of the rubber determines its resistance to wear and tear.

The material property governing the hysteresis and heat generation is the viscosity of rubber. This can also be represented by an appropriate damping ratio or a loss coefficient for rubber. Heat generated by internal friction in rubber is then transferred within the material governed by its thermal diffusivity and conductivity. Mechanical, thermal and chemical properties of rubber are affected by temperature to a considerable level. Therefore, it is clear that viscous properties of rubber play an important role in tire/pavement friction, directly by dissipating energy and indirectly by affecting the properties of rubber.

Physical properties of pavement materials also influence the amount of friction. Elasticity and hardness are the dominant properties. In asphalt concrete pavements in particular, the viscosity of asphalt cement could affect the frictional levels at elevated temperatures.

Slip is a measure of the difference of the circumferential linear velocity of the tire to the linear velocity of the center of the tire (i.e. speed of the vehicle). It is an important variable in developing frictional forces at the tire/pavement contact. If the radius of the wheel is $r$, and the translational and rotational velocities of the wheel hub are $v$ and $\omega$, respectively, the slip speed ($v_r$) and the longitudinal slip ratio ($s$) can be defined as,

$$s=\frac{r\omega-v}{v}=\frac{v_r}{v} \qquad \text{(for braking)} \tag{1a}$$

$$s=\frac{r\omega-v}{r\omega}=\frac{v_r}{r\omega} \qquad \text{(for driving)} \tag{1b}$$

The normal load on the tire determines the apparent and the actual contact area. The higher the load, the higher will be the area available for adhesion and hysteresis mechanisms to generate friction force. Tire/pavement friction varies with tire dynamics. Tire speed ($v$) and slip ($s$) are the most commonly used independent variables against which $\mu$ is measured and plotted in practice. On many occasions, $\mu$ is also expressed as a one variable function of slip speed ($v_r$) as shown in Figure 1.3.

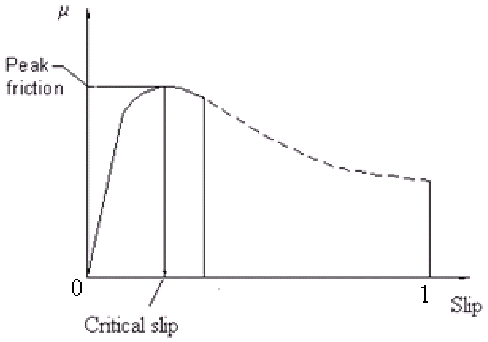

Figure 1.3: Typical behavior of tire/pavement $\mu$ vs. slip speed ($sv$)

The $\mu$ in Figure 1.3 is obtained during a continuous braking operation ranging from a no-slip condition ($s = 0$) to a locked-wheel condition ($s = 1$), while traveling at a constant speed on a wet pavement. One important feature of Figure 1.3 is the peak friction occurring at a certain critical slip speed. This behavior of friction is experienced in both dry and wet pavements.

Tire/pavement friction observed under dry conditions does not show any significant variation with the traveling speed ($v$). However, under wet conditions, $\mu$ decreases exponentially with increasing speed. Figure 1.4 shows the combined variation of $\mu$ with both speed ($v$) and slip ($s$) under wet conditions.

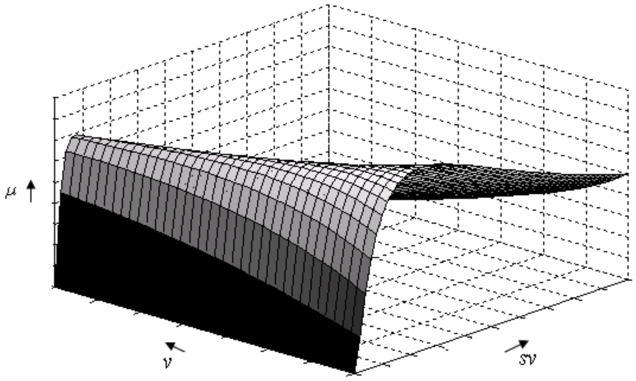

Figure 1.4: Variation of tire/pavement $\mu$ vs. slip speed ($v_r$) and traveling speed ($v$) under wet conditions

The most common contaminant affecting tire/pavement interaction is water, and hence the friction evaluation standards call for wetting the pavement before measurement. Friction is reduced due to the presence of a water film at the interface because of the following reasons. On a wet pavement, a part of the normal force at the contact is supported by water, thus reducing the effective tire/pavement direct contact and the normal load component transferred to the pavement asperities. At locations where water is trapped in between the two surfaces, the friction on the tire is solely provided by the viscous shear force exerted at the water film boundary. These viscous shear forces are significantly smaller compared to adhesion on dry pavements. In addition, filling of water in asperities reduces the hysteresis effects.

Under wet pavement conditions, the footprint can be divided into three regions (Figure 1.5).

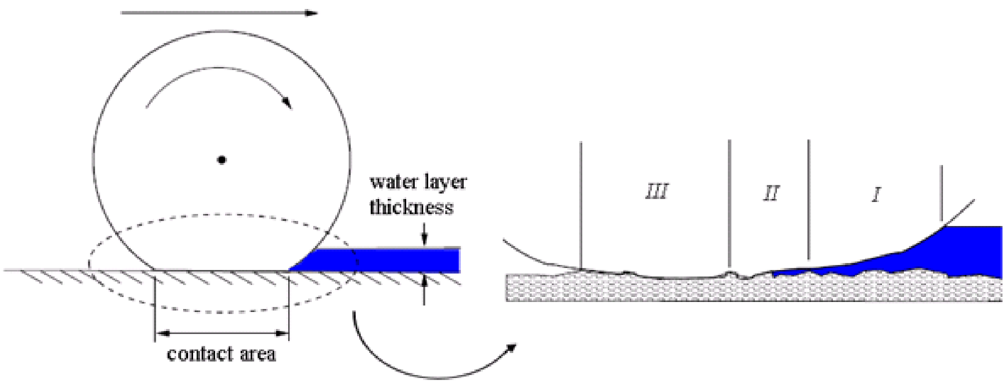

Figure 1.5: Regions in the footprint under wet conditions

(i) Floating region

In this region, the tire floats on a water film converging toward the footprint.

(ii) Transition region

In this region, the water film is partially broken and the tire begins to drape over the pavement asperities and establishes contact.

(iii) Contact region

In this region, the water film is squeezed out of the interface and contact conditions similar to those under dry conditions exist.

It is obvious that the above three regions do not have clearly defined boundaries. The final thickness of the water film is a function of the speed of the tire and the initial thickness of water layer on the pavement. The higher the travel speed and the greater the water layer thickness, the more the direct contact between the tire and the pavement will be reduced. As the speed is increased beyond a certain speed on a wet pavement, the direct contact between the tire and the pavement is completely lost. This phenomenon is called dynamic hydroplaning.

In contrast, viscous hydroplaning is a phenomenon that occurs when the water layer is not thick enough to produce dynamic hydroplaning. This occurs when the combined texture (mostly at the micro scale) of the two surfaces is insufficient to drain the trapped water and direct contact between the surfaces is lost (Clark, 1981).

## 1.3 Devices for Evaluation of Pavement Friction and Texture

It is important to identify the difference between a wheel of a regular vehicle and a friction testing wheel as dynamic systems, which are used to obtain certain outputs by feeding multiple inputs. Table 1.2 shows the inputs and outputs for each system. According to the description given in Table 1.2, slip should be provided as an input to a friction testing wheel. If not, the frictional behavior measured will not be representative of surface properties only. However, many more parameters (e.g. water level and temperature) have to be considered to define the complete systems. Only the need to control the slip and the inability to use a regular automotive tire as a standard pavement friction measuring device are emphasized here.

Table 1.2: Vehicle wheel and friction test wheel as systems

| Dynamic System | Inputs | Outputs |
|---|---|---|
| Wheel of a general vehicle | torques & forces on the axle,<br>driving/braking torque on hub,<br>pavement surface properties | friction force,<br>slip |
| Friction testing wheel | torques & forces on the axle,<br>pavement surface properties,<br>slip,<br>speed of vehicle | friction force |

Both friction and texture evaluation devices are used in the state-of-the-art of pavement friction measurement. Those measurement devices, considered in this dissertation research, are discussed in section 1.3.1.

### 1.3.1 Pavement Friction Measuring Devices (PFMDs)

As stated in section 1.1, it is the common practice adopted in the industry to estimate $\mu$ of wet pavements by measuring the shear force and the normal forces at the tire/pavement interface. Dependence of $\mu$ on the speed of travel and the slip ratio (Figure 1.4) is well known and hence, most of the PFMDs operate under standard speed and slip conditions. Measured $\mu$ is expected to represent the frictional input from the surface characteristics, and extensively used for safe runway and highway operation and maintenance. Several widely used PFMDs are described below. Pictures of the PFMDs described in this section can be found in Appendix A.

#### 1.3.1.1 Spot Measuring PFMDs

These PFMDs measure dynamic $\mu$ at discrete locations on the pavement. The British Pendulum Tester (BPT) and the Dynamic Friction Tester (DFT) are examples of such PFMDs.

(i) British Pendulum Tester (BPT)

BPT measures friction of a pavement surface based on the loss of potential energy during half a swing (cycle) of a rubber padded pendulum that is made to brush the pavement during its swing. This device has been used for pavement friction measurement for several decades. However, after the advent of DFT which gives a complete plot of friction variation within a range of speeds, the use of BPT has been limited.

(ii) Dynamic Friction Tester (DFT)

The DFT (Saito et al, 1996) consists of a horizontal flywheel under which a horizontal disk is attached. Three rubber pads mounted on metal strips are fixed axi-symmetrically on a circular path on the disk (Figure A.1). The rubber pads come into contact with the pavement during the test. DFT provides the variation of friction with tangential velocity at the rubber pads during the period of deceleration of the disk. Starting speed for a DFT test can vary between 80 – 100 km/h. Figure 1.6 shows a typical $\mu$ vs. speed test produced by the DFT.

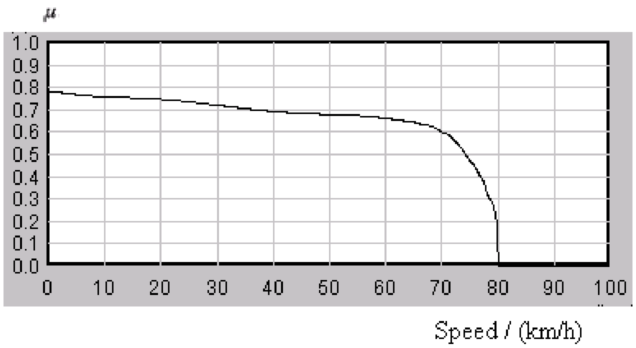

Figure 1.6: Friction data provided by a typical DFT test

Due to the repeatability of DFT, it is used as the standard device in harmonizing PFMDs according to the ASTM International Friction Index (IFI) (ASTM E1911, 2009) calculation procedure which will be discussed in chapter 2. According to this standard, DFT $\mu$ value at 20 km/h extracted from the DFT $\mu$ vs. velocity measurement is considered as a standard indicator of the micro-texture of the pavement.

### 1.3.1.2 Continuous Friction Measuring Equipment (CFME)

These PFMDs provide a continuous estimate of $\mu$ on a selected straight segment of a pavement. There is a wide range of operating mechanisms and different wheels are used on them. As illustrated in Table 1.2, the pre-defined input of slip is the main difference between a test wheel and regular wheels in a vehicle. This facility provides a means of observing the 3-dimensional (3-D) behavior of $\mu$ shown in Figure 1.4. The most common categorization of these PFMDs is based on the slip at which they measure friction.

Variable slip PFMDs are specified in ASTM E1859 (ASTM E1859, 2006). However, they are not widely used even though they can be used to evaluate the variation of friction with respect to both $v$ and $s$. The devices ROAR and RUNNAR, manufactured by Norsemeter, Norway, are typical examples of these PFMDs. The usefulness of the devices of this type in comprehensive pavement friction estimation is obvious from Figure 1.4.

Fixed-slip PFMDs use a constant slip ratio which is built-into the testing mechanism. They are used to measure pavement friction at a given constant speed, and hence provide $\mu$ data at desired velocities, but on a particular constant slip plane in Figure 1.4. Two widely used fixed-slip PFMDs are described below. Data from these two devices were used in the analysis presented in this dissertation.

#### (i) Locked Wheel Skid Tester (LWST)

LWST (Figure A.2) can be put in the fixed-slip category, considering the fact that it measures and reports pavement friction in the locked wheel condition at any desired constant speed. LWST is used to evaluate the average pavement friction in the locked wheel state as outlined in ASTM E274 (ASTM E274, 2006) and measure the peak pavement friction as outlined in ASTM E1337 (ASTM E1337, 2008). Forced sliding of the locked wheel on a pavement generates large drag forces, and therefore, this device employs a trailer to house the test wheel. This device is the most commonly used pavement friction measuring device in the United States. All fifty state Departments of Transportation (DOTs) have been using this device to collect pavement friction data for many years (Feighan, 2006).

Figure 1.7 shows typical data collected during a LWST test. A plot in the format in Figure1.7 is obtained using the *Winskid* software developed by the International Cybernetics Corporation (ICC), Largo, Florida, to analyze the raw data obtained from the LWSTs manufactured by ICC. The data typically collected at each data point include, distance from the starting point of data collection, traveling speed ($v$) ('*VehSpd*' in the graph), circumferential speed of the test wheel ($v$ - $sv$) ('*TestSpd*' in the graph), normal load on test wheel ('*Load*' in the graph) and longitudinal frictional force ('*Force*' in the graph) on the test wheel. *Winskid* also provides the skid data at each data point which can be opened in a spreadsheet. One can use the *Winskid* graph (Figure 1.7) in combination with the spreadsheet of skid data to extract required ranges of raw data. The movable cursor on the graph with visualized data point facilitates this task.

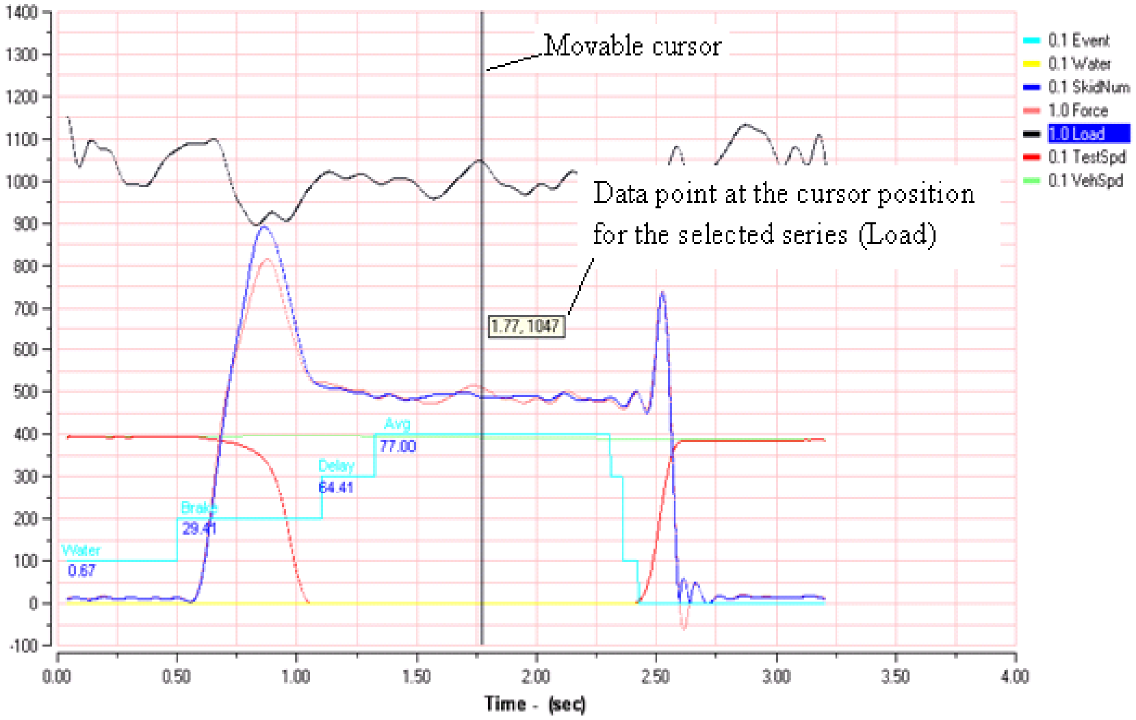

Figure 1.7: Typical skid data provided by LWST plotted by the *Winskid* software.

(ii) Runway Friction Tester (RFT)

The RFT (Figure A.3) is a typical example for a fixed-slip device. RFT has a separate test wheel to measure friction. A typical RFT operates at a constant slip ranging between 0.1 and 0.15. However, the test mechanism is attached at the rear of a truck behind the rear-wheel axle. Friction measurements obtained by this device tend to be higher than those from a LWST, because it operates at a level of slip at which the frictional force is closer to its maximum with respect to slip (see Figure 1.4). A typical plot of RFT data is shown in Figure 1.8. In Figure 1.8, the skid number is defined as $100 \times \mu$, and it is a common practice in pavement friction measurements. The reported RFT data is averaged at every foot of the tested length.

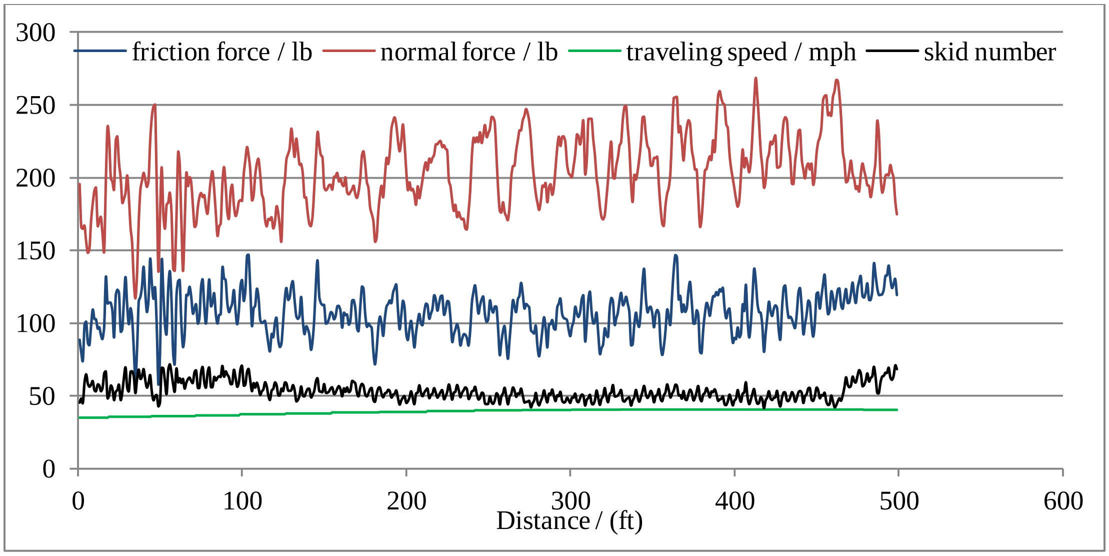

Figure 1.8: Typical skid data provided by RFT

### 1.3.2 Macrotexture Measurement Devices

Since the direct determination of micro-texture (Table 1.1) in the field is tedious indirect measurements such as DFT are often sought. However, macro-texture is measured in the field relatively easily using a variety of methods. These include conventional methods such as the Sand Patch Test, the Outflow Volumetric Test and relatively more accurate and sophisticated methods based on laser technology (Feighan, 2006).

The Circular Track Meter (CTM) (Figure A.4) specified in ASTM E2157 (ASTM E2157, 2009), is one of the widely used macro-texture measuring devices that employs laser technology. At a given location the CTM evaluates the macro-texture on the path where $\mu$ is evaluated by its companion DFT. The Mean Profile Depth (MPD) given by this device, which is an average profile depth calculated according to ASTM E1845 (ASTM E1845, 2009), is used as the macro-texture representation in the current standardization procedure (ASTM E1960, 2007). A typical CTM profile is shown in Figure 1.9.

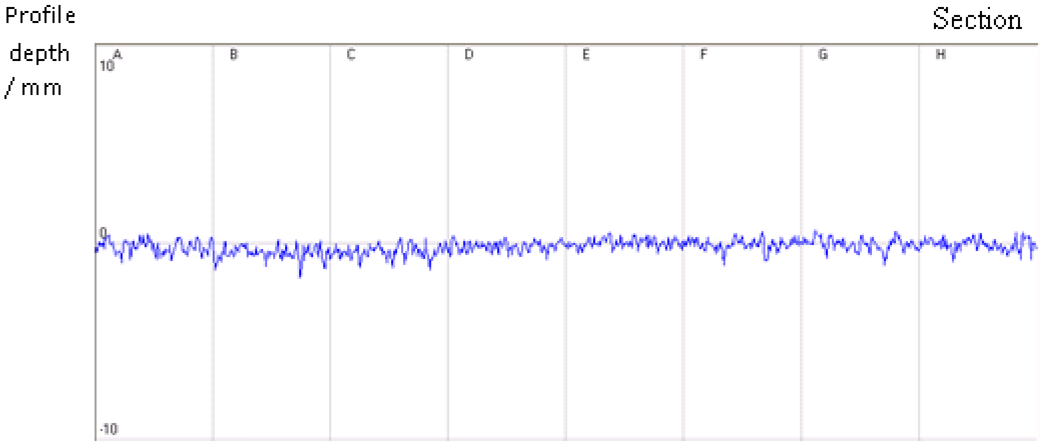

Figure 1.9: Typical texture data provided by CTM on an asphalt pavement

The CTM divides the profile measurement to eight sections (labeled A through H in Figure 1.9) and calculates MPD at each section. The average MPD for the profile shown in Figure 1.9 was reported as 0.57 mm.

# CHAPTER 2

# PROBLEMS IN COMPARING PAVEMENT FRICTION MEASUREMENTS

In this chapter, the friction measurements from different PFMDs will be presented to illustrate their disparity. The current standard procedure for harmonizing the measurements from different PFMDs (ASTM E1960, 2007) and the associated problems will also be explained. The friction measurements presented in this chapter were taken at the annual NASA Wallops workshop which has been conducted to harmonize measurements from different PFMDs.

## 2.1 NASA Wallops Friction Workshop

The annual NASA Wallops Runway Friction Workshop has been conducted for more than a decade, and the test procedures adopted are specifically focused in comparing the readings from different PFMDs that are brought to the workshop from around the world. During this workshop, different types of friction and texture measuring devices from different manufacturers and users are evaluated at the same set of runway surfaces under similar conditions. These readings are used to derive empirical harmonization equations between the PFMDs. PFMDs with measured data that do not conform to the harmonization procedure are considered to be unreliable. Therefore, this workshop is considered as a place where standard tire/pavement friction data are collected.

During the workshop, different PFMDs measure friction at test Sections of different pavement types. The spot measuring devices and CFME are operated separately. When the CFME are operated, the test vehicles are lined up as a convoy and several replicates of measurements are made at each test speed.

## 2.2 Need for Standardization

In 2007, 14 PFMDs of 11 different types were brought to the workshop. Figure 2.1 shows the disparity in friction measurements from 5 devices of different types on 7 different pavement surfaces (labeled A through G).

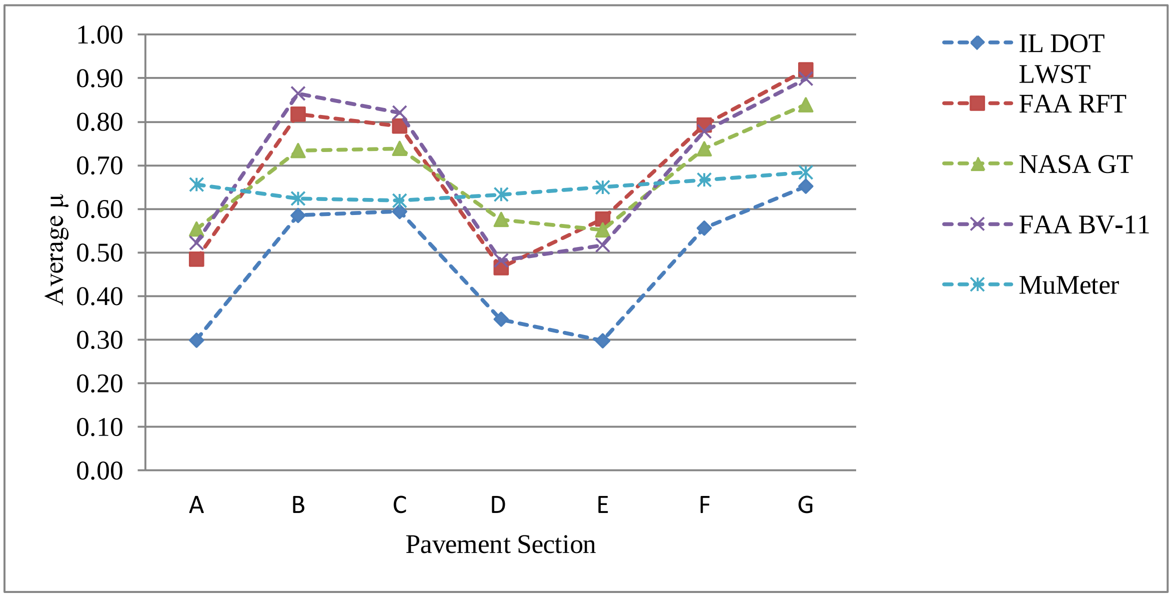

Figure 2.1: Disparity in average friction measurements from different types of PFMDs

In Figure 2.1, the Grip Tester (GT) and the BV-11 Skiddometer are two fixed-slip devices. The MuMeter is a side-force measuring device that evaluates friction in the lateral direction in contrast to most of the other PFMDs that measure friction in the longitudinal direction.

The inevitable variation in measured $\mu$ is due to the different mechanisms employed by different devices to measure friction. For example, in LWST, the wheel slip ($s$) during the measurement is 1, and in RFT it is 0.13.

Due to the disparity in the types of PFMDs employed to measure tire/pavement friction in different parts of the world, and the variety of practices adopted in reporting friction, confusions are unavoidable at the operational level especially in situations such as runway operations. Therefore, an obvious need for standardization exists and the current ASTM procedure to achieve this (ASTM E1960, 2007) will be discussed in section 2.3.

## 2.3 Current Standard for Harmonization

The need for standardization of pavement friction measurements from different devices was shown in section 2.2. The most obvious way of achieving this is to restrict pavement friction measurement to a single type of device that operates under well-defined conditions. However, this solution is impractical for any global industry that evolves with leaps and bounds. Hence, the current approach for standardizing tire/pavement friction measurement can be identified as a diplomatically pragmatic approach that accommodates different PFMDs developed by different manufacturers around the globe. Standards for designing, manufacturing, operating and maintaining different types of devices are available. Following are some examples of such standards set up by the American Society for Testing and Materials (ASTM).

(i) ASTM Standard E274 – 06 (ASTM E274, 2006), Standard Test Method for Measuring Skid Resistance of Paved Surfaces Using a Full-Scale Tire

(ii) ASTM Standard E1911– 09AE1 (ASTM E1911, 2009), Standard Test Method for Measuring Paved Surface Frictional Properties Using the Dynamic Friction Tester

(iii) ASTM Standard E2157 – 09 (ASTM E2157, 2009), Standard Test Method for Measuring Pavement Macro-texture Properties Using the Circular Track Meter

(iv) ASTM Standard E1337 – 90 (ASTM E1337, 2008), Standard Test Method for Determining Longitudinal Peak Braking Coefficient of Paved Surfaces Using a Standard Reference Test Tire

(v) ASTM Standard E1859 – 97 (ASTM E1859, 2006), Standard Test Method for Friction Coefficient Measurements Between Tire and Pavement Using a Variable Slip Technique

(vi) ASTM Standard E1960 – 07 (ASTM E1960, 2007), Standard Practice for Calculating International Friction Index of a Pavement Surface

(vii) ASTM Standard E524 – 08 (ASTM E524, 2008), Standard Specification for Standard Smooth Tire for Pavement Skid-Resistance Tests

Of the above, this dissertation primarily focuses on the standard harmonization procedure ASTM E1960. The development of this procedure and its details are discussed in section 2.3.1.

### 2.3.1 Standardization Model and Procedure

The Pennsylvania State University (PSU) model (Henry, 1978) is the basic friction model used in the standardization of pavement friction evaluation. This model can be expressed by a statistically developed exponential equation (Eq. 2) which can be used to predict friction at any desired slip speed using the friction data obtained at the operating slip speed of the measuring device.

$$\mu(v.s) = \mu_0 . e^{-\left(\frac{v.s}{V_0}\right)} \tag{2}$$

Here the two model parameters $\mu_0$ ($\mu$ at slip speed = 0) and $V_0$ (an exponential constant) can be calibrated to predict $\mu$ at any slip speed, by fitting several measured data points to Eq. (2).

As an outcome of a comprehensive experiment conducted by the World Road Association with international collaboration, a procedure to harmonize the friction measurements from devices operated at different slip speeds has been standardized. This experiment is called the PIARC (Permanent International Association of Road Congresses or the World Road Association) experiment. The PSU model (Eq. 2) served as the basis for this procedure (Wambold et al, 1994). Eq. (3) expresses the PIARC model.

$$\mu(v.s) = \mu(v.s_1). e^{\left(\frac{v.s_1 - v.s}{S_p}\right)} \tag{3}$$

When the parameter $S_p$ (the speed constant representing the macro-texture of the pavement) is known, Eq. (3) can be used to obtain the friction at any desired slip speed ($v.s$), using the friction measured at the operating slip speed ($v.s_1$). Both the PSU and the derived PIARC models limit their applicability to the post-peak portion of the plot shown in Figure 1.3, since these models do not incorporate tire parameters that determine the pre-peak portion of the $\mu$ plot in Figure 1.3. Nonetheless, the PIARC model (Eq. 3) is used as the basis for the current ASTM standard practice for harmonizing pavement friction measuring devices (ASTM E1960). $S_\mathrm{p}$ is computed using Eq. (4) with the Mean Profile Depth (MPD) value given by the Circular Track Meter (CTM) specified in the ASTM E2157 test method. According to ASTM E1960, the PIARC model is used to adjust the friction values measured at different slip speeds ($FR_S$) to a common slip speed of 60 km/h using Eq. (5a). The adjusted friction values ($FR_{60}$) are then harmonized with friction numbers ($F_{60}$) obtained using Eq. (5b) with the measurements from the Dynamic Friction Tester (DFT) evaluated at 20 km/h ($DFT_{20}$). DFT is used as the standard friction measuring device due to its repeatability and precision. The harmonization is achieved using a linear regression shown by Eq. (6), where *A* and *B* are the regression parameters.

$$S\mathrm{p} \ = \ 14.2 \ + \ 89.7 \times MPD \tag{4}$$

$$FR_{60} = FR_S . e^{\left(\frac{v.s-60}{S_p}\right)} \tag{5a}$$

$$F_{60} = 0.081 + 0.732 \times DFT_{20} . e^{\left(\frac{-40}{S_p}\right)} \tag{5b}$$

$$F_{60} = A + B \times FR_{60} \tag{6}$$

The above standard practice (ASTM E1960) for calculation of the International Friction Index (IFI) provides a definitive means of correlating the friction readings from different devices operating at various slip speeds.

At the aforementioned NASA Wallops annual friction workshop, the friction measuring devices are calibrated using the above IFI calculation procedure and the regression constants specific to each calibrated device are estimated. These regression constants are then expected to be used in subsequent measurements involving the calibrated devices to make their friction measurements comparable.

### 2.3.2 Problems in the IFI Procedure

Inconsistencies in the current IFI procedure have been observed on many occasions. Complaints about the inadequacy of the model in meeting the runway operational needs were common (especially from aviation professionals) in the two most recent Wallops workshops. These inconsistencies can be demonstrated simply by using the two distinct calibration constants ($A$ and $B$ in Eq. 6) for a certain device to predict the $F_{60}$ evaluated on the same surface. Furthermore, $FR_{60}$ values from the same device estimated from measurements at two different speeds on the same pavement have shown considerable disagreements. Figure 2.2 shows the quality of the IFI calibration achieved for two devices (Federal Aviation Administration (FAA) RFT and Virginia Department of Transportation (VDOT) LWST) tested at the Wallops 2007 workshop. The inconsistency in using data collected at different speeds can be seen from both Figure 2.2 (a) and (b). Furthermore, the major assumption of linearity between $F_{60}$ and $FR_{60}$ (Eq. 6) does not seem to be valid, especially in the calibration at 96 km/h shown in Figure 2.2 (b).

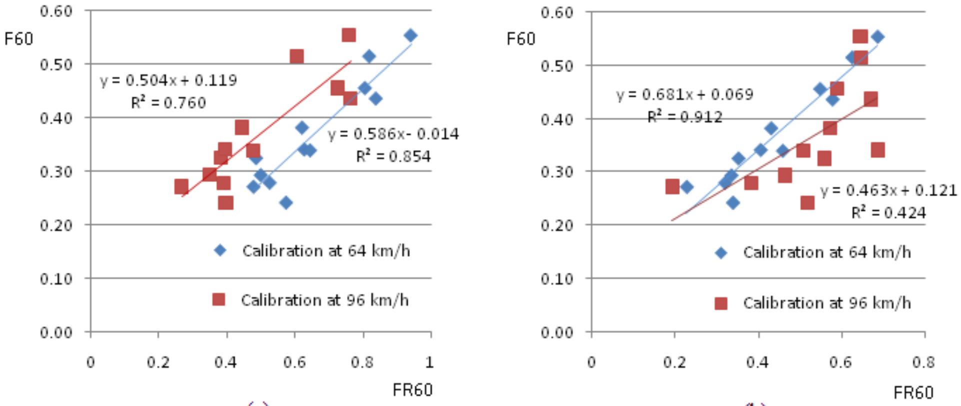

(a) (b)

Figure 2.2: Quality IFI calibration achieved at 2007 Wallops workshop for two devices, (a) FAA RFT, (b) VDOT LWST

The IFI procedure standardizes the pavement friction measurements from different devices based on empirical modeling that only considers the effects of slip speed and texture of the pavements. In Figure 2.3, the friction measured during eight repeated test runs on pavement Section A at the NASA Wallops flight facility by VDOT LWST is plotted. The range of $\mu$ is more than 0.1 and the values have a decreasing trend. This can be a result of an increase in the water level when many devices are operated on the same wheel path over a short period of time. However, the IFI model is not capable of handling this kind of scenario.

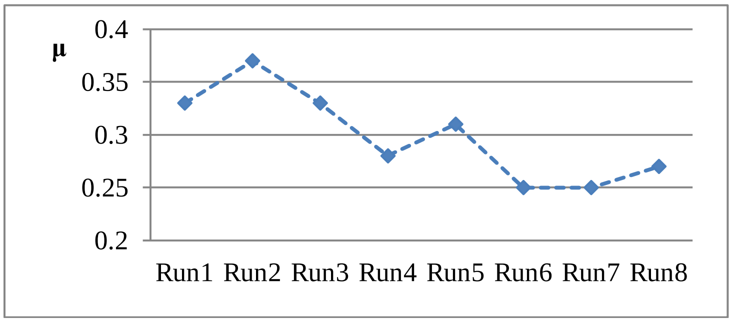

Figure 2.3: Variation of VDOT LWST measurements on pavement Section A

Moreover, the IFI method fails to compensate for the disparity in the measurements due to possible differences in parameters of the measuring mechanism between two devices of the same type. Figure 2.4 shows a systematic deviation in measurements taken from two Grip Testers. The NASA GT measured higher friction than DND GT on all of the pavement Sections. On some occasions the difference is as large as 0.1. This systematic difference can be attributed to a difference in tire properties, probably caused by different inflation pressures, which again is beyond the scope of the IFI method.

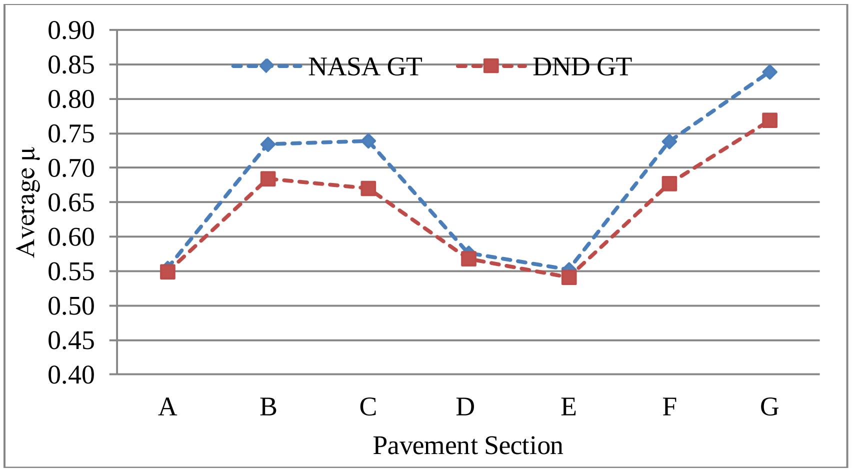

Figure 2.4: Systematic deviation in average $\mu$ measurements from two GTs

The CTM MPD reading is essential in calculating the standard $\mu$ value using Eqs. (4), (5a) and (6). Therefore, an extra set of spot texture measurements on the surface is required by the IFI procedure. This is simply impractical in places like busy runways. Because of the above reasons, the reliability of the current standardization has been questioned during the recent past. A model addressing the above issue is therefore essential in achieving sufficiently accurate harmonization between different PFMDs.

# CHAPTER 3

# RESEARCH METHODOLOGY

It was shown in chapter 2 that the standardization procedure involving the calculation of IFI (ASTM E1960) produces inconsistent results when the calibrated model is used to correlate subsequently measured data. One obvious reason for the inconsistency is the exclusion of important physical parameters such as tire properties and water film thickness in the friction model. The parameters of the current model represent only the pavement texture, speed, and to a limited extent, the variation of slip ratio between the measuring devices. Furthermore, the micro-texture representation itself is based on another friction measuring device (DFT).

The best approach to solve this problem is to model tire/pavement friction using an analytical model with physically meaningful and quantifiable parameters. Using appropriate parameters, such a model can be used to interpret the disparity between various PFMDs operating under different conditions. Moreover, by calibrating a more representative analytical friction model with due care, it is possible to achieve a physically meaningful comparison between measurements from different PFMDs. It can also allow a physically intuitive adjustment of parameters for a given device, such as the construction, size and pressure of the tire in order to fine-tune its measurements to an acceptable range of values. Most importantly, knowledge of the physically meaningful model parameters for the standard version of a particular type of device provides a means of condition monitoring and preventive maintenance. In addition, from the point of view of pavement design and management, use of this type of a model can enhance the accuracy of prediction of the frictional performance from a given combination of texture, geometry and contamination level.

Considering the facts explained above, an analytical friction model was proposed to develop a more consistent harmonization method. The model is the LuGre friction model (Canudas-de-Wit et al, 1995), which derives its name from the “Lund Institute of Technology,” Sweden and the “Laboratoire d'Automatiquede Grenoble,” France, where the initial work to develop the model was carried out. The LuGre model was originally developed to model general sliding friction for control purposes and it was later applied to longitudinal tire dynamics (Canudas-de-Wit et al, 1999). It showed great promise to provide physically meaningful comparisons between different PFMDs. Deriving the governing equations for different PFMDs had already been accomplished by the research team prior to the beginning of this dissertation research (Seneviratne et al, 2009)..

The starting point for this research was the effective application of previously derived governing equations (Seneviratne et al, 2009) to analyze PFMD data. The previous attempt was to calibrate several PFMDs simultaneously using a handful of measured data points that included representative measurements from all the devices that were compared.

A detailed literature survey on modeling tire/pavement friction based on the LuGre model was conducted. The superiority of the LuGre model over the existing PFMD harmonization method was then confirmed by a comparative study. Although many previous publications remarked the analytical nature of the LuGre tire model, none of those had successfully validated the physical significance of the model parameters. All the applications were limited to calibrating the model equations using various fitting procedures to predict measured tire/pavement friction responses (Canudas-de-Wit et al, 1999, Deur et al, 2001 and Canudas-de-Wit et al, 2003). Therefore, verification of the physical meanings of the LuGre model parameters pertaining to tire/pavement friction became an important objective for this research. The model parameters were analytically related to directly measurable properties and parameters affecting tire/pavement interaction. A set of laboratory tire experiments was designed and carried out at a renowned independent tire testing facility. The data from these experiments were then used to estimate the LuGre model parameters, which were then compared with the parameters obtained by the traditional data fitting approach.

The effect of the amount of water in the tire/pavement interface on friction, which had been overlooked, subjected to approximations, or handled with excessive detail resulting in practical restrictions for the applications intended herein, was studied using a combined experimental and analytical procedure. As a result, a practical and straightforward method was developed to include the effect of water on tire/pavement friction in the LuGre model.

After successful validation of the model for tire/pavement friction testing applications and validating the physical meaning of the model parameters, the sensitivity of the frictional output of the model to the model parameters was determined by a statistically based sensitivity analysis. The results of the sensitivity analysis were used to prioritize the model parameters in terms of their contribution toward the frictional output, and to determine critical model parameters that can be adjusted by introducing practically feasible modifications in the measuring mechanisms of selected PFMDs. This ability to propose physical modifications whose effects can be quantified using the LuGre tire model was used to develop an effective harmonization procedure. The physically meaningful harmonization between two widely used PFMDs envisioned by this method is shown in Figure 3.1. As the next step, an experimental program was conducted to validate the above mentioned physically meaningful PFMD harmonization method.

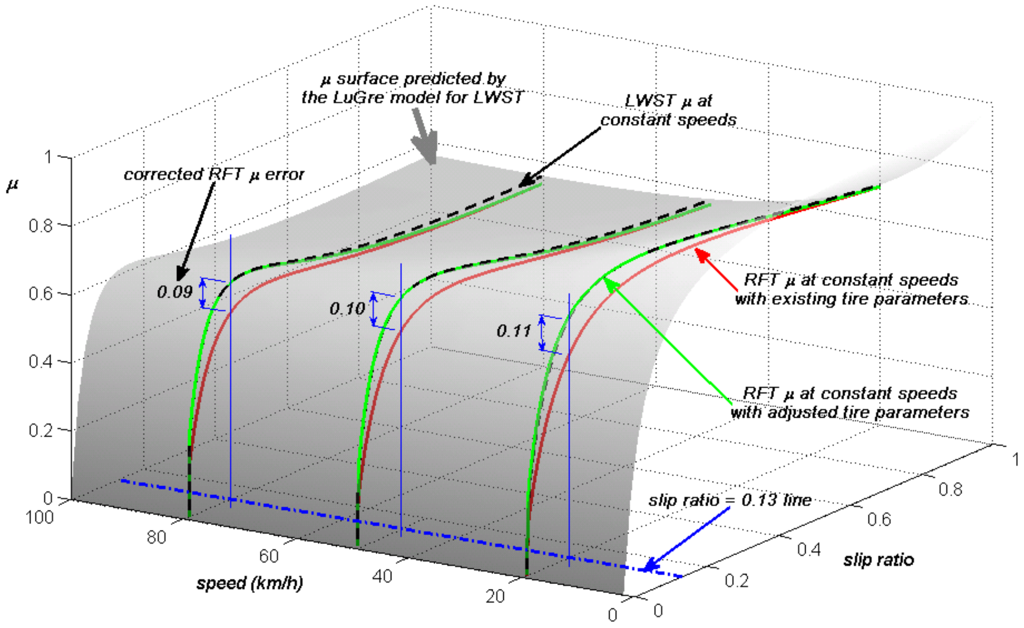

Figure 3.1: Expected physically meaningful harmonization between LWST and RFT

## 3.1 List of Research Tasks

The following is the list of the components of the research program carried out for the fulfillment of the requirements for this dissertation.

(i) Development of computational methods for the analysis of PFMD data using the tire/pavement friction models considered in the research program

(ii) Evaluation of the LuGre model for its capability to characterize pavement friction

(iii) Comparison of the accuracy of the LuGre model in predicting PFMD measurements with that of the model used in the current standardization

(iv) Detailed literature study on the development and applications of the LuGre model

(v) Validation of the physical meanings of the tire parameters of the LuGre model by measuring them using specially designed experiments

(vi) Development of a practical method to calibrate the LuGre tire model to capture the effect of the amount of water at the tire/pavement interface on friction

(vii) Statistical sensitivity analysis to determine the relative significance of the LuGre model parameters according to their contribution to model the friction force development at the tire/pavement interface

(viii) Development of a demonstrative harmonization method for two widely used PFMDs; LWST and RFT

(ix) Experimental validation of the developed harmonization method

# CHAPTER 4

# PREVIOUS WORK ON LUGRE MODEL AND ITS APPLICATION TO TIRE/PAVEMENT FRICTION MODELING

The main intent of this research was to develop a practical and effective method to harmonize PFMDs based on an analytically sound tire/pavement friction model. The model should have an ability to provide physically quantifiable guidelines to introduce adjustments to PFMDs in order to bring them to an acceptable harmonization. Therefore, it should be able to characterize all of the basic parameters that contribute to tire/pavement friction development while fulfilling the computational simplicity required by a standard procedure. In this chapter, a detailed literature survey is presented on the development of analytical friction models toward the LuGre tire model. Due to the wide spectrum of applications of this model, specific attention was paid to development of the model and its application to tire/pavement interaction, particularly longitudinal tire dynamics which governs majority of PFMDs.

## 4.1 Evolution of Dynamic Friction Models towards LuGre Model

Although, modeling of friction has evolved through centuries, capturing important frictional behavior in both static and sliding conditions using a single model had been problematic until the LuGre model was introduced in 1995 (Canudas-de-Wit et al, 1995). The development of friction models toward the LuGre model is discussed in the following sections of this chapter.

### 4.1.1 Classical Models for Friction

Figure 4.1 shows different components of friction (Armstrong-Helouvry, 1991). Static friction phenomena only have a static dependency on velocity. The first static friction model was the classic model of friction from Leonardo Da Vinci (1452 – 1519); friction force is proportional to load, opposes the direction of motion, and is independent of contact area. Coulomb (1785) further developed this model and the friction phenomena described by the model became known as Coulomb friction (Figure 4.1(b)). Morin (1833) introduced the idea that frictional force opposes the direction of motion when the sliding velocity is zero (Figure 4.1(a)). Reynolds (1866) developed expressions for the friction force caused by the viscosity of lubricants. The term viscous friction is used for this friction phenomenon (Figure 4.1 (c)). Stribeck (1902) observed that for low velocities, the friction force decreases continuously with increasing velocities and not in a discontinuous manner as described above. This phenomenon of decreasing friction at low, increasing velocities is called the Stribeck friction or effect. The Stribeck effect is described by the parameter called Stribeck velocity. Small values of Stribeck velocity produce a rapidly decreasing Stribeck effect and vice-versa (Figure 4.1 (f)).

The classical friction models use different combinations of Coulomb friction, viscous friction and Stribeck friction and they are described by static maps between velocity and friction force (Armstrong-Helouvry, 1991). Initial development of these friction models for control systems had considerable attention paid to modeling of the zero velocity and velocity reversal nature of friction while modeling sliding friction.

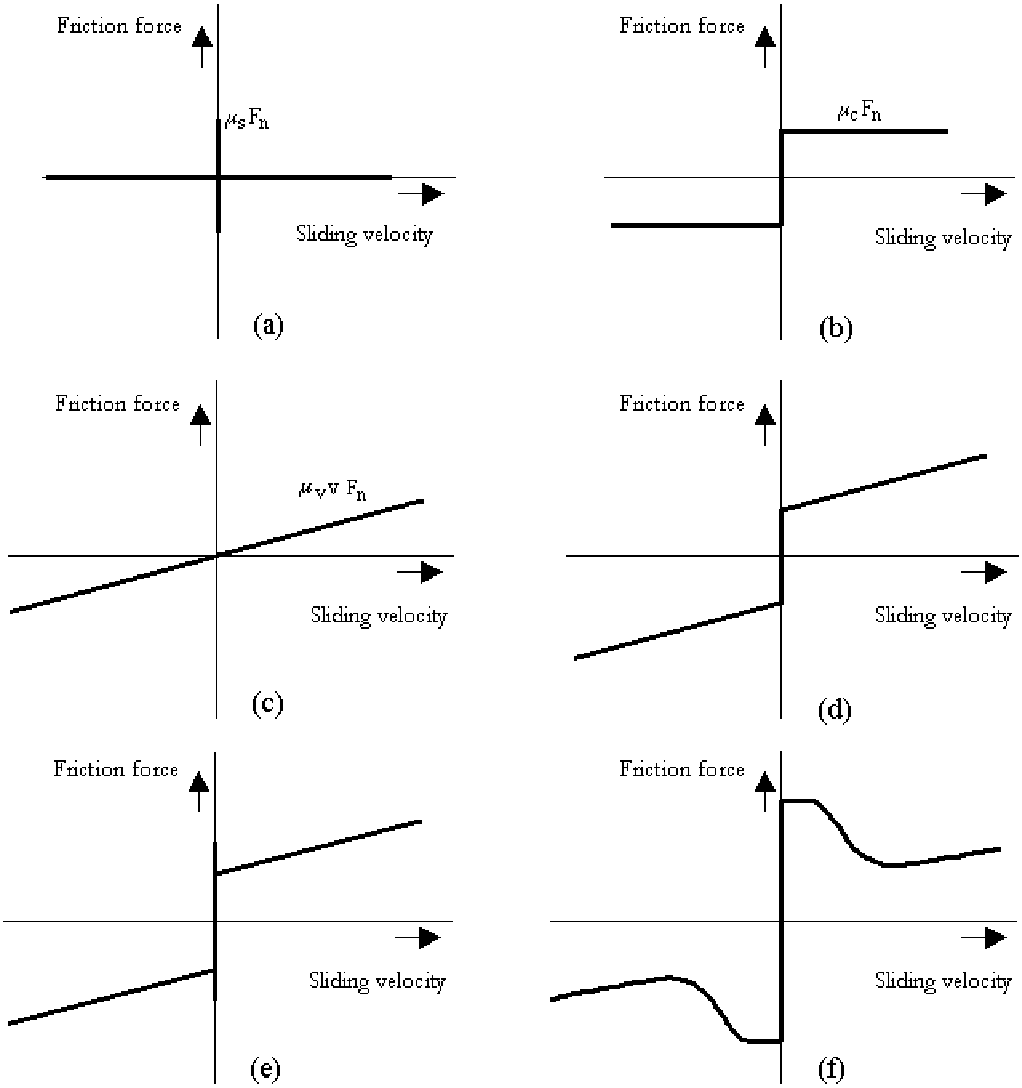

Figure 4.1: Components of friction, (a) static friction, (b) Coulomb friction, (c) viscous friction (d) Coulomb + viscous friction, (e) static + Coulomb + viscous friction, (f) static + Coulomb + viscous friction with Stribeck effect

Since zero velocity and velocity reversal are not experienced in tire/pavement friction measuring devices, the above condition is beyond the scope of this research. Therefore, early attempts to achieve the above purpose such as Karnopp model (Karnopp, 1985) and Armstrong's model (Armstrong-Hélouvry et al, 1994) are not discussed in detail in this review. However, the static models do not explain observations such as the hysteresis behavior of friction with varying velocity, variation of the limiting static frictional force and small displacements at the interface during stiction. Thus, the use of classical models is not reliable especially in terms of precision at low velocity control (Canudas-de-Wit et al, 1995).

### 4.1.2 Dynamic Friction Models

Models that can incorporate dynamic effects must be used for more accurate description of friction under certain practical conditions. The first motivation for development of dynamic friction models was precision and friction compensation requirements in controls. The Dahl model (Eq. 7) (Dahl, 1968) is a very early model formulated to serve this purpose.

$$\frac{dF}{dx} = \sigma\left[1 - \frac{F}{\mu_c} sgn(v)\right]^{\alpha} \tag{7}$$

In Eq. (7) $x$, $F$, $\sigma$, and $\mu_c$ are the displacement, friction force, material stiffness and Coulomb friction, respectively, while $\alpha$ is a parameter defining the shape of the $F$ vs. $x$ curve which is kept at unity in most cases. The Dahl model captures neither the Stribeck effect nor stiction (Olsson et al, 1998). Typical $F$ vs. $x$ behavior obtained from the Dahl model is shown in Figure 4.2.

In Haessig et al, 1991, two dynamic friction models were introduced to model the stick-slip behavior. The bristles modeling the contact points in the stiction model presented in Haessig et al, 1991 capture the random nature of the contact. The second model called the reset integrator model does not capture stiction adequately, however, it is numerically more efficient than the bristle model (Haessig et al, 1991).

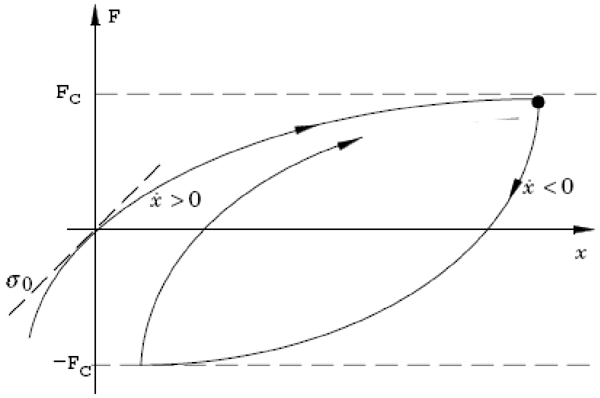

Figure 4.2: Typical *F* vs. *x* curve provided by the Dahl model (Dahl, 1968)

### 4.1.3 The LuGre Dynamic Friction Model

Origin of the model by Canudas-de-Wit et al, 1995 is the motivation to compensate friction in control systems based on analytical models. In the formulation of this model, it is assumed that the two rigid surfaces make contact through elastic bristles like in the bristle model (Haessig et al, 1991). Under the application of a shear force, the deflection of the bristles results in the friction force. The deflection will be random depending on the nature of the textures of the two surfaces and quantified by the normal pressure distribution on the contact area. If the deflection is sufficiently large, the bristles start to slip, and the average bristle deflection under steady-state motion is determined by the velocity. The bristle deflection is lower at low velocities, which implies that the steady-state deflection decreases with increasing velocity. This models the phenomenon that the surfaces are pushed apart by the lubricant producing the Stribeck effect (Olsson et al, 1998). The average deflection of the bristles is denoted by $\bar{z}$ and given by,

$$\frac{d\bar{z}}{dt} = v_r - \frac{|v_r|}{g(v_r)}\bar{z} \tag{8a}$$

The frictional force generated from the bending of the bristles is described by Eq. (8b) where $\mu$ is the previously defined coefficient of friction.

$$\frac{F_s}{F_n} = \sigma_0 \bar{z} + \sigma_1 \frac{d\bar{z}}{dt} + \sigma_2 v_r \tag{8b}$$

$$\operatorname{sgn}(v_r).\mu = \frac{F_s}{F_n} \tag{8c}$$

The parameter $\sigma_0$ is the stiffness of the bristles, $\sigma_1$ is the damping coefficient, and $\sigma_2$ is the viscous damping coefficient. They are normalized by the normal force $F_n$. Function $g(v_r)$ (Eq. 9a) has been selected to represent the components of friction illustrated in Figure 4.1.

$$\sigma_0 g(v_r) = \mu_c + (\mu_s - \mu_c) e^{-\left|\frac{v_r}{v_s}\right|^2} \tag{9a}$$

with $\mu_c$ , $\mu_s$ and $v_s$ are the Coulomb friction, static friction and the Stribeck velocity, respectively.

In Canudas-de-Wit et al, 1995, the properties and behavior of the LuGre model are discussed in detail. It is proven that *z*, given in Eq. (8a) is bounded for all *t* values provided the initial *z* is finite and bounded. The dissipative nature of *z*, which is important in characterizing hysteresis, is also addressed in the model. The pre-sliding lag of friction is modeled with selected parameters and plotted as shown in Figure 4.3. Furthermore, frictional hysteresis due to velocity transients is also modeled (Figure 4.4 (a)) and compared qualitatively with experimental data (Figure 4.4 (b)) which had already been published independently (Hess et al, 1990).

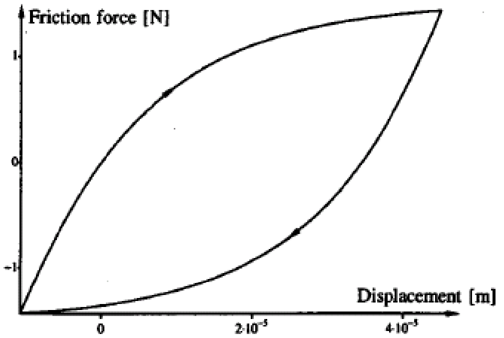

Figure 4.3: Presliding displacement modeled by the LuGre model with suitable parameters (Canudas-de-Wit et al, 1995)

Moreover, stick-slip motion can also be demonstrated with this model, and its application for control purposes has also been discussed in detail (Canudas-de-Wit et al, 1995). Since these effects are beyond the scope of the intended research, they will not be discussed here.

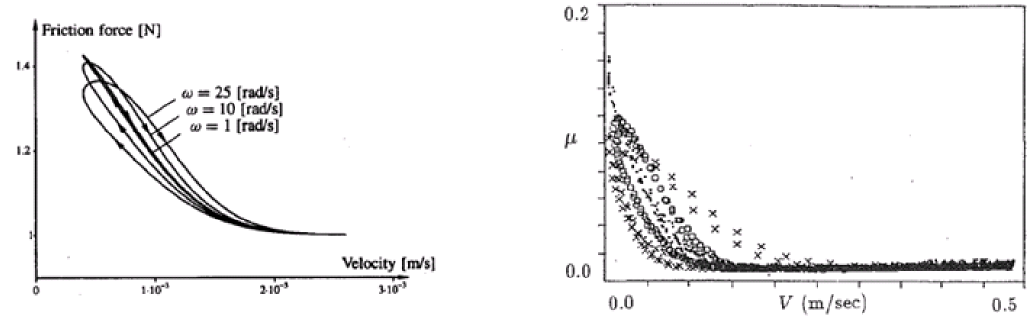

(a) LuGre predictions of hysteresis with varying velocity

(b) Experimental data at different velocity frequencies; . - 0.63 rad/s, o - 6.3 rad/s, x - 31.5 rad/s

Figure 4.4: Prediction of frictional hysteresis with varying velocity by the LuGre model (a) and comparison to independent experimental data (b)

## 4.2 Steady-State Models for Tire/Pavement Friction

Before 1999, tire friction modeling was limited to steady-state friction models. These models had been developed basically in two fields, independent of each other. One is the tire/pavement friction measuring field and the other is the vehicle dynamics analysis field. PSU (Henry, 1978), PIARC (Wambold et al, 1994) and Rado (Rado, 1994) friction models were developed in the field of pavement friction evaluation. The PSU and PIARC models were discussed in section 2.3.1 of this dissertation.

The Rado friction model (Eq. 10) (Rado, 1994) which is another empirical model developed using the PIARC experimental data, considers both the effects of tire properties and pavement texture properties on $\mu$ vs. slip speed characteristics of a wet pavement.

$$\mu(s.v) = \mu_{peak}.e^{\left[\frac{-\left(ln\frac{s.v}{S_c}\right)^2}{C^2}\right]} \tag{10}$$

In Eq. (10), $\mu_{peak}$ is the maximum friction observed during a continuous linear braking phase from free rolling to the locked wheel condition at a constant traveling speed, $S_c$ is the slip speed at which $\mu_{peak}$ is observed and $C^2$ is a texture related parameter equivalent to $S_p$ in the PIARC model (Eq. 2). The Rado model (Eq. 10) is capable of describing the friction-slip speed behavior in the entire slip range shown in Figure 1.3.

The Pacejka model (Pacejka et al, 1991) is the most widely cited tire friction model found in vehicle dynamics literature. The consistency of this model seen in comparison with steady-state experimental data has led this model to be called the "magic formula". Consequently, this model is extensively used as a benchmark for assessing new models (Canudas-de-Wit et al, 1999). In this model, the tire/pavement friction force is expressed as,

$$F\,(s) = c_1 \sin(c_2 \arctan(c_3 s - c_4 (c_3 s - \arctan(c_3 s)))) \tag{11}$$

Where, $c_1$, $c_2$, $c_3$ and $c_4$ are primary parameters dependent on the tire/pavement characteristics and $s$ is the slip. Parameters $c_1$, $c_2$, $c_{3,}$ and $c_4$ are dependent on many secondary parameters stemming from tire characteristics, pavement conditions and tire operational conditions. They are determined by fitting Eq. (11) to experimental data. However, the drawback of this model is that it obviously needs a large amount of experimental data for calibration and the model parameters do not have physical significance.

In general, steady-state models are simple but restricted to constant slip speed and constant normal load analysis. However, in reality, the tire/pavement interaction is essentially of a dynamic nature so the need for dynamic tire models has been important for the evaluation of pavement friction and vehicle dynamics.

## 4.3 The LuGre Model for Tire/Pavement Friction

The LuGre model was initially developed for lubricated sliding contact of general materials. This is evident from the typical model parameters (material properties) selected for the model simulations presented in (Canudas-de-Wit, 1995). Four years after its origination, in 1999, the LuGre model was first applied to tire/pavement interaction (Canudas-de-Wit et al, 1999), specifically, to longitudinal tire dynamics.

### 4.3.1 Longitudinal Tire Dynamics

Longitudinal tire dynamics (Figure 4.5) is a simplified consideration of the mechanics of the automotive tire, neglecting any lateral effects in the direction of the wheel axle.

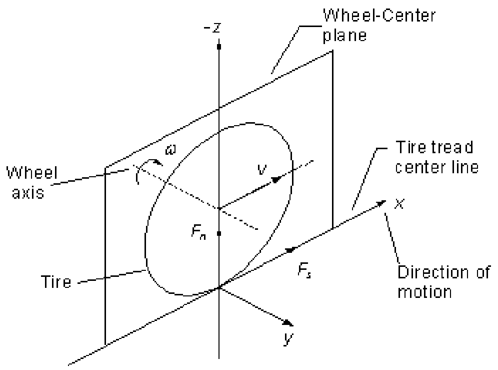

Figure 4.5: An illustration of longitudinal tire dynamics

For this simplified case, the equations of motion for the tire are as follows.

$$F = m\ddot{x} \tag{12a}$$

$$T - rF = J\dot{\omega} \tag{12b}$$

where, $F$ - longitudinal frictional force, $m$ - mass of the wheel, $\ddot{x}$ - longitudinal acceleration at wheel center, $T$ - braking or accelerating torque on the wheel, $r$ - wheel radius, $J$ - moment of inertia of the wheel, and $\dot{\omega}$ - angular acceleration of the wheel.

It must be noted that in the case of most pavement friction measuring devices, the dynamics are restricted to the longitudinal direction. On the other hand, some devices do have lateral effects arising either from the geometry of the measuring mechanism or the dynamics.

### 4.3.2 Tire Modeling Using a Brush Representation

Modeling of tires with brushes attached to a rigid carcass has been used for analyzing cornering resistance in Pacejka et al, 1991. Figure 4.6 illustrates the details of this tire brush model, where the bristle deformation is generally a function of both the bristle position along the tire footprint and time.

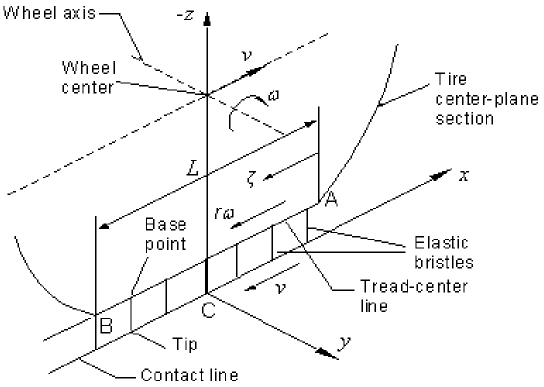

Figure 4.6: Tire brush model (Pacejka et al, 1991)

Two basic versions of tire modeling, lumped modeling and distributed modeling, are shown in Figure 4.7 (Canudas-de-Wit et al, 2003). Lumped modeling only considers a single state of the tire deflection at a given time while distributed modeling discretizes the tire footprint and considers the variation in the deflection along the footprint.

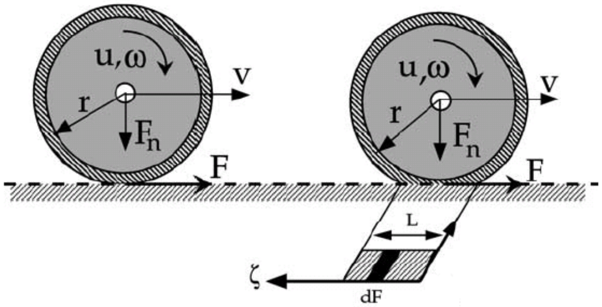

Figure 4.7: One-wheel system with lumped friction (left) and distributed friction (right)

### 4.3.3 Application of the LuGre Model to Longitudinal Tire Dynamics

The distributed version of the LuGre model incorporates both time and space variations of the bristle deflection. The simplified lumped model does not consider any variation along the tire footprint. Therefore, it has the same model equations as Eqs. (8) with the exception of having a *z*, that is only dependent on time, in place of an average bristle deflection $\bar{z}$.

Considering the behavior of a tire moving along the pavement as shown in Figure 4.6, Figure 4.8 shows the movement of an element of the tire footprint during a $\delta t$ time interval from $t$ to $t+\delta t$.

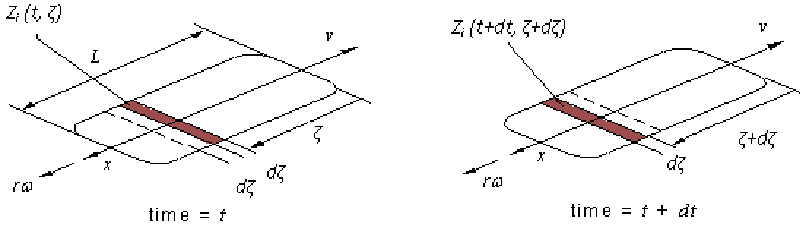

Figure 4.8: Time dependent position of an element on the tire footprint

The distributed model (Canudas-de-Wit et al, 2003) considers the variation of bristle deformation, $z$ with time $t$ and position along the tire footprint length $\zeta$ (Figure 4.8). However, the distributed model developed in Canudas-de-Wit et al, 1999 has a significant deficiency as discussed in Deur, 2001. That is, the standard derivative $\frac{dz}{dt}$, which is used to multiply the bristle damping coefficient $\sigma_1$, damps the tire force oscillations both in time as well as in space. This has been modified in the analysis presented in Canudas-de-Wit et al, 2003. The formulation presented here gives equations to estimate $\mu$, whereas the focus in Canudas-de-Wit et al, 2003 is more toward providing equations for the frictional force developed at the interface.

The footprint element shown in Figure 4.8 moves backwards along the pavement with the rotation of the tire at $r|\omega|$ velocity. Therefore,

$$z = z(\zeta, t) \tag{13a}$$

$$dz(\zeta, t) = \frac{\partial z(\zeta, t)}{\partial \zeta} d\zeta + \frac{\partial z(\zeta, t)}{\partial t} dt \tag{13b}$$

$$\frac{d\zeta}{dt} = r|\omega| \tag{13c}$$

Eliminating $dz/dt$ from the modified Eq. (8a) for the lumped model, and using Eqs. (13) produces the partial differential equation governing the bristle deformation as,

$$\frac{\partial z(\zeta, t)}{\partial t} = v_r - \frac{\sigma_0 |v_r|}{g(v_r)} z(\zeta, t) - r|\omega| \frac{\partial z(\zeta, t)}{\partial \zeta} \tag{14}$$

For a specific problem, the solution to Eq. (14) can be found using appropriate time and space boundary conditions. As the tire footprint conditions are assumed to be invariant in the lateral direction, analysis is limited to the longitudinal derivation. Assuming a unit width for the tire footprint, the longitudinal horizontal frictional force, $F_s$ can be related to the normal force, $F_n$ by,

$$F_s = \int_0^L f_s(\zeta) d\zeta \tag{15a}$$

Using Eq. (8b),

$$F_s = \int_0^L \left( \sigma_0 z(\zeta, t) + \sigma_1 \frac{\partial z}{\partial t} + \sigma_2 v_r \right) f_n(\zeta) d\zeta \tag{15b}$$

And,

$$\mathrm{sgn}(v_r).\mu F_n. = \mathrm{sgn}(v_r).\mu\int_0^L f_n(\zeta)d\zeta \tag{15c}$$

Where, $f_n(\zeta)$ is the normal force per unit length at the position $\zeta$ on the tire footprint and $L$ is the length of the tire footprint. In the LuGre tire model, $g(v_r)$ given in Canudas-de-Wit et al, 2003 and Deur, 2001, have a slight difference having Stribeck exponent as a parameter ($\alpha$) despite the constant value of 2 in Eq. (9a). However, in Canudas-de-Wit et al, 1999, a different constant exponent of 0.5 was used. $\sigma_0$ was dropped from the equation, and the equation for *z* (Eq. 8a) was adjusted by multiplying the $z$ term by $\sigma_0$.

$$g(v_r) = \mu_c + (\mu_s - \mu_c)e^{-\left|\frac{v_r}{v_s}\right|^{\alpha}} \tag{9b}$$

$$\frac{d\bar{z}}{dt} = v_r - \frac{sgn(v_r)v_r\sigma_0}{g(v_r)}\bar{z} \tag{8d}$$

Assuming a suitable normal force distribution (Pottinger, 1982) over the tire footprint (e.g. a constant or linearly varying), the apparent coefficient of friction $\mu$ can be determined. Under unsteady conditions, $\mu$ is a function of time, *t*, reducing Eq. (14) to,

$$\frac{\partial z(\zeta,t)}{\partial t} = v_r - \frac{\sigma_0|v_r|}{g(v_r)}z(\zeta,t) - r|\omega|\frac{\partial z(\zeta,t)}{\partial\zeta} = 0 \tag{16}$$

Since the bristles that are not in contact with the pavement are not deflected, the following boundary condition can be assumed for all times,

$$z(0,t)=0 \tag{17}$$

Then the solution to Eq. (16) becomes,

$$z(\zeta)=\operatorname{sgn}(v_r)\frac{g(v_r)}{\sigma_0}\left(1-e^{-\zeta/C}\right) \tag{18a}$$

Where,

$$C=-\left|\frac{v_r}{\omega r}\right|\frac{g(v_r)}{\sigma_0} \tag{18b}$$

By substituting for *z* in Eq. (15b), with $\partial z/\partial t=0$,

$$F_s=\int_0^L\left(\sigma_0 z(\zeta)+\sigma_2 v_r\right)f_n(\zeta)d\zeta \tag{18c}$$

Meanwhile, from Eqs. (15a) and (15c) one can obtain,

$$\mu=\frac{\operatorname{sgn}(v_r)F_s}{\int_0^L f_n(\zeta)d\zeta} \tag{18d}$$

Finally, $\mu$ is calculated using Eqs. (18c) and (18d), assuming a suitable distribution of normal force along the footprint. A more realistic force distribution on a tire footprint of an accelerating tire is as shown in Figure 4.9 (Canudas-de-Wit et al, 2003 and Moore, 1975).

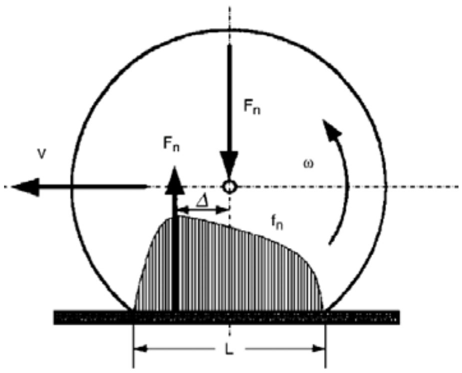

Figure 4.9: Typical normal force distribution on the tire footprint of an accelerating tire

In Canudas-de-Wit et al, 2003, simplified normal force distributions (Eq. 19a) such as a uniform distribution are used to begin with.

$$f_n(\zeta) = \frac{F_n}{L} \tag{19a}$$

Then, the equation for $\mu$ can be expressed as,

$$\mu(v_r) = \mathrm{sgn}(v_r).g(v_r)\left\{1 - \frac{C}{L}\left(1 - e^{-\frac{L}{C}}\right)\right\} + \sigma_2 v_r \tag{19b}$$

Since, realistically the normal force at the footprint boundaries must be zero as shown in Figure 4.9, a distribution combining sinusoidal and exponential shapes would suffice.

An average lumped model, which simplifies this analysis while capturing the effects of bristle position, has also been derived by averaging the bristle deformation along the tire footprint (Canudas-de-Wit et al, 1999, Deur, 2001 and Canudas-de-Wit, et al, 2003). In the latter model, a mean friction state $\bar{z}$ is defined as follows.

$$\bar{z}(t) = \frac{1}{F_n}\int_0^L z(\zeta, t) \times f_n(\zeta)\, d\zeta \tag{20a}$$

It follows that,

$$\dot{\bar{z}}(t) = \frac{1}{F_n}\int_0^L \frac{\partial z(\zeta, t)}{\partial t} \times f_n(\zeta)\, d\zeta \tag{20b}$$

Then, using Eq. (14), mathematical manipulation of the LuGre equations results in

$$\frac{\partial \bar{z}}{\partial t} = v_r - \frac{\sigma_0 |v_r|}{g(v_r)}\bar{z} - K(t)|r\omega|\bar{z} \tag{21a}$$

And,

$$\operatorname{sgn}(v_r).\bar{\mu}(t) = \sigma_0 \bar{z}(t) + \sigma_1 \frac{\partial \bar{z}(t)}{\partial t} + \sigma_2 v_r \tag{21b}$$

Where,

$$K(t) = \frac{1}{F_n \bar{z}(t)}\left\{ \left[ z(\zeta, t) f_n(\zeta) \right]_0^L - \int_0^L z(\zeta, t) \frac{\partial f_n(\zeta)}{\partial \zeta} d\zeta \right\} \tag{21c}$$

The expression *K(t)* captures the distributed nature of the model expressed by Eqs. (14) and (15) in terms of its integral term, while the term $\left[ z(\zeta, t) f_n(\zeta) \right]_0^L$ reflects the boundary conditions. For zero boundary conditions,

$$K(t) = -\frac{\int_0^L z(\zeta,t)\frac{\partial f_n(\zeta)}{\partial \zeta}d\zeta}{\int_0^L z(\zeta,t)\times f_n(\zeta)d\zeta} \tag{22}$$

Based on Eq. (22), $K(t)$ can be estimated for different normal force distributions. Deur, 2001 and Canudas-de-Wit et al, 2003 show how expressions for $K(t)$ are derived with reasonable assumptions and approximations. By separating the effects of the two variables in *z* (Eq. 23), the time dependence of *z* is first eliminated from Eq. (22).

$$z(\zeta,t) = \psi(\zeta).\theta(t) \tag{23}$$

Then, for different combinations of $f_n(\zeta)$ and $\psi(\zeta)$, *K* can be estimated. Some combinations and the corresponding expressions for *K* are given in Table 4.1 (Canudas-de-Wit et al 2003).

Deur, 2001 makes an approximation for $K_0(t)$ by choosing steady-state solutions of the average lumped model and the distributed model resulting in the same frictional force. This yields,

$$K_0(t) = K_0(C) = \frac{1-e^{-L/C}}{1-\frac{C}{L}\left(1-e^{-L/C}\right)} \tag{24}$$

Furthermore, Deur, 2001 shows that 0 < $K_0(t)$ < 2 for all $t \geq 0$.

Selection of a constant value for $K_0$ was suggested in Deur, 2001 significantly affecting in the steady-state solutions of distributed and average lumped models. The steady-state solutions with constant and time varying $K_0$ are compared with the Magic formula (Eq. 11), and excellent matching has been shown in Canudas-de-Wit et al, 2003.

Table 4.1: *K* expressions with different approximations and assumptions

| $f_n(\zeta)$ distribution | Assumption for $\psi(\zeta)$ | Expression for *K* | Notes |
|---|---|---|---|
| $f_n(\zeta)=\frac{F_n}{L}$ | $\psi(\zeta)=\zeta$ | $K=\frac{2}{L}$ | - $\psi(0)=0$ |
| | $\psi(\zeta)=\zeta^{0.5}$ | $K=\frac{7}{6L}$ | - rate of increase of deflection is decreasing with ζ |
| | $\psi(\zeta)=b.sat(\zeta/b)$<br>$0<b<1$ | $K=\frac{2b(3-2b)}{L(b^3-2b^2+2)}$ | - tire footprint is divided into two parts; adhesive and sliding regions<br>- *b* determines the transition from adhesion to sliding |
| $f_n(\zeta)=e^{-\lambda(\zeta/L)}f_{n0}$ | See Notes (column IV) | $K=\frac{\lambda}{L}$<br>(for large $\lambda$) | - $f_n$ is not zero at boundaries<br>- $\psi(\zeta)$ does not appear<br>- variable separable assumption is not made in this case<br>- $\lambda>0$ |
| $f_n(\zeta)=e^{-\lambda(\zeta/L)}f_{n0}$ | See Notes (column IV) | $K=\frac{K_0(t)}{L}$ | - $\lambda=0$, $f_n(\zeta)$ becomes uniform<br>- $f_{n0}=\frac{F_n}{L}$<br>- $z(L,t)\approx K_0(t).\bar{z}$ |

### 4.3.4 Experimental Validation of the Model

Use of constant $K_0$ versus time varying $K_0$ has not made considerable difference in the experimental validation of the model. However, the experimentation presented in Canudas-de-Wit et al, 2003 has a major restriction, in that, the slip and speed could not be controlled independently. Nevertheless, the model shows excellent matching with the experimental results for these limited data.

Figure 4.10 (Canudas-de-Wit et al, 2003) demonstrates the matching of the friction values predicted by the LuGre steady-state average lumped model to test data collected in an experiment in which both slip and speed are varied. First, the steady-state equations have been applied using the mean speed for one test, and model parameters (except the dynamic damping parameter $\sigma_1$) have been estimated by solving the nonlinear least-squares problem using MATLAB.

Then, using the time history of the same data, $\sigma_1$ has been estimated. Figure 4.11 shows the comparison of the predictions with three sets of experimental data using constant $K_0$ values. Comparisons are shown in Figure 4.12 for the same tests with time varying $K_0$. According to the above results, the improvement in the accuracy of modeling achieved by using varying $K_0$ is insignificant, and a constant $K_0$ would be adequate to capture the frictional behavior.

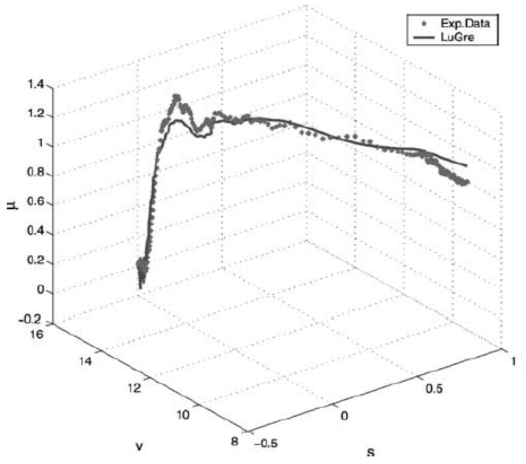

Figure 4.10: Comparison of experimental data with steady-state average lumped model predictions (Canudas-de-Wit et al, 2003)

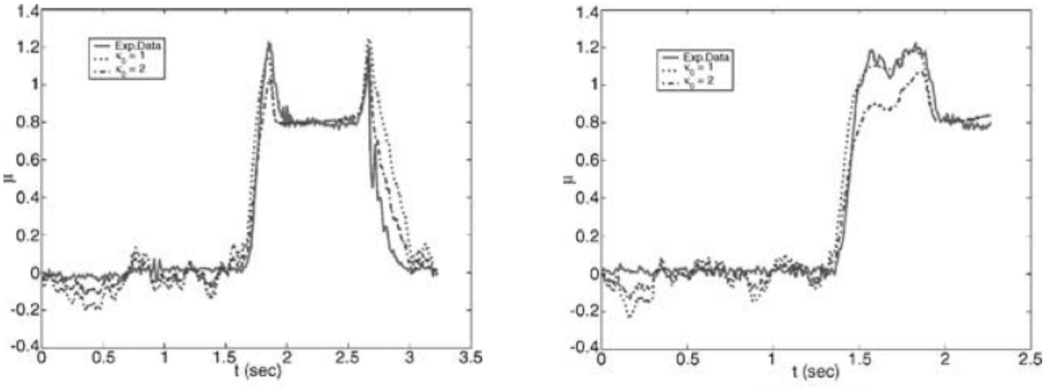

(a) Braking #1

(b) Braking #2

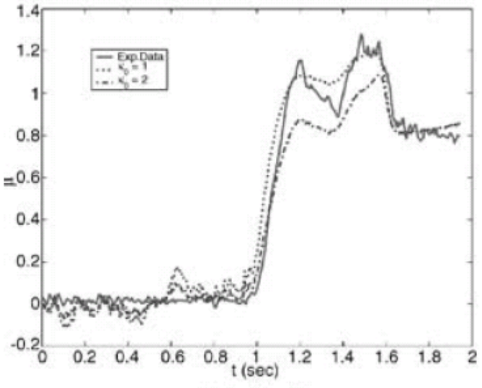

(c) Braking #3

Figure 4.11: Dynamic model predictions with $K_0$ kept constant (Canudas-de-Wit et al, 2003)

The model parameters for the plots in Figures 4.10, 4.11 and 4.12 were $\sigma_0$ = 178 m$^{-1}$, $\sigma_1$ = 1 sm$^{-1}$, $\sigma_2$ = 0 sm$^{-1}$, $\mu_c$ = 0.8, $\mu_s$ = 1.5, $v_s$ = 5.5 ms$^{-1}$ and $\alpha$ = 2.

Figures 4.11 and 4.12 show the validity of this model for tire/pavement friction applications. Therefore, along with its physically significant parameters, the selection of the LuGre model over the other friction models for the solution of the pavement friction measurement problem is justified.

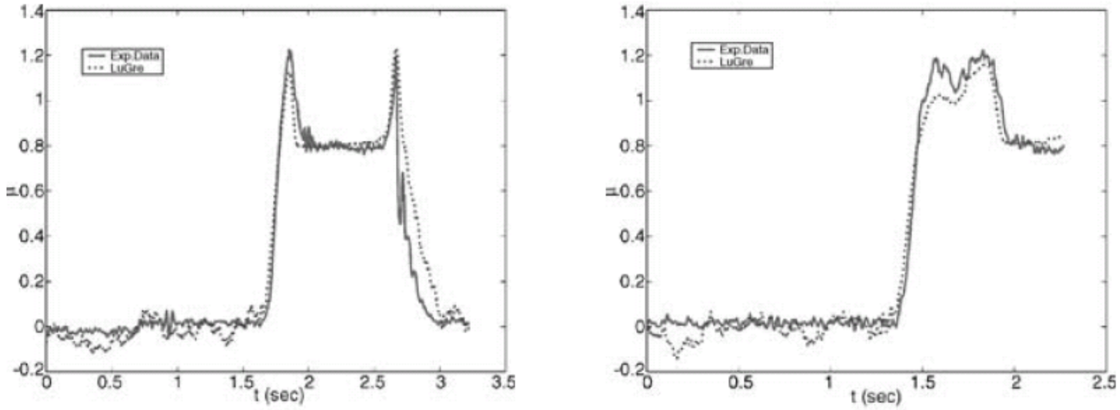

(a) Braking #1

(b) Braking #2

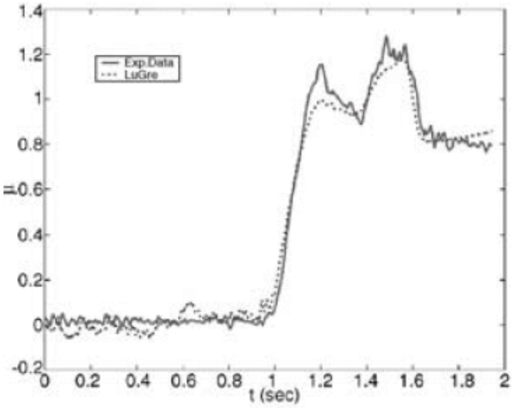

(c) Braking #3

Figure 4.12: Dynamic model predictions with varied $K_0$ (Canudas-de-Wit et al, 2003)

## CHAPTER 5

# VALIDATION OF LUGRE TIRE MODEL FOR MODELING TIRE/PAVEMENT FRICTION MEASUREMENTS

The LuGre model was identified as an analytical model that had the potential to meet the objectives of the research project. Then, to investigate the applicability of the model to the specific project tasks, the PFMDs had to be modeled using the LuGre model. The LWST and the RFT were the two main PFMDs used for the analyses carried out in this research. Most of the United States' Departments of Transportation (DOT) and many international transportation agencies use these devices for measuring runway and highway pavement friction.

Application of the LuGre friction model to the above mentioned devices was achieved with satisfactory validation by continuing the initial work published in Seneviratne et al, 2009. Later, the data from the Wallops 2008 workshop were analyzed to further validate the capability of the model to characterize the friction of different pavements. After the preliminary validation of the model, it was compared with the currently used model for PFMD harmonization. Then, the physical significance of the model's parameters and its accuracy of predicting tire/pavement friction were studied in detail using carefully controlled friction measurements collected by the LWST. The dynamic version of the LuGre model was then employed to study its capability to model real-world dynamic friction data. The LWST is the main test device used in this validation, because it provides sufficiently detailed data that facilitates the calibration of the LuGre model, both steady-state and dynamic. RFT data were also analyzed to understand the limitations of not having the slip data.

### 5.1 Interpretation of LWST and RFT Measurements with the LuGre Tire Model

Eqs. (21a) and (21b) are the average lumped longitudinal LuGre tire model equations and they can be written as follows to represent the dynamic data from the LWST or data from any other device that collects dynamic tire/pavement friction data of similar nature. Function $g$ is given by Eq. (9b).

$$\bar{\mu}(t) = \sigma_0 \bar{z} + \sigma_1 \frac{\partial \bar{z}}{\partial t} + \sigma_2 v_r \tag{25a}$$

$$\frac{\partial \bar{z}}{\partial t} = v_r - \frac{\sigma_0 v_r}{g(v_r)} \bar{z} - \frac{K_0}{L}(v - v_r)\bar{z} \tag{25b}$$

For steady-state braking, $\bar{\mu}$ can be derived from Eqs. (25) as follows.

$$\bar{\mu} = \frac{\sigma_0 v_r}{\left[\frac{\sigma_0 v_r}{g(v_r)} + \frac{K_0}{L}(v - v_r)\right]} + \sigma_2 v_r \tag{26a}$$

$$\bar{\mu}.\mathrm{sgn}(v_r) = \sigma_0 \bar{z}(t) + \sigma_2 v_r \tag{26b}$$

The measuring arrangement in the RFT controls the slip of the test wheel to be a constant value ($s = s_{RFT}$) using a hydraulic mechanism. $s_{RFT}$ can be a constant value between 0.10 and 0.15 for a given RFT device, and the most commonly used value is 0.13. The average lumped model equations for an RFT are the same as those for an LWST (Eqs. 26) with $v_r$ being equal to $v.s_{RFT}$. Therefore, in Eqs. (26), $v_r = v$ for LWST steady-state data measured at a slip ratio of 1, and $v_r = v \times 0.13$ for RFT data.

## 5.2 Preliminary Calibration of the LuGre Model

In the preliminary calibration presented in Seneviratne et al, 2009, the LuGre model was calibrated using LWST and DFT data collected from a field test performed on a 300 ft pavement stretch on McKinley Drive, Tampa, Florida. In the validation presented in this section, the LWST remained as the major test device, and the RFT data were analyzed considering the long term goal of harmonizing different PFMDs. Due to the significant differences in its measurement approach and the related LuGre model equations (Seneviratne et al, 2009), DFT was not considered in the harmonization.

### 5.2.1 Testing Procedure for Preliminary Calibration

For validation of the model, data from varied speed and slip conditions are needed. All of the PFMDs available for this research project were fixed-slip devices, thus limiting the accuracy and versatility of the data fitting procedure adopted to calibrate the LuGre model parameters. The only possible deviation that could be achieved with respect to traditional test procedures was in terms of speed. However, this problem could be solved to some extent using the traditionally unused portion of the data collected by the LWST during its braking phase. Therefore, the LWST was used to collect test data required to validate the LuGre tire model for pavement friction testing applications.

LWST data collection starts at a designated lead time before the brakes are applied to bring the wheel from its free rolling state to a locked state and continues until it returns to the free rolling state. This testing protocol provides means of accessing some important data at continuously varied slip, while braking and releasing of brakes. These data include the transient data for $s \in [-1,0]$ at the speed at which the test is conducted.

Such data collected at different constant speeds were used to calibrate the model and obtain a 3-D prediction of friction with slip and speed. Simultaneous variation of both slip and speed, which can provide dynamic data with respect to both variables, is not feasible using a standard LWST, because the device and the test control software are not designed to accommodate such extreme conditions.

Velocity control for testing is achieved by the cruise control system of the test vehicle. The cruise control system is sufficient for the main purpose of the device, which is to measure the friction at $s = 1$, where the force variations are minimal provided the pavement conditions are consistent throughout the test. The high rate of velocity change during short term wheel locking can affect the velocity control and as a result, degrade the quality of data collected during braking. The rate of braking can be dropped significantly by reducing the pneumatic pressure applied during braking.

For the preliminary calibration presented in Seneviratne et al, a reasonably level and straight 300 feet long asphalt pavement stretch on the right lane of South Bound McKinley Drive, Tampa, Florida was tested with an ICC LWST using a standard smooth test tire (ASTM E524, 2008). Tests were carried out at 32, 48, 64 and 80 km/h (20, 30, 40 and 50 mph) traveling speeds on a dry sunny day. Four 25 m (75 ft) Sections were demarcated and four repetitions were carried out within each Section at each speed. DFT and CTM tests were also conducted along the LWST test path, with one test per Section, in dry weather conditions similar to those prevailed during the LWST tests.

Table 5.1: Summary of test data used for the analysis

| | | **Sec.1** | **Sec.2** | **Sec.3** | **Sec.4** | **Average** |
|---|---|---|---|---|---|---|
| ***CTM Texture*** | ***MPD*** | 0.57 | 0.61 | 0.59 | 0.8 | 0.59 |
| ***DFT Friction*** | $DFT_{20}$ | 0.79 | 0.83 | 0.79 | 0.79 | 0.8 |
| ***IFI Parameters*** | $S_p$ | 65.33 | 68.92 | 67.12 | 85.96 | 67.12 |
| | $F_{60}$ | 0.29 | 0.3 | 0.3 | 0.34 | 0.29 |
| ***LWST Friction*** | ***32 km/h*** | 0.54 | 0.57 | 0.55 | 0.56 | 0.55 |
| | ***48 km/h*** | 0.5 | 0.53 | 0.54 | 0.53 | 0.52 |
| | ***64 km/h*** | 0.48 | 0.49 | 0.51 | 0.48 | 0.49 |
| | ***80 km/h*** | 0.44 | 0.46 | 0.44 | 0.44 | 0.44 |
| ***LWST*** $FR_{60}$ | ***32 km/h*** | 0.35 | 0.37 | 0.38 | 0.40 | 0.37 |
| | ***48 km/h*** | 0.42 | 0.45 | 0.44 | 0.46 | 0.44 |
| | ***64 km/h*** | 0.51 | 0.54 | 0.52 | 0.50 | 0.52 |
| | ***80 km/h*** | 0.6 | 0.59 | 0.62 | 0.56 | 0.59 |

Table 5.1 illustrates the summary of LWST, DFT and CTM test data obtained from McKinley test site according to the standard ASTM practice (ASTM E1960, 2007). The LWST data shown in Table 5.1 are the average $\mu$ values measured during the locked wheel phase ($s$ = 1). It is seen that the test data are consistent for all four Sections, without much variation from each other. The only major deviation is the CTM MPD at the fourth Section, which is much higher than that for the other three Sections. Since this measurement does not represent the typical texture of the tested pavement segment, it was discarded in computing the average MPD and $S_p$. This type of variation in the CTM MPD measurements can occur due to removed gravel particles on local spots of the pavement.

Data from Section 3 in Table 5.1 were used for the analysis presented here, because they represent the average characteristics of the pavement best.

### 5.2.2 Calibration of the LuGre Model Using LWST Data

Data points collected during the braking phase of the LWST test wheel were first considered as independent steady data points, neglecting the actual transient effects. This assumption permitted the use of steady-state LuGre equations for LWST (Eqs. (25)). Table 5.2 shows the LuGre model parameters calibrated using the LWST data.

Table 5.2: LWST parameters from preliminary calibration

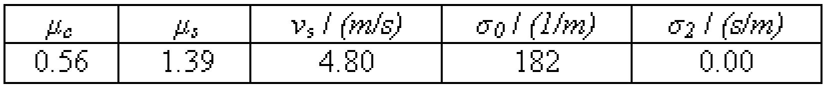

| $\mu_c$ | $\mu_s$ | $v_s$ / (m/s) | $\sigma_0$ / (1/m) | $\sigma_2$ / (s/m) |
|---|---|---|---|---|
| 0.56 | 1.39 | 4.80 | 182 | 0.00 |

The LuGre model parameters for the LWST data presented in Table 5.2 were obtained by optimizing the model equations to fit the observed LWST test data. The *lsqnonlin* function available in MATLAB was used for this purpose. As implied by its name, *lsqnonlin* solves nonlinear the least-squares problems, including data fitting problems. Starting with some initial values and physically acceptable ranges for the model parameters, the least-squares problem was solved, and the optimum parameters were obtained. A MATLAB function (*ode45*) implementing an explicit Runge-Kutta formula was used to solve the differential equations.

Calibrated model parameters in Table 5.1 were used to predict the $\mu$ vs. slip behavior at each test speed. Comparisons of model predicted and observed $\mu$ at each tested speed are shown in Figure 5.1. The average Root Mean Square (RMS) error of $\mu$ for all four tested speeds was 0.10.

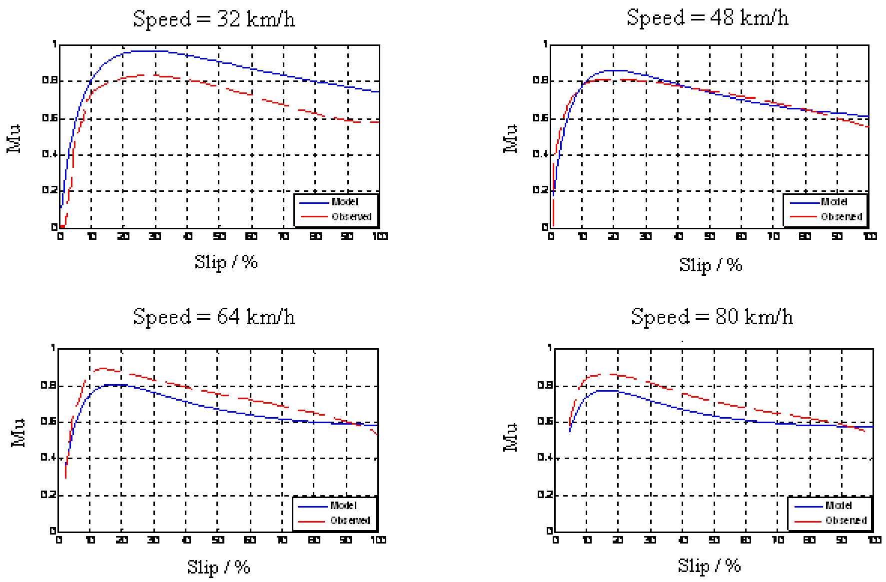

Figure 5.1: Variation of LuGre model predicted vs. observed LWST $\mu$

### 5.2.3 Comparison with the Currently Used Model for PFMD Standardization

The predictions of the LuGre model presented in section 5.2.2 were compared with those from the empirical model currently used in the ASTM standardization procedure for PFMDs. This model, namely, the PIARC friction model (Wambold et al, 1994), which is derived from the PSU friction model (Henry, 1978), has been described in section 2.3.1 of this dissertation. However, neither of the above models can describe the complete 3-D variation of friction with wheel slip and traveling speed alone. In Andresen et al, 1999, a 3-D tire/pavement friction model was derived based on the PSU model and the Rado friction model (Rado, 1993) (Eq. 10).

The PSU-Rado model equation is given as,

$$\mu(v,s) = \mu_0 . e^{-\left(\frac{v}{V_0}\right)} . e^{\frac{-\left(ln\frac{v.s}{S_C}\right)^2}{c^2}} \qquad (27)$$

The PSU component of this model (Eq. 2) is slightly different in the sense that it has speed (*v*), in place of slip speed (*s.v*) in the exponent. However, it is the best approach to take in comparing the currently used model with the LuGre model, which can accommodate both *s* and *v* variations of $\mu$ by default. Figure 5.2 shows the results when the PSU-Rado model is used to model the same data set (Table 5.1) modeled by the LuGre model in Figure 5.1. The same data fitting method used for the LuGre model analysis explained in section 5.2.2 was used with the PSU-Rado model as well.

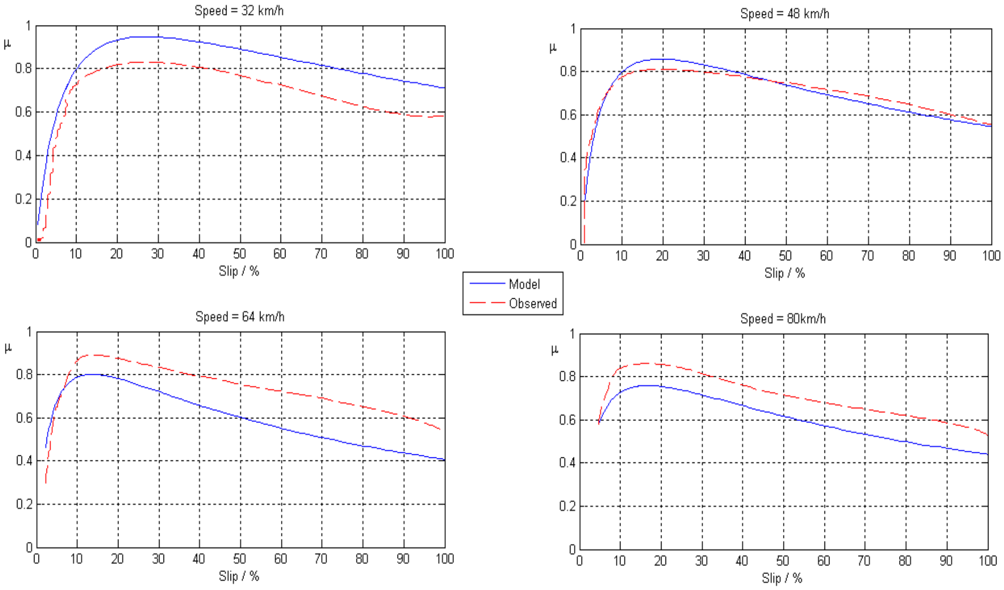

Figure 5.2: Variation of PSU-Rado model predicted vs. observed LWST $\mu$

The predictions of the PSU-Rado model shown in Figure 5.3 have a 20% higher average RMS $\mu$ error (0.12) compared to that of the LuGre model.

The successful preliminary calibration of the LuGre model for the LWST with reasonably accurate predictions suggest that a properly calibrated LuGre model can be used to predict PFMD measurements to a higher accuracy. The relatively higher error coupled with the empirical nature of the PSU-Rado model makes it less appealing than the LuGre model for the intended applications. Furthermore, the LuGre model can be improved further to adapt to specific test conditions demanded by different PFMDs.

## 5.3 Adequacy of the LuGre Tire Model for Characterizing the Friction Level of Pavements

One of the main objectives of this research was to model the deviations in physical properties of different PFMDs to explain the disparities in their friction measurements. Therefore, to validate the model for this purpose, PFMDs that exert different measurement conditions must be considered, and data collected on different types of pavements have to be analyzed as well.

The LuGre model is used to model the tire/pavement frictional behavior affected by tire properties, pavement properties and contaminants (water in the case of standard LWST tests). Although, there are several parameters overlooked in the LuGre model, some of them, such as tire inflation pressure and temperature mainly affect friction by indirectly changing the tire properties. However, the water film thickness between the tire and pavement directly affects the footprint area and the effective load carried by the pavement. Therefore, these parameters that are not taken into account in the model were controlled during the data collection.

The capability of the LuGre tire model to predict the measured friction data, accuracy level of estimated model parameters and their physical impact are presented in this section. The majority of the material presented here was published in Rajapakshe et al, 2010. Estimated model parameters in the LuGre model are tuned to fit measured data using nonlinear least-squares optimization. Then, the degree of fit is determined by using coefficient of determination ($R^2$) and RMS error of predicted $\mu$. The next step in this evaluation procedure is using the model with optimum parameters to predict measurements not used for the parameter optimization. The model accuracy is considered to be high in predicting measurements when the $R^2$ value is high and RMS error for $\mu$ is low. By observing the dispersion of measured data with model predicted $\mu$, systematic errors can be identified. Continuous clustering of measured $\mu$ above or below the predicted $\mu$ suggests that the model is ineffective in capturing certain important physical aspects of the phenomenon (Motulsky et al, 1987).

Variation of the model parameters when tuned with several similar data sets quantifies consistency and singularity of the model parameters. If the optimization algorithm outputs similar values for a certain model parameter with similar data sets, then the model is more reliable for predicting measurements with actual physical meanings of the parameters.

Since the LuGre model parameters have physical significance, the parameters should be checked for misrepresentation. Parameters representing the tire properties should remain same for data collected on different pavement surfaces whereas the other parameters that represent the tire/pavement interface should vary.

### 5.3.1 Collection of Controlled LWST Data for Accurate Calibration of the LuGre Model

First, the friction data collected from LWST on several surfaces at the NASA Wallops Runway Friction Workshop 2008 were used for the analysis. In this workshop, several PFMDs were tested on different pavement surfaces with the goal of harmonizing their measurements. However, the data were found to be inconsistent due to the flooding of pavement surfaces caused by repeated testing by PFMDs and other variations such as inflation pressure and temperature. Since the original LuGre model does not capture the effect of water film thickness, and the actual water film thickness data were unavailable, the initial results from the LuGre model were found to be inconsistent. However, on the grooved surfaces, where the trapped water is allowed to escape from the footprint, the results were found to be relatively consistent. Therefore, data collected from grooved surfaces (Table 5.3) were used for the final analysis. Data measured at four different speeds on each Wallops pavement surface mentioned in Table 5.3 were considered in the analysis.

Table 5.3: Different pavement types available at NASA Wallops flight facility

| Runway Section | Description of pavement type | General $\mu$ trend experienced in the Past |
|---|---|---|
| B | Grooved 25x6x6 mm canvas belt concrete | 0.94 |
| C | Grooved 25x6x6 mm burlap drag-finished concrete | 0.92 |
| F | Grooved 50x6x6 mm small aggregate asphalt | 0.86 |
| G | Grooved 25x6x6 mm small aggregate asphalt | 1.02 |

Since the initial analysis of Wallops data showed some inconsistency, more controlled tests were carried out on a selected pavement Section on Fowler Avenue, Tampa, Florida. The selected pavement on Fowler Avenue has an open-graded friction course (FC-5), which facilitates water drainage from the contact patch. All of the measurements were carried out under similar weather conditions and during the same time period over several days. Furthermore, the order of the test speeds was randomly changed to eliminate systematic errors coming from the variations of tire temperature, ambient temperature and water film thickness. To avoid considerable variations in those parameters, no more than three data sets were taken on the same day.

Figure 5.4 shows plots of the averages and standard deviations of the ten sets of observed $\mu$ at each test speed (in km/h) versus the percentage slip. Data are available at 2% slip intervals, from 2% to 100% slip. Plots of the averages in Figure 5.3 have been made continuous only for ease of visualization of the variation of $\mu$ vs. slip.

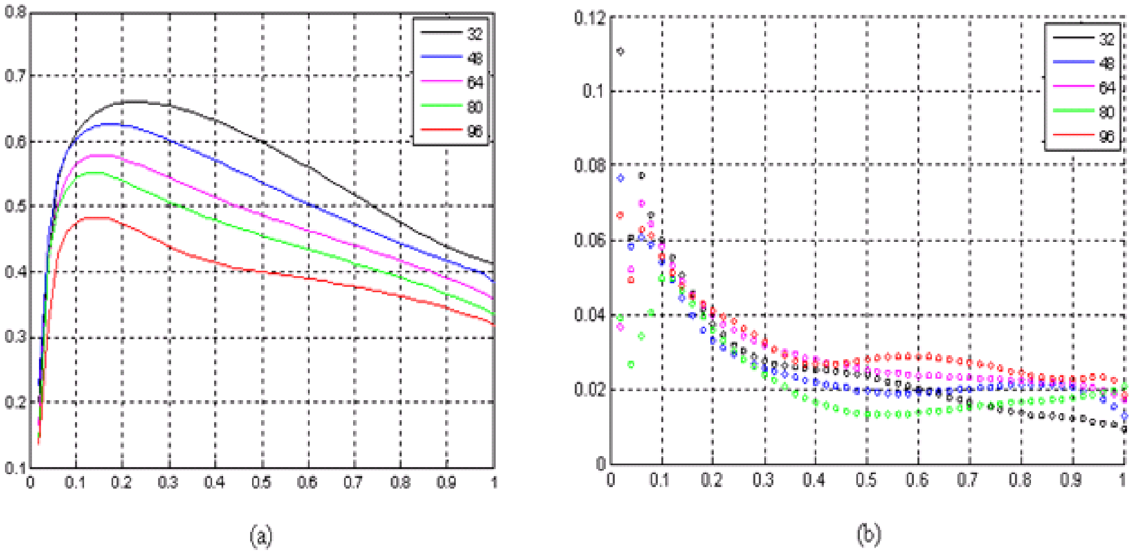

Figure 5.3: Tampa data at five different speeds (a) Average, (b) Standard deviation.

### 5.3.2 Accurate Calibration Using Controlled LWST Data

LWST data from the selected pavement Sections explained in section 5.3.1 were used to calibrate the steady-state LuGre model equations for the LWST (Eqs. 25). First, a steady-state calibration was carried out at each Section separately, as done in the preliminary calibration. Data collected at four different speeds were available. In the initial calibration, three speeds were selected for calibration, and predictions were made for the fourth speed using the calibrated model. This analysis was repeated for all four possible combinations of three speeds. This was performed to verify both the model and the computational procedure. The accuracy of the calibrated model was evaluated based on the average RMS error of model predictions compared to the measurements.

Tuning of all parameters was done initially except for $\alpha = 1$. Based on the results, values of several parameters were fixed as follows. The value for $K_0$ was tuned in all cases close to 2.00 and hence fixed at that value. The viscous parameter, $\sigma_2$, turned out to be 0.0008 s/m for all the cases, and therefore, was kept at that constant value. Table 5.4 contains the detailed optimum parameters after fixing $K_0$ and $\sigma_2$.

Table 5.4: Tuned parameters from initial calibration with Wallops data.

| Runway | Pred Speed (km/h) | Pred Error | Optimum Parameters | | | | Cal Error |
|---|---|---|---|---|---|---|---|
| | | | $\mu_c$ | $\mu_s$ | $v_s$ ( m/s) | $\sigma_0$ ($m^{-1}$) | |
| F | 48 | 0.062 | 0.525 | 1.397 | 6.8 | 157 | 0.063 |
| | 64 | 0.096 | 0.545 | 1.460 | 5.4 | 148 | 0.053 |
| | 80 | 0.055 | 0.550 | 1.464 | 5.8 | 170 | 0.065 |
| | 96 | 0.087 | 0.536 | 1.394 | 6.4 | 183 | 0.055 |
| C | 48 | 0.101 | 0.605 | 1.422 | 6.6 | 184 | 0.049 |
| | 64 | 0.062 | 0.612 | 1.334 | 5.9 | 202 | 0.066 |
| | 80 | 0.042 | 0.615 | 1.371 | 6.1 | 192 | 0.070 |
| | 96 | 0.061 | 0.626 | 1.498 | 4.8 | 179 | 0.066 |
| B | 48 | 0.085 | 0.530 | 1.309 | 10.6 | 245 | 0.053 |
| | 64 | 0.085 | 0.610 | 1.681 | 5.4 | 184 | 0.051 |
| | 80 | 0.048 | 0.632 | 1.651 | 5.2 | 200 | 0.063 |
| | 96 | 0.063 | 0.555 | 1.505 | 7.2 | 218 | 0.059 |
| G | 48 | 0.088 | 0.567 | 1.434 | 9.9 | 241 | 0.039 |
| | 64 | 0.070 | 0.584 | 1.330 | 9.2 | 242 | 0.046 |
| | 80 | 0.031 | 0.604 | 1.427 | 8.2 | 240 | 0.056 |
| | 96 | 0.064 | 0.609 | 1.431 | 7.6 | 228 | 0.051 |

Each parameter in Table 5.4 lies within a unique range. However, variations in parameters of the $g(v_r)$ function are too low among the surfaces, inconsistent within the same surface and do not show any relationship with the actual frictional trend given in Table 5.3. Furthermore, tire stiffness parameter, $\sigma_0$ also has a considerable variation. These are signs of misrepresentation from parameters estimated using the optimization procedure. These adverse effects can be attributed to inconsistencies in data resulting from lower control over the parameters such as water film thickness and temperature.

The more controlled data measured on the Fowler Avenue site (Figure 5.4) were analyzed next, and Table 5.5 shows the estimated parameters. As can be seen, the estimated parameters are far more consistent than the parameters estimated from the Wallops data. However, there is a slight inconsistency in friction prediction for speeds outside of the range of calibration (i.e. predictions at 32 and 96 km/h). Overall, prediction errors are lower for the more controlled data measured at Tampa, than for the Wallops data.

Table 5.5: Tuned parameters from calibration with Tampa data

| Pred Speed / km/h | Pred Error | Optimum Parameters | | | | Cal Error |
|---|---|---|---|---|---|---|
| | | $\mu_c$ | $\mu_s$ | $v_s$ (m/s) | $\sigma_0$ ($m^{-1}$) | |
| 32 | 0.042 | 0.321 | 0.944 | 6.6 | 160 | 0.024 |
| 48 | 0.024 | 0.338 | 0.954 | 5.6 | 164 | 0.028 |
| 64 | 0.026 | 0.336 | 0.976 | 5.4 | 167 | 0.028 |
| 80 | 0.029 | 0.335 | 0.972 | 5.5 | 167 | 0.027 |
| 96 | 0.037 | 0.346 | 0.942 | 5.7 | 186 | 0.025 |

Calibration results for the Tampa data at the prediction speed of 64 km/h are shown in Figure 5.4 (i.e. data at 64 km/h have not been used for estimation of parameters and the estimated parameters have been used with the model to predict observed data at that speed). $R^2$ values and RMS errors (see Figure 5.4 title) in the model-predicted $\mu$ can be used to compare observed and model-predicted $\mu$. Figure 5.6 shows prediction results at 64 km/h with the estimated parameters (given in the row for 64 km/h in Table 5.5).

Although the plots in Figures 5.4 and 5.5 show signs of slight systematic errors, these plots are not suitable for making conclusions about those errors, since the actual observed data have been averaged to obtain the data used for model parameter estimation. To observe any clustering of data around the predicted curves, the observed data should be scattered with model predictions. Figure 5.6 shows two views of a plot consisting of $\mu$ vs. slip and speed variation predicted by the model, and the actual measured data points scattered at each speed. Figure 5.6 (a) shows a view of the plot from a top perspective and Figure 5.6 (b) shows it in a bottom perspective. According to the views in Figure 5.6, the measured data are scattered on both sides of the predicted surface showing no signs of continuous clustering of the measured data. Only exception is at 32 km/h, where measured data points are continuously clustered below the model predicted surface for higher slips (> 60 %).

As the next step, the consistency and singularity of the model parameters were evaluated by using similar data to estimate model parameters. Ten similar sets of data were created by randomly picking values for normal load and friction force at each (speed, slip) data point. These random values were picked from normal distributions with means and standard deviations of measured values at the particular data point. The ten similar sets of data were then used to separately estimate model parameters with the same optimization procedure used with the Tampa average data. Means and standard deviations of those estimated parameters are given in Table 5.6.

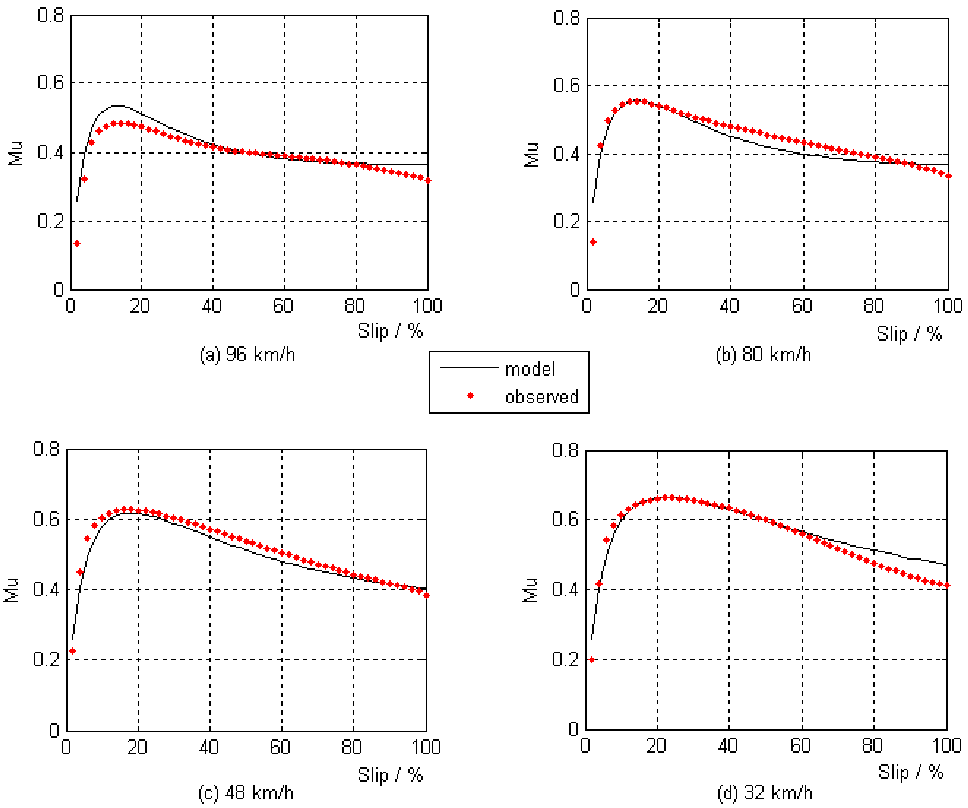

Figure 5.4: Calibration results with observed data from Tampa; (a) Calibration at 96 km/h ($R^2$ = 0.76, RMS Error = 0.029), (b) Calibration at 80 km/h ($R^2$ = 0.86, RMS Error = 0.029), (c) Calibration at 48 km/h ($R^2$ = 0.93, RMS Error = 0.023), (d) Calibration at 32 km/h ($R^2$ = 0.92, RMS Error = 0.028).

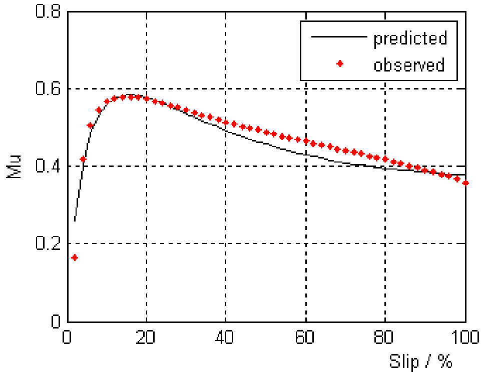

Figure 5.5: Prediction results of Tampa data at 64 km/h with estimated model parameters using observed data at other 4 speeds ($R^2$ = 0.90, RMS Error = 0.025).

Table 5.6: Level of consistency of model parameters estimated using similar measured data.

| Parameter | Mean | Standard Deviation as a % of Mean |
|---|---|---|
| $\mu_c$ | 0.334 | 3.20 |
| $\mu_s$ | 0.957 | 4.40 |
| $v_s$ (m/s) | 5.63 | 10.06 |
| $\sigma_0$ ($m^{-1}$) | 174 | 5.86 |
| RMS Error | | |
| Calibration | 0.043 | 2.85 |
| Prediction | 0.043 | 11.37 |

The $v_s$ and $\sigma_0$ parameters have shown considerably higher variations (standard deviations higher than 5 %) as shown in Table 5.6. Also these two parameters show higher variation in the actual measured data illustrated in Table 5.5. Therefore, it can be concluded that these parameters are more sensitive to variations in measured data, and in some factors which are not adequately explained by the model.

Parameter $v_s$ is a measure of the slip speed ($v_r$) at which the minimum of $g(v_r)$ occurs, and beyond that $v_r$, $g(v_r)$ increases due to the increase in viscous friction force from water. Therefore, the inconsistency in $v_s$ can be partly attributed to neglecting the exact amount of water under the tire. The inconsistency in $\sigma_0$ can be avoided if an exact value for it can be found by some other means. Since $\sigma_0$ represents the stiffness of tire, the best evaluation would be by measurement. However, considering the fact that the same tire was used under the standard conditions for all the tests, a constant value of 180 $m^{-1}$ was assumed for $\sigma_0$ for the remainder of the analysis. This value was selected based on the results from the above analyses and past literature (Canudas-de-Wit et al, 2003).

With $\sigma_0$ fixed at 180 $m^{-1}$, a second stage of calibration was done using the data collected in the Wallops workshop. Table 5.7 shows the results of the calibration.

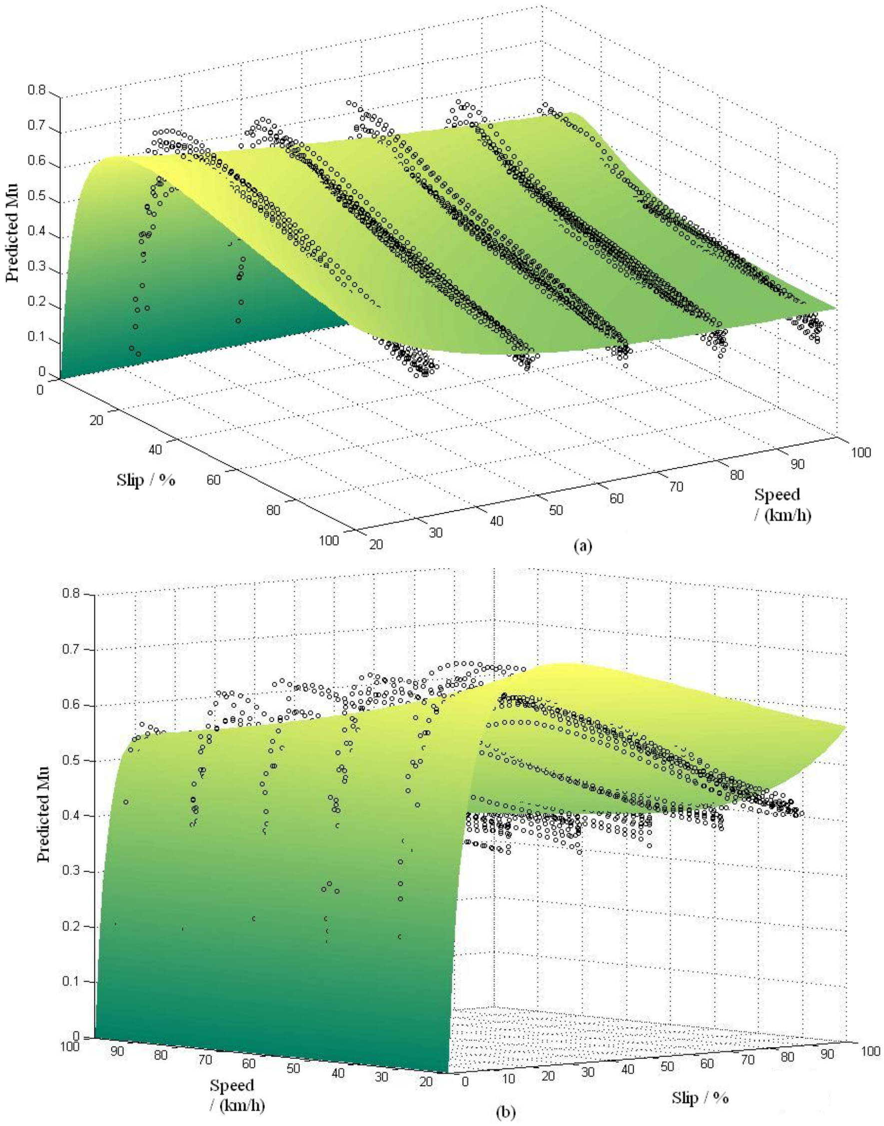

Figure 5.6: Dispersion of measured data around model predicted results (a) view from a top angle, (b) view from a bottom angle.

Parameters $\mu_c$ and $\mu_s$ in Table 5.7 show proportionality with general friction observations on the surfaces. This suggests that, by tuning for parameters, friction can be evaluated in terms of static and Coulomb friction without the effects of other parameters such as tire properties. However, a single parameter representing the frictional performance of the pavement, which is dependent mainly on the texture of the pavement, cannot be identified according to these results. Furthermore, the accuracy of the selected

$\sigma_0$ value and the consistency of the data are not guaranteed, preventing any strong conclusions regarding real physical significance of the parameters.

Table 5.7: Tuned parameters for LWST from second stage of calibration with constant $\sigma_0$

| Runway Section | LuGre Parameters | | | RMS $\mu$ Error | | General $\mu$ Level Experienced in the Past |
|---|---|---|---|---|---|---|
| | $\mu_c$ | $\mu_s$ | $v_s$ (m/s) | Calibration | Prediction | |
| F | 0.52 | 1.27 | 7.4 | 0.063 | 0.062 | 0.86 |
| C | 0.62 | 1.48 | 5.3 | 0.064 | 0.061 | 0.92 |
| B | 0.61 | 1.8 | 5.2 | 0.061 | 0.059 | 0.94 |
| G | 0.66 | 1.84 | 5.3 | 0.057 | 0.057 | 1.02 |

### 5.3.3 Calibration of Dynamic LuGre Model Equations Using LWST Data

In all of the above analyses, the actual dynamic nature of the data was not considered. Hence the applicability and significance of the results are limited, and the real dynamic capability of the model is not tested. Therefore, the analysis was next extended to include the dynamic parameter $\sigma_1$. Eqs. 25 were used. The value for $\sigma_1$ was found by tuning the parameters, while maintaining $\sigma_0$, obtained by the steady-state calibration, as a constant. This could only be done with data from a single run of the tester because of the dynamics. Table 5.8 shows the details of tuned parameters for four data sets. These data sets were selected from the Wallops data by reviewing and extracting the observed $\mu$ variation with slip during the measurement in order to select a representative data set of typical frictional behavior. In the first column of Table 5.8, the Wallops pavement Section and the speed of the test run in km/h are given.

Table 5.8: Calibration of dynamic LuGre model using LWST data

| Data | $\mu_c$ | $\mu_s$ | $v_s$ / m/s | $\sigma_1$/ m$^{-1}$ | Avg. $\mu$ Error | Compare with |
|---|---|---|---|---|---|---|
| B-80 | 0.518 | 1.592 | 8.26 | 0.501 | 0.038 | 0.041 |
| B-96 | 0.600 | 1.454 | 8.21 | 0.496 | 0.039 | 0.041 |
| G-80 | 0.632 | 1.702 | 6.00 | 0.556 | 0.032 | 0.036 |
| G-96 | 0.637 | 1.959 | 6.06 | 0.505 | 0.040 | 0.043 |

The $\mu$ parameters and $v_s$ have been changed from the values obtained with the steady-state model. The decreased average errors cannot be directly compared with the ones given in Table 5.7, because of the use of data at only one speed. The values given in the last column in Table 5.8 are suitable for this particular comparison only, since they are from a steady-state calibration that includes only the particular set of data. However, the order of magnitude of the $\sigma_1$ values obtained here are not comparable with what is seen in the literature (Canudas-de-Wit, 2003).

## 5.4 Calibration of RFT Data Using the LuGre Model

The other CFME for which raw data was available was the RFT. A calibration procedure similar to that for the LWST also had to be followed for the RFT data. In this fixed-slip device, the conditions are presumed to be steady and it possesses a normal force control mechanism, which restricts very high normal load variations. Although the RFT is meant to be a fixed-slip device the hydraulic method of controlling the slip produces slight variation of slip due to the changes in the forces during a test run. Therefore, not having the tire slip data was a major shortcoming of the RFT data when the LuGre model was calibrated.

The LuGre model parameters were tuned using the RFT data, which resulted in $\mu$ vs. $v$ variations at the constant $s$ value of 0.13 for RFT. As a result, for a particular RFT test conducted at a particular $v$, a constant $\mu$ value is predicted by the model. However, the deviation of measured data from the predicted average value is considerably high because of the slip variation as explained above. This can be expected because the RFT operates in the proximity of the peak slip region (Figure 1.3), and on certain pavements, if the RFT operates on either side of the peak of the $\mu$ vs. $v_r$ curve, a slight variation of $s$ could create a considerable variation in $\mu$. To support this explanation, the effect of a slight change in slip on RFT friction measurement predictions using the LuGre model is shown in Figure 5.7. According to Figure 5.7, the traditional data provided by the RFT are quite insufficient to calibrate the LuGre model accurately. Because of this, calibration of the RFT data was highly inconsistent and the only important observation of the calibration was that the $\sigma_0$ value for the RFT tire (220 $m^{-1}$) is higher than that for the LWST.

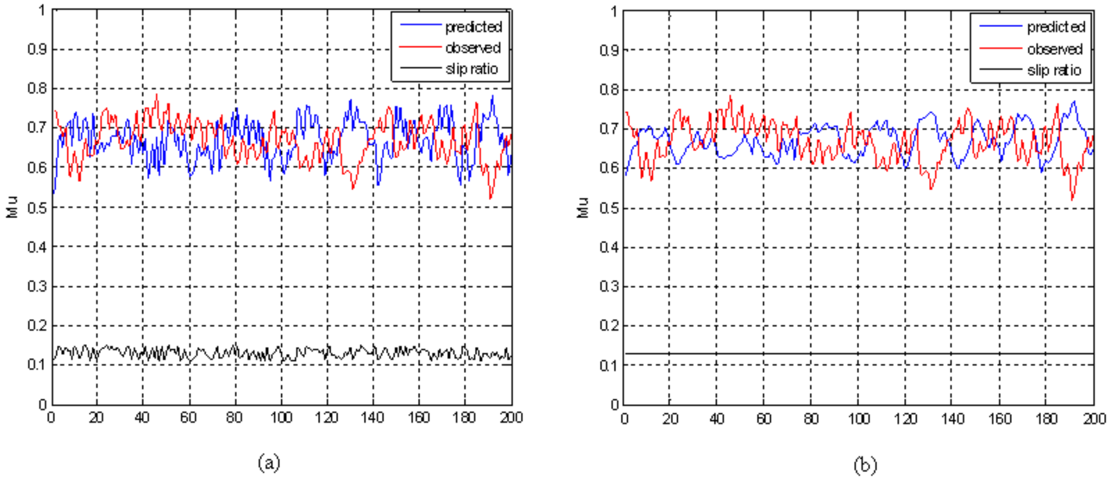

(a)

(b)

Figure 5.7: Effect of a random change of slip on predictions of RFT data by LuGre model random variation of slip 0.11 ~ 0.15 (b) constant slip

## 5.5 Discussion of Validation Results

According to the analysis and findings of this chapter, the steady-state average lumped LuGre tire friction model can be recognized as a potentially useful model to forecast the frictional behavior of the tire/pavement contact based on parameters estimated using measured data from the same tire. The capability of the LuGre model to represent frictional characteristics of different pavements in terms of parameters $\mu_c$ and $\mu_s$ is an important observation from the results with Wallops data. However, the value of the tire parameter $\sigma_0$ must be known beforehand to achieve this using the parameter estimation procedure used in this analysis.

Although the parameters in the LuGre model can be physically interpreted, parameters such as bristle stiffness and damping have not been directly measured. Therefore, the relationships of these parameters to the measurable parameters and properties such as tire stiffness, inflation pressure, loss coefficient of the tire rubber and tire geometry have to be established. These relationships can then be used effectively for model based comparison, condition monitoring and maintenance of PFMDs.

Although the LuGre model shows immense potential for fulfilling the objectives of this research, it requires several improvements to provide more accurate results. The model yields promising results with more controlled data (Tampa data, Table 5.5). However, in general testing conditions (Wallops data, Table 5.4) the accuracy levels of predictions are considerably low, suggesting modifications or improvements to the model to increase its versatility. In this respect, parameters that are overlooked in the model need to be incorporated without affecting the physical nature of the model. Based on the results of the preliminary calibration and validation, the effect of the water film thickness on the pavement should be included in the model. Variation of model parameters during a dynamic test is another concern.

From the results presented in this chapter, it can be concluded that the validation of the LuGre model for modeling runway friction measuring devices has been successful. From the LWST analysis, it is clear that if the data required for the model are provided by the device to be calibrated, the results can be satisfactory. For devices that do not provide such detailed data, special arrangements must be made to collect the data in the required format. For example, slip data for an RFT can be invaluable in accurately calibrating the LuGre model equations. To conduct a comprehensive comparison, it is advisable to use data from several other types of devices that utilize testing mechanisms distinct from those discussed in this dissertation. Variable slip devices are one important example of such devices.

# CHAPTER 6

# SENSITIVITY ANALYSIS OF LUGRE TIRE MODEL

## 6.1 Motivation for Sensitivity Analysis

An analytical approach that forms the basis of PFMD standardization must be able to model tire/pavement friction with physically meaningful and quantifiable parameters. With sufficiently accurate parameter estimation, such an analytical model can be used to understand the deviations between friction measurements made using different PFMDs under different conditions. Moreover, it can lead to physically intuitive modifications in the measurement devices to bring the measurements to an acceptable range. From the point of view of pavement design and management, the use of this type of a model can increase the ability to predict the effects of tire properties, pavement texture or contamination level on the frictional performance of the pavement. The LuGre tire friction model (Canudas-de-Wit et al, 1995, Canudas-de-Wit et al, 1999, Canudas-de-Wit et al, 2003 and Deur, 2001) was validated in chapter 5 for pavement friction testing applications (Rajapakshe et al, 2010 and Seneviratne et al, 2009).

In this chapter, the suitability of the LuGre tire friction model as a foundation for a physically intuitive standardization procedure for pavement friction testing has been studied based on a sensitivity analysis of the model. Global and local sensitivity analysis methods (Saltelli et al, 2000) were used to determine the significance of LuGre model parameters that represent various $\mu$ phenomena analytically. The uncertainty of the model-predicted frictional output produced by the uncertainties of the input parameters has also been studied to determine the reliability of the model. Based on the results of the sensitivity analysis, a demonstrative harmonization between LWST and RFT is presented in chapter 8 as a step toward a potential physically intuitive harmonization procedure.

To perform the global sensitivity analysis, the Design of Experiment (DOE) features available in the MINITAB statistical software package (Mathews, 2005) have been used in this work in combination with the statistical tools available in MATLAB. Both the tasks of the implementation of the LuGre model and the local sensitivity analysis have been carried out using MATLAB. The function, *lsqnonlin* available in MATLAB for solving nonlinear least-squares optimization problems has been used to optimize LuGre model parameters to fit measured PFMD data.

## 6.2 Sensitivity Analysis of the LuGre Tire Model

In any modeling task, an understanding of the uncertainty of the outputs of the model and their sensitivity to the inherent uncertainties of the inputs is invaluable. Thus, a Sensitivity Analysis (SA), which enables identification of the most significant input parameters in the model by quantifying the contribution from different inputs to the model outputs, is an essential aspect of model formulation.

Of the input variables to the dynamic LuGre model given by Eqs. (25) and (9b), the wheel slip must be input as a function of time, representing the variation of driving or braking torque (that is, $s = s(t)$). This is an essential requirement to solve the differential equation (Eq. 25b) for bristle deflection. When using an LWST to measure friction, variation of the braking torque determines the dynamics of the test tire (Rajapakshe et al, 2010 and Seneviratne et al, 2009). The time taken from initial application of brakes on the wheel until it is fully locked is a function of the initial travel speed, brake torque and friction force at the tire/pavement contact. This braking time lies typically within 0.2 – 0.8 seconds in LWST tests. In the SA performed in this work, a fixed time variation was input for *s*, assuming that it corresponds to the variation of torque applied during braking. Figure 6.1 shows a comparison of the selected input *s* with experimental *s* variations experienced by the LWST on two asphalt pavements at different speeds.

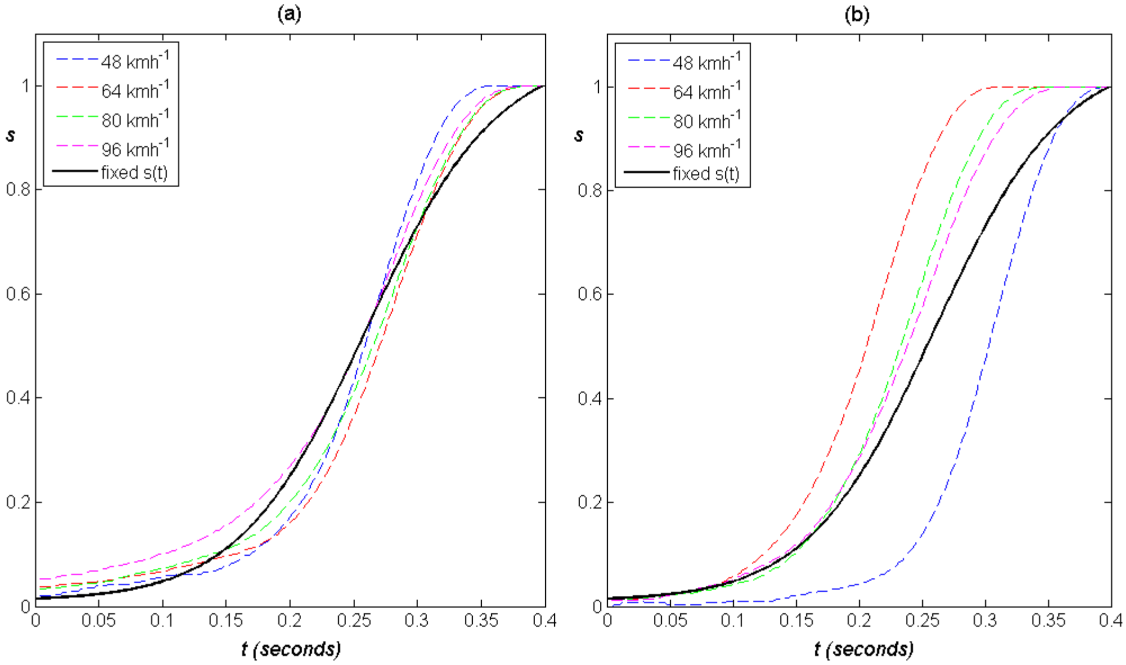

Figure 6.1: Comparison of the fixed *s* used in the SA with actual *s* variations; (a) on Wallops G, (b) on Fowler Avenue

## 6.3 Significance of the Input Parameters

When empirical models are formulated using experimental data, parameter screening methods (SM) are used to eliminate relatively insignificant parameters based on their minor contribution to the model output. This can be performed by Design of

Experiment (DOE) to analyze the model outputs for an exhaustive list of input parameter combinations spanning the entire parameter space. Although parameter screening is irrelevant for an analytical model like the LuGre model, in which all the parameters are physically meaningful; a DOE analysis can be helpful in deciding the impact of each of the input parameters on the model output. If some physical parameters turn out to be relatively less significant, they can be fixed at reasonable values without affecting the integrity of the analytical model.

Several statistical software packages are available to implement DOE, and of them MINITAB was chosen in this work to assist MATLAB in the analysis performed for the LuGre tire model (Mathews, 2005). For a realistic DOE analysis, practical ranges for all the inputs to the model should be known. Results of previous work (Canudas-de-Wit et al, 1999, Canudas-de-Wit et al, 2003, Deur, 2001, Rajapakshe et al, 2010 and Seneviratne et al, 2009) were used to determine these ranges, especially in the cases of $\sigma_0$ and $\sigma_1$ , because the only method used for their estimation was data fitting. The selected ranges for the parameters can be visualized in Figure 6.2. For each parameter, several values were picked within the selected range. The output from the LuGre Eqs. (25), $\bar{\mu}$ was evaluated for all possible combinations of selected parameter values.

In the presentation of DOE results, Figure 6.2 shows the variation of $\mu_{avg}$ at different $s$ levels, plotted against each model parameter. $\mu_{avg}$ is an average of the $\bar{\mu}$ values obtained for a selected parameter value at a given $s$ level when the other parameters were assigned all possible combinations of their respective values. For example, $\mu_{avg}$ value for $\sigma_0$ = 150 m$^{-1}$ at $s$ = 0.25 is an average of 5×5×5×5×3×3×4×3×3 = 200625 $\bar{\mu}$ values which were evaluated using Eqs. (25), and (9b) for the 200625 possible combinations of all the values selected for the other parameters.

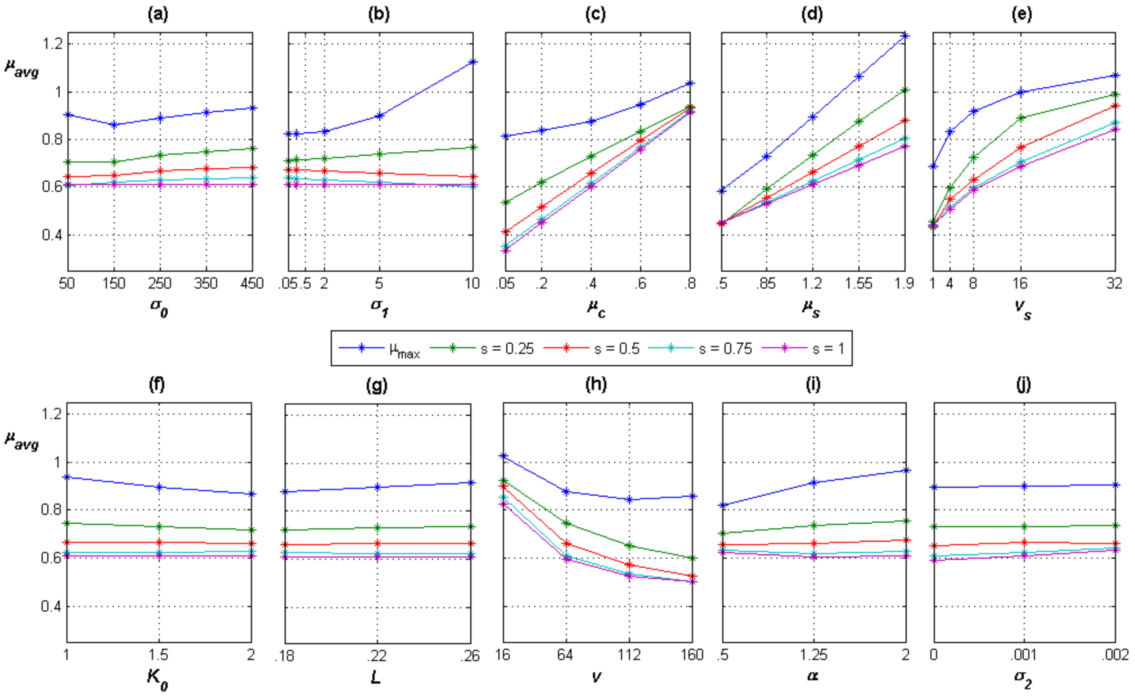

Figure 6.2: Characteristic plots for tire/pavement friction as predicted by LuGre model

The plots in Figure 6.2 characterize $\mu$ with respect to each contributory parameter as predicted by the LuGre tire model. Since the LuGre model has already been identified and validated as a reasonably accurate model for analyzing $\mu$ (Rajapakshe et al, 2010 and Seneviratne et al, 2009), these plots can be considered to exhibit actual $\mu$ characteristics. Hence, these characteristic plots, coupled with the physical significance of the model parameters, enable better visualization and explanation of $\mu$ phenomena. The variations in $\mu$ that are less than 0.01 are considered to be insignificant in this analysis. This threshold suits most of the practical applications of pavement friction such as vehicle control, runway operations and pavement management. As observed in Figure 6.2, all of the parameters in the LuGre tire model are significant in determining the complete tire/pavement frictional behavior. A high significance of $s$ is shown by consistent and considerable disparity among $\mu_{avg}$ curves at different slip levels for all the parameters. All the parameters except $\mu_c$ and $\sigma_2$ are more significant at relatively low $s$ levels, where high $\mu$ values are experienced.

The LuGre characteristic plots for $\mu$ shown in Figure 6.2 can be invaluable in drawing conclusions regarding the $\mu$ behavior, $\mu$ measurements and also in comparison of those measurements obtained using different PFMDs that employ different measurement mechanisms. Several examples of such applications are outlined below.

(i) Provision guidelines for design of measuring mechanisms for PFMDs

The characteristic plots in Figure 6.2 illustrate the $\mu$ behavior with respect to parameters that are known to have major impacts. Therefore, the designer of a new device can use these plots to make important decisions on the basic measurement mechanism that required to build a device that is relatively consistent in its measurements and hence more competitive in the market. As an example, it can be seen from Figures 6.2 (a), (b), (f) and (g), that the impact of parameters $\sigma_0$, $\sigma_1$, $K_0$ and $L$ are relatively insignificant at high $s$ levels, specifically at $s$ = 1. This observation explains the higher consistency of LWST compared to the devices that operate at lower $s$ values.

(ii) Identification and characterization of the effect of water trapped in the contact interface

As the characteristic plots in Figure 6.2 illustrate, the LWST measured $\mu$ at $s$ = 1 is mainly dependent on $\mu_c$, $\mu_s$, $v_s$, $v$ and $s$. The impact of all the other parameters on $\mu$ at $s$ = 1 can be neglected by comparing Figures 6.2 (c), (d), (e) and (h) with the others. Of the above significant parameters, the impact of the vehicle kinematic parameters $v$ and $s$ on $\mu$ is well understood. Furthermore, in the physical scenario, the terms $\mu_c$ and $\mu_s$ represent the frictional properties of the contact surfaces governed by their surface properties, including texture. The parameter ranked next to the surface properties in terms of the contribution to LWST measured $\mu$ is the amount of water trapped in the tire/pavement interface. This argument points to $v_s$ as the major parameter that represents the amount of water trapped at the interface. It must be noted that $v_s$ has been considered as a lubrication-dependent parameter in the original formulation of the LuGre friction model as well (Canudas-de-Wit et al, 1995). According to Figure 6.2 (e), $v_s$ should decrease with an increase in the amount of water trapped at the interface.

Upon identifying $v_s$ as the factor that determines the effects of water on $\mu$, it can be seen from Figure 6.2 (e) that the effects of water are linear at higher slips and nonlinear at lower slips, where higher $\mu$ values are experienced. Therefore, for accurate determination of water effects on $\mu$ using data measured at the locked-wheel condition, a linear regression model can be used. On the other hand, if the measurement device is operated at a lower slip, a nonlinear curve can be fit to the experimental data.

(iii) Development of a systematic and physically intuitive procedure to standardize pavement friction measurement

A procedure of this type can be initiated by categorization of the LuGre model parameters as (i) contact-specific and (ii) device-specific ones. Based on this categorization, the parameters $\mu_c$ and $\mu_s$ are contact-specific, while the parameters $\sigma_0$,

$\sigma_1$, $K_0$ and $L$ are device-specific. On the other hand, the parameter $v_s$, which represents the amount of water trapped in the contact interface depends on pavement texture, tire tread geometry and amount of water sprayed by the wetting system of the PFMD, and hence can be put into either of the two categories.

The contact-specific model parameters determined using the LuGre model with data collected by different devices on the same pavement must be identical, provided that similar contact conditions (tire tread material, nominal water film thickness, temperature, etc.) prevail at the tire/pavement interface during the time of measurement. Significant device-specific parameters for different PFMDs can be identified by generating the LuGre characteristic plots valid for the devices. It should be noted that the plots in Figure 6.2 are valid for most of the devices that use tires for sensing friction. These significant parameters can then be estimated by fitting experimental data or by direct measurement. Knowing the device-specific parameters for a certain device, the contact-specific parameters determined using another device on a given pavement can readily be used to predict the frictional response of the former device on the same pavement. Since the device-specific parameters are known and physically identified, factors affecting these parameters such as the tire construction, inflation pressure, etc. can be adjusted so that different measuring devices would produce comparable friction measurements on the same pavement under similar contact conditions. Furthermore, LuGre model equations with appropriate device-specific parameters can be used to facilitate the prediction of the behavior of a vehicle or an aircraft operating on a pavement on which the pavement-specific parameters have been already determined using a PFMD. Applications of the

LuGre model for standardizing pavement friction measurement are discussed in detail in chapter 8.

## 6.4 Uncertainty of the LuGre Tire Model Output

To evaluate the uncertainty of the LuGre model output due to the uncertainty associated with the input parameters, a global SA has to be performed. A global SA can consist of one or both of the following approaches; (i) varying all the input parameters simultaneously, (ii) allowing each parameter to vary over its entire range (Saltelli et al, 2000). The DOE presented in section 6.2 is a global SA based on both of the above mentioned approaches. A method based solely on the first approach mentioned above allows simultaneous variation of several or all the input parameters within relatively small tolerances. Such a method can evaluate the uncertainty of the model output (Saltelli et al, 2000) at a nominal set of model parameters. In this section, a nominal set of LuGre model parameters was varied simultaneously within the practically encountered ranges of variation to obtain the gross uncertainty of the frictional output. However, the sensitivity obtained by a procedure involving simultaneous variation of multiple model parameters does not represent the isolated effect of any single parameter on the model output. The sensitivity of the model output to individual parameters was obtained using a local SA, and the results are presented in section 6.5.

### 6.4.1 Friction Data Used to Obtain Nominal Model Parameters

Some of the PFMD data collected in the NASA Wallops Runway Friction Workshop (2008) and used for the model validation presented in chapter 5 (Rajapakshe et al, 2010) were used in this analysis for the purpose of determining typical values for the

LuGre parameters. In the Wallops workshop, PFMDs used by all the participating agencies collect friction data along the same wheel path on the pavement Sections that are tested. Both LWST and RFT data collected at the pavement Sections given in Table 6.1 were used for the analyses presented in this chapter. All of the pavements mentioned in Table 6.1 are transversely grooved, with an identical groove geometry of 25 mm × 6 mm × 6 mm (spacing × depth × width). In addition, data collected on Fowler Avenue in Tampa, FL was also used for some of the analyses. The asphalt pavement surface of Fowler Avenue has an open-graded friction course (FC-5) that enhances water drainage.

### 6.4.2 Nominal LuGre Parameters for LWST and RFT

All of the device-dependent LuGre parameters for USF's LWST except $\sigma_1$ are known from the work presented in chapter 5 (Rajapakshe et al, 2010 and Seneviratne et al, 2009). The corresponding parameters for USF's RFT were determined by a separate parameter calibration that is similar to the ones performed for LWST in Rajapakshe et al, 2010 and Seneviratne et al, 2009. However, several assumptions had to be made in determining some of the RFT parameters, because RFT data do not contain the details of $\mu$ variation with respect to variations in slip ratio.

According to the characteristic plot given in Figure 6.2 (b), $\bar{\mu}$ is only sensitive to $\sigma_1$ at low $s$ values, where the maximum $\mu$ is experienced. Moreover, considerable sensitivity of $\bar{\mu}$ to $\sigma_1$ is only shown at relatively high $\sigma_1$ values. The general LuGre model (Eqs. 25 and 9b) was used with the Wallops 2008 data mentioned in section 6.3.2 to evaluate the $\sigma_1$ parameter for the LWST. The other model parameters previously estimated with the steady-state assumption (Rajapakshe et al, 2010) were used as initial estimates in this nonlinear least-squares optimization. Using friction data collected at different speeds (48, 64, 80 and 96 km/h) on the three pavement Sections given in Table 6.1, $\sigma_1$ was consistently tuned to a value around 0.5 s/m, without considerably affecting the calibration accuracies obtained using the steady-state assumption (Rajapakshe et al, 2010). The above result is compatible with the lower sensitivity of the model output to $\sigma_1$ (Figure 6.5 (b)), especially for a relatively low value of 0.5 s/m as characterized in Figure 6.2 (b).

Table 6.1: Details of the NASA Wallops runway pavement Sections and data collected on them

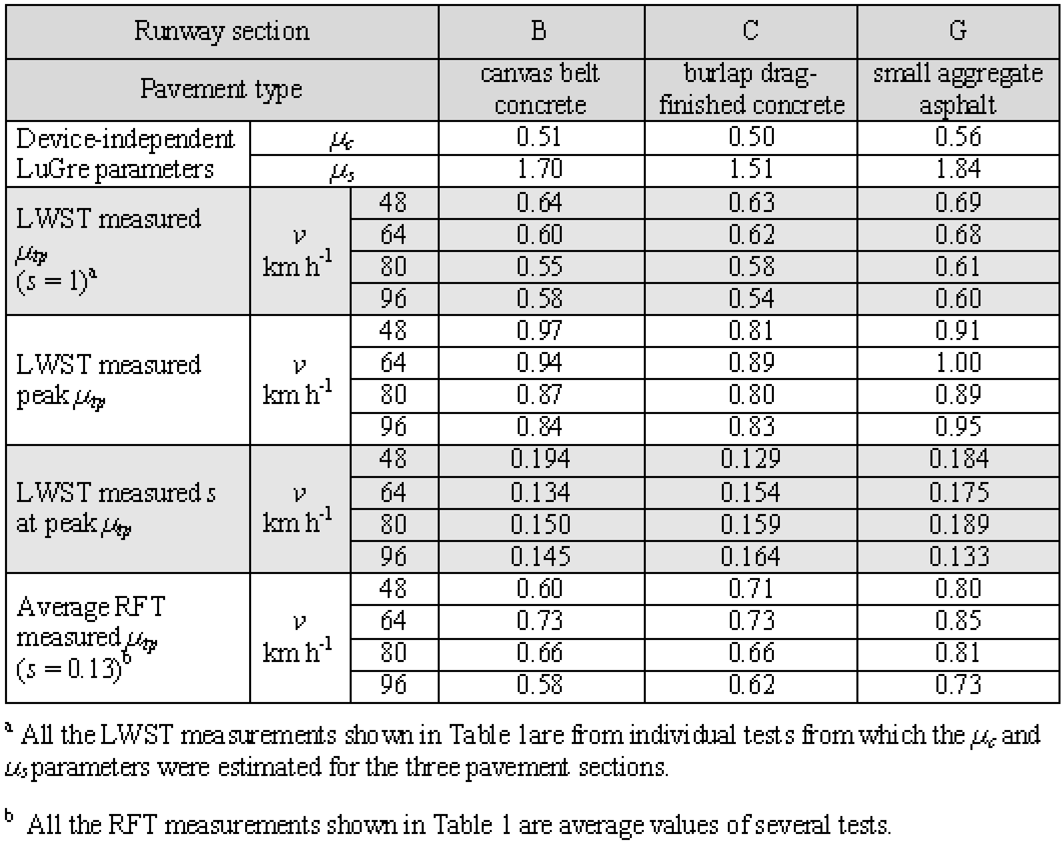

| Runway section | | | B | C | G |
|---|---|---|---|---|---|
| Pavement type | | | canvas belt concrete | burlap drag-finished concrete | small aggregate asphalt |
| Device-independent LuGre parameters | $\mu_c$ | | 0.51 | 0.50 | 0.56 |
| | $\mu_s$ | | 1.70 | 1.51 | 1.84 |
| LWST measured $\mu_{tp}$ $(s = 1)^{a}$ | $v$ km $h^{-1}$ | 48 | 0.64 | 0.63 | 0.69 |
| | | 64 | 0.60 | 0.62 | 0.68 |
| | | 80 | 0.55 | 0.58 | 0.61 |
| | | 96 | 0.58 | 0.54 | 0.60 |
| LWST measured peak $\mu_{tp}$ | $v$ km $h^{-1}$ | 48 | 0.97 | 0.81 | 0.91 |
| | | 64 | 0.94 | 0.89 | 1.00 |
| | | 80 | 0.87 | 0.80 | 0.89 |
| | | 96 | 0.84 | 0.83 | 0.95 |
| LWST measured $s$ at peak $\mu_{tp}$ | $v$ km $h^{-1}$ | 48 | 0.194 | 0.129 | 0.184 |
| | | 64 | 0.134 | 0.154 | 0.175 |
| | | 80 | 0.150 | 0.159 | 0.189 |
| | | 96 | 0.145 | 0.164 | 0.133 |
| Average RFT measured $\mu_{tp}$ $(s = 0.13)^{b}$ | $v$ km $h^{-1}$ | 48 | 0.60 | 0.71 | 0.80 |
| | | 64 | 0.73 | 0.73 | 0.85 |
| | | 80 | 0.66 | 0.66 | 0.81 |
| | | 96 | 0.58 | 0.62 | 0.73 |

[a] All the LWST measurements shown in Table 1are from individual tests from which the $\mu_c$ and $\mu_s$ parameters were estimated for the three pavement sections.

[b] All the RFT measurements shown in Table 1 are average values of several tests.

RFT friction data are collected under steady-state conditions, and therefore cannot be used to estimate $\sigma_1$ by fitting to the dynamic LuGre equations. However, the $\sigma_1$ value for an RFT can be assumed to be lower than that for an LWST (0.5 s/m) due to the higher inflation pressure and smaller size of the RFT tire (Table 6.2). Therefore, considering the relatively insignificant impact of lower $\sigma_1$ values on $\bar{\mu}$ (Figure 6.2 (b)), a value of 0.25 s/m was assumed for $\sigma_1$ of the RFT. The parameter $L$ was directly measured for the two devices, and $K_0$ was kept constant at 2 (Rajapakshe et al, 2010). Table 6.2 presents some important physical characteristics, and the device-specific LuGre parameters for LWST and RFT tires.

Table 6.2: LWST and RFT test tire characteristics and their corresponding LuGre parameters

| Tire | Outer diameter | Tread width (width of the footprint) | Standard inflation pressure | $\sigma_0$ | $\sigma_1$ | $L$ |
|---|---|---|---|---|---|---|
| Unit | m | m | k Pa (psi) | $m^{-1}$ | $s\ m^{-1}$ | m |
| LWST (ASTM E524 [12]) | 0.703 | 0.149 | 165.5 (24) | 180 | 0.5 | 0.21 |
| RFT (ASTM E1551) [13] | 0.417 | 0.061 | 206.8 (30) | 220 | 0.25 | 0.10 |

### 6.4.2.1 Determination of $v_s$ Parameter for LWST and RFT

As explained in section 6.2, the parameter $v_s$ is dependent on both the drainage properties governed by pavement texture and tire tread pattern, and the level of self-wetting of the PFMD. The test tires used in LWST and RFT have smooth treads (ASTM E1551, 2008 and ASTM E524, 2008) to facilitate characterizing the isolated effects of pavement texture on measured $\mu$. According to the current ASTM standards (ASTM E1911, 2009, ASTM E2340, 2006 and ASTM E274, 2006) the water flow from the self-wetting system of a PFMD is controlled to provide a specific nominal water film thickness at all traveling speeds. A perfectly smooth contact interface is assumed in defining this nominal water film thickness. The intent of such specifications is to maintain similar water effects in different PFMDs, so that their measurements are comparable. For the LWST, the standard nominal water film thickness is 0.56 mm (ASTM E274, 2006). However, ASTM does not define a specific nominal water film thickness for fixed-slip PFMDs (ASTM E2340, 2006), which is understandable because of the variation allowed in the slip ratio. The manufacturer of the RFT owned by USF has selected the nominal water film thickness for the device to be 1 mm. However, the differences in the properties of the test tires used in the two devices (Table 6.2) affect the drainage of water from the tire/pavement contact interface differently. The relatively higher inflation pressure and footprint aspect ratio (length/width) of the RFT tire facilitate drainage of water from the contact interface, and compensate for the higher amount of water supplied by its self-wetting system. Therefore, the increase in nominal water film thickness for the RFT is intuitive in terms of the need for maintaining consistent water effects compared to the LWST, which is an older and more widely used PFMD. Hence, considering the similar drainage properties of the pavements used in the analysis, the parameter $v_s$ has been assumed to be equal for the LWST and the RFT. In this section, a numerical justification for the above assumption is provided using already available knowledge on the hydroplaning potential of tires on wet pavements. If the effects of water in LWST and RFT are similar and the combined effects of all the other contributory factors of hydroplaning are the same, the hydroplaning speeds for the two tires should be equal.

Hydroplaning or aquaplaning has been subjected to extensive study for a period of more than over 50 years. The NASA hydroplaning equation (Eq. 28) (Dreher et al, 1963) is one widely used outcome of the previous research in hydroplaning. It predicts the critical speed for hydroplaning, $v_c$ , of a tire having an inflation pressure of $p$. The constant $K$ in Eq. (28) has to be empirically evaluated for the conditions at the tire/pavement contact interface. Based on an understanding of the mechanisms of hydroplaning, the constant $K$ has been expanded as in Eq. (28) (van Es G. W. H., 2001). $L$ and $W$ in Eq. (28) are the length and width of the tire footprint, respectively. The remaining constant $k$, represents the effects of all the other contributory factors including pavement texture, tire tread pattern and the amount of water present at the contact interface.

$$v_c = K\sqrt{p} \tag{28}$$

$$v_c = k\frac{L}{W}\sqrt{p} \tag{29}$$

The nominal or expected water film thickness of a PFMD can be assumed to directly represent the amount of water present at the contact interface. If the constant $k$ in Eq. (29) is further expanded and the water film thickness $T$ is included as a separate variable, the resulting equation becomes Eq. (30) in which the exponent $\delta$ of $T$ and the constant $\lambda$ are to be evaluated empirically.

$$v_c = \lambda\frac{1}{T^{\delta}}\frac{L}{W}\sqrt{p} \tag{30}$$

It has been empirically found (Huebner et al, 1986) that the hydroplaning speed is linearly correlated to $T^{-0.5}$ for $T < 2.5$ mm. The data for the empirical analysis in (Huebner et al, 1986) was obtained from (Agrawal et al, 1977) and the exponent -0.5 for $T$ was selected with reference to (Gengenbach, 1968). Therefore, Eq. (31) can be used to calculate the hydroplaning speed for the LWST and RFT tires in terms of $\lambda$, assuming that the factors represented by $\lambda$, including pavement texture and tire tread pattern, are kept constant.

$$v_c = \lambda \frac{L}{W}\sqrt{\frac{p}{T}} \tag{31}$$

Using Eq. (31), the hydroplaning speeds for LWST and RFT test tires can be found by substituting the inflation pressures and footprint dimensions presented in Table 6.2, and the water film thicknesses for the two devices. Eqs. (32) and (33) show the results after the substitutions.

$$v_c^{LWST} = \lambda \frac{21}{14.9}\sqrt{\frac{165.5}{0.56}} = 24.23\lambda \tag{32}$$

$$v_c^{RFT} = \lambda \frac{10}{6.1}\sqrt{\frac{206.8}{1}} = 23.57\lambda \tag{33}$$

According to Eqs. (32) and (33), the hydroplaning speeds for LWST and RFT test tires are approximately equal when the factors represented by $\lambda$ are kept constant. This result shows that the water effects that lead to hydroplaning are similar for the two devices. Therefore, it is reasonable to assume the same $v_s$ parameter value in the LuGre tire model equations for LWST and RFT on pavements having similar drainage properties.

In the analyses presented in this chapter, the $v_s$ parameter determined for LWST by fitting the LuGre model equations (Eqs. 25) to measured data on the three pavement Sections mentioned in Table 6.1 was used for both the devices. The assumption of an identical $v_s$ of 5.75 m/s for both ofthe devices operated on the three pavements having identical groove geometries was further justified by the consistent results presented in chapter 8.

### 6.4.3 Uncertainty Analysis of the Model Output

The uncertainty of the model output was studied in the most general version of the longitudinal average lumped LuGre tire model (Eqs. 25), which can be used to directly analyze LWST data collected during the braking process of a free rolling wheel to a fully locked condition. A nominal set of model parameters that can be used to model a standard LWST test on an arbitrary pavement was used for the analysis. This uncertainty analysis was carried out in MATLAB. The results of a similar analysis carried out for a nominal set of parameters that represents the RFT is presented in Appendix B.

In the uncertainty analysis presented here, the parameters have been assigned practically realistic variances with respect to their nominal values. Parameters $\mu_c$, $\mu_s$, $\sigma_0$, $L$ and $v$ were assigned a 10% variance, while $v_s$ and $\sigma_1$ were assigned a 20% variance, considering their higher variability. $\alpha$, $K_0$ and $\sigma_2$ were assigned a lower variance (5%) considering the fact that these parameters can be kept constant in most of the practical analysis (Canudas-de-Wit et al, 1999, Canudas-de-Wit et al, 2003, Deur, 2001, Rajapakshe et al, 2010 and Seneviratne et al, 2009). The variances for the parameters in this uncertainty analysis were assigned to represent normal test conditions, and hence do not reflect the ones obtained in section 5.3.2 using replicate data generated from controlled experiments. Figure 6.3 shows the nominal parameter values or the respective means, and the 1000 random sample values assigned using Latin Hypercube Sampling (LHS) for each parameter within the above mentioned variances. LHS is a special random sampling method that draws samples equally distributed within and only within the designated range for a random variable (Saltelli et al, 2000).

The output $\mu$ was then evaluated for the 1000 sets of random parameter samples, and the resulting statistics of output $\mu$ are presented in Figure 6.4. In Figure 6.4 (a), the average model output ($\mu_{avg}$) for the 1000 sets of random parameters overlaps with the $\mu$ variation given by the nominal set of parameters. The standard deviation of the output $\mu$ has been evaluated as a percentage of the mean $\mu$ and plotted in Figure 6.4 (b). These plots were consistent for multiple sampling exercises, showing that 1000 samples are adequate for an accurate analysis. According to Figure 6.4 (b), the average standard deviation ($\mu_{err}$) in output $\mu$ is approximately 2.5% of the mean, which is lower than the variances introduced to most of the input parameters. When a constant variance of 10%, which is unrealistic, is introduced to each parameter, the variance in output $\mu$ turned out to be 5% showing that the variance introduced to the parameters was halved in the model output. A similar trend was observed for other magnitudes of constant variance introduced to all the input parameters.

## 6.5 Local Sensitivity of the Output

It is important to gauge the local sensitivity of the LuGre model's frictional output to parameters such as $\sigma_0$ and $\sigma_1$ as well, since that knowledge is helpful for a physically intuitive PFMD harmonization procedure, as explained in chapter 8. A local SA facilitates identifying the critical parameters that have the most significant impact on the frictional output of a specific measuring device. Mathematically, local sensitivity is the partial derivative of the output with respect to each parameter evaluated at a nominal set of input parameter values. It can be determined by explicit evaluation of the partial derivative from the model equations or by numerical evaluation based on isolated variation of the respective input parameter within a reasonably small interval close to the nominal parameter value. In this section, a local SA is used to numerically evaluate the sensitivity of the LuGre model output to each input parameter at the same nominal set of input parameter values used in the uncertainty analysis for LWST presented in section 6.3. The same analysis was performed for the RFT and the results are presented in Appendix A.

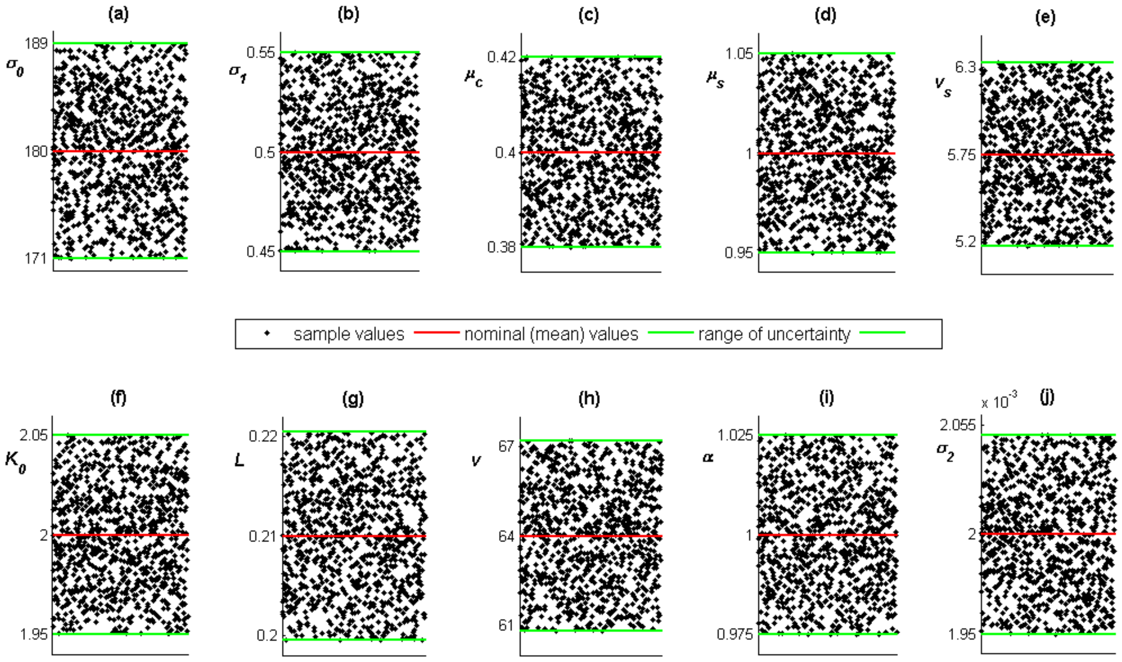

Figure 6.3: Nominal values and the sample values of the parameters for the uncertainty analysis representing LWST testing

In the numerical evaluation performed using MATLAB, each parameter was separately assigned an equal variance (±5%) with respect to their nominal values. LHS was used to select equally distributed samples for each parameter. A set of local characteristic plots similar to the global characteristic plots shown in Figure 6.2 were generated to study the effects on the output $\mu$ of the ±5% local variance introduced to each nominal input parameter. The local characteristic plots shown in Figure 6.5 indicate that the variation of $\mu$ due to local uncertainty in the input parameters has the same trends seen in the global characteristic plots in Figure 6.2.

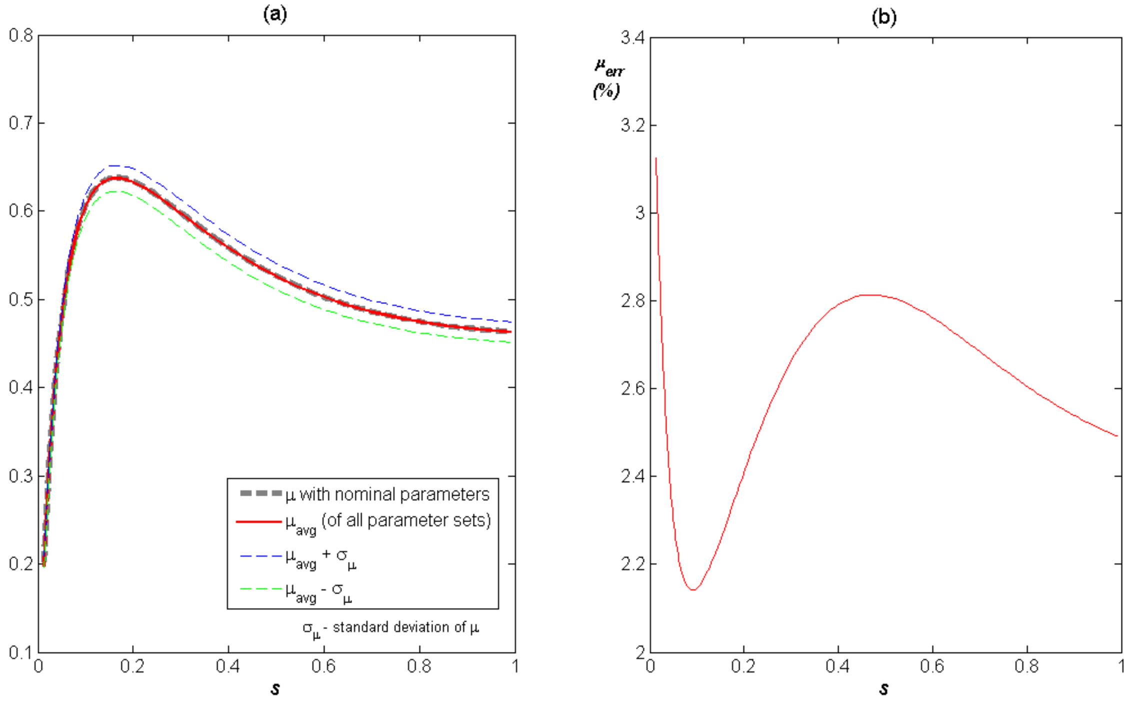

Figure 6.4: Uncertainty in the model output due to uncertainty of the parameters for LWST testing; (a) quality of the uncertainty analysis, (b) % standard deviation from the actual value due to the uncertainty introduced to the input parameters

Figure 6.6 illustrates the local sensitivity of the output $\mu$ to each parameter by presenting the variation of standard deviation in the output $\mu$ ($\mu_{err}$) against slip. The higher the $\mu_{err}$, the higher is the sensitivity of the output $\mu$ to the parameter that was varied. According to Figures 6.6 (b) and (j), the output $\mu$ is relatively insensitive to parameters $\sigma_1$ and $\sigma_2$ within the complete range of slip. This observation explains the reasonable prediction accuracies reported in (Rajapakshe et al, 2010 and Seneviratne et al, 2009) even when the effect of $\sigma_1$ was neglected in analyzing LWST friction data based on a steady-state assumption in the LuGre model (Eqs. 26). The relevant plots in Figure 6.6 show that $\mu$ is more sensitive to parameters $\sigma_0$, $\mu_s$, $v_s$, $K_0$, $L$ and $v$ at lower slip ratios, at which the maximum $\mu$ is experienced, and $\mu$ is more sensitive to the two remaining parameters ($\mu_c$ in specific) at higher slip ratios. Therefore, at the selected set of nominal parameter values that represents the LWST, it is more appropriate to evaluate the frictional properties of pavements at the fully locked-wheel ($s$ = 1) condition where $\mu$ is highly sensitive to a single pavement-dependent parameter, $\mu_c$. Furthermore, at the fully locked-wheel condition, $\mu$ is relatively insensitive to device-dependent parameters. This fact confirms the superior capability of the LWST as a consistent and accurate device for measuring frictional properties of pavements under dynamic operational conditions.

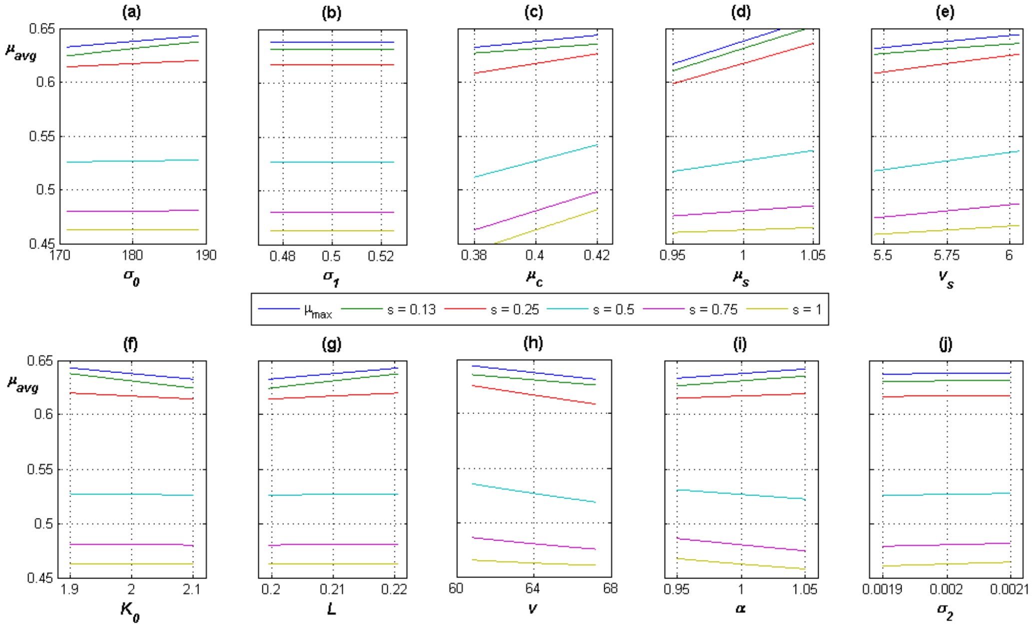

Figure 6.5: Local sensitivity of the LuGre model output at a nominal set of parameters representing LWST testing

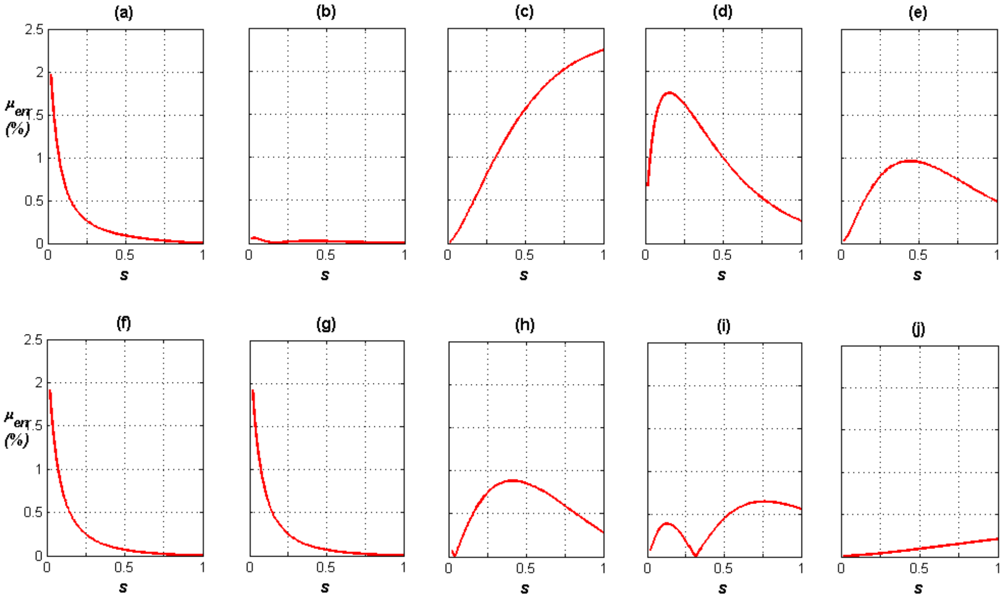

Figure 6.6: Standard deviation of the output $\mu$ as a percentage of its nominal value vs. slip ratio for ±5% local variation in the nominal parameter values for (a) $\sigma_0$ , (b) $\sigma_1$ , (c) $\mu_c$ , (d) $\mu_s$ , (e) $v_s$ , (f) $K_0$ , (g) $L$ , (h) $v$ , (i) $\alpha$ , (j) $\sigma_2$ representing LWST testing

# CHAPTER 7

# PHYSICALLY MEANINGFUL METHODS FOR ESTIMATING LUGRE TIRE MODEL PARAMETERS

In the past applications, the LuGre tire friction model has always been empirically calibrated by tuning its parameters to fit measured tire/pavement friction data or an already calibrated friction model. However, the physical significance of the model parameters is an important advantage of this widely-used analytical tire friction model. In the context of this research, it enables the model to provide physically intuitive guidelines for harmonizing different tire/pavement friction measuring devices by introducing modifications to their measurement mechanisms.

In modeling dynamic tire forces using the LuGre model, the mechanical properties of the tire are represented by the normalized stiffness and damping parameters ($\sigma_0$ and $\sigma_1$) of the brushes/bristles that model the contact surface of the tire. As identified previously, in the sensitivity analysis presented in chapter 6, the parameter $v_s$ captures the effect of water on tire/pavement friction while the parameters $\mu_c$ and $\mu_s$ model the texture-related frictional properties pertaining to the tire/pavement contact.

In the study presented in this chapter, laboratory tire tests were carried out to measure the properties of the standard smooth test tires used in the LWST and RFT (ASTM E524, 2008 and ASTM E1551, 2008). The properties were measured in vertical, lateral and longitudinal directions, and were used to derive the corresponding lumped LuGre tire parameters. A set of controlled LWST friction experiments was carried out to validate the applicability of the parameter $v_s$ for modeling the effect of water level on tire/pavement friction. Further, a simple experimental method was devised using the LWST to estimate the parameters $\mu_s$ and $\mu_s$.

## 7.1 Derivation of LuGre Tire Parameters Using Laboratory Tests

The physical meanings of the LuGre model tire parameters $\sigma_0$ and $\sigma_1$ are respectively the stiffness ($k$) and damping coefficient ($c$) of the bristles that are used to model the tire contact with the pavement. $k$ and $c$ are normalized by the total axial load carried by the bristles to obtain $\sigma_0$ and $\sigma_1$. When the lumped version of the model is considered, two values for $\sigma_0$ and $\sigma_1$ exist. Therefore, for the longitudinal lumped LuGre tire model that is applicable to most of the PFMDs, including the LWST and RFT is considered in this research. The tire parameters are given by Eqs. (34).

$$\sigma_{0x} = {}^{k_x}/_{F_z} \tag{34a}$$

$$\sigma_{1x} = {}^{c_x}/_{F_z} \tag{34b}$$

In Eqs. (34), the coordinate system shown in Figure 4.5 has been used, hence, $k_x$ is the longitudinal lumped stiffness and $c_x$ is the longitudinal lumped damping coefficient of the tire while $F_z$ is the normal load on the tire. Similar parameters can be defined in the lateral direction as well. Load versus displacement measurements must be made on the tire in the directions of interest to estimate the corresponding $k$ and $c$ values.

### 7.1.1 Methods to Measure *k* and *c* of a Tire

Two approaches may be taken to estimate the *k* and *c* values of a tire from load versus displacement measurements collected in the lateral, longitudinal and vertical directions. In both methods, the tire must be excited at its footprint in the ranges of frequencies and amplitudes that cover the operational conditions of the tire.

The most straightforward method is to use the equation for frequency response (Inman, 2006) of a single degree of freedom (SDOF) vibration system (Eq. 35) and back calculate the *k* and *c* values. In Eq. (35), $X$ – amplitude of the displacement excitation, $F_0$ – amplitude of the force response, $\omega$ – frequency of the excitation, $\omega_n$ – natural frequency of the system, and $\zeta$ – damping ratio of the system.The value of *c* can be obtained from Eq. (36).

$$\frac{X}{F_0} = \frac{\omega_n^2/k}{\sqrt{\left(\omega_n^2-\omega^2\right)^2+(2\varsigma\omega_n\omega)^2}} \tag{35}$$

$$c = {}^{2\zeta k}/_{\omega_n} \tag{36}$$

The frequency response method for the estimation of *k* and *c* parameters is well established. Once the variation of $F_0$ and $X$ vs. $\omega$ is known from the experimental data, *k* and *c* can be determined by nonlinear fitting of the data to Eq. (35). However, this method requires data to be collected over a sufficiently large frequency range that preferably includes the natural frequency of the SDOF system. Furthermore, the method is incapable of capturing any variations in *k* and *c* with the frequency or amplitude of excitation.

The second method that can be used for determining the *k* and *c* of the tire was found in the literature (Lazan, 1968) for the analysis of the viscoelastic properties of materials. It utilizes the hysteresis loop formed by the load versus deflection curve of a cyclically loaded linear viscoelastic material to estimate its stiffness and damping properties. Figure 7.1 illustrates the use of the hysteresis loop in this method.

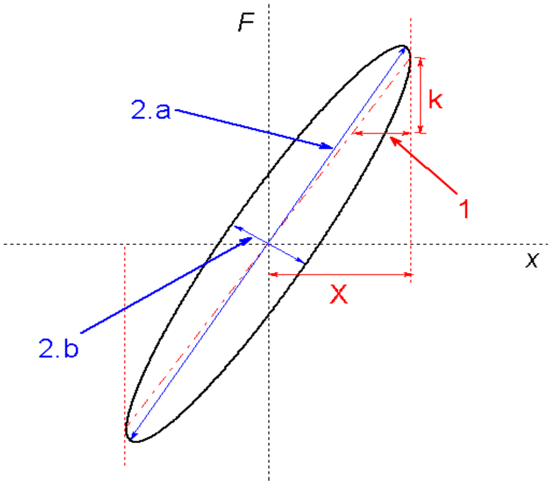

Figure 7.1: Properties of the hysteresis loop used for estimating *k* and *c* of a linear viscoelastic material

The stiffness of the material is calculated as shown in Figure 7.1 (Lazan, 1968), and it can be given by,

$$k = \frac{F_{x_{max}} - F_{x_{min}}}{x_{max} - x_{min}} \tag{37}$$

The total strain energy (*U*) supplied to the material and the energy loss due to damping (*D*) during the loading cycle are given by Eq. (38) and Eq. (39), respectively. The loss coefficient of the viscoelastic material and its relationship to the *k* and *c* parameters are given by Eq. (40) and Eq. (41) (Lazan, 1968). Finally, the damping coefficient, *c*, can be determined from Eq. (42) by using Eqs. (38 – 41).

$$D = \pi ab \tag{38}$$

$$U = {}^{kX^2}/_{2} \tag{39}$$

$$\eta = {}^{D}/_{2\pi U} \tag{40}$$

$$\eta = {}^{c\omega}/_{k} \tag{41}$$

$$c = {}^{ab}/_{\omega X^2} \tag{42}$$

For material behaviors that can be modeled approximately by linear viscoelasticity, the latter method can be used to estimate the $k$ and $c$ parameters at different frequencies and amplitude levels, irrespective of the natural frequency of the SDOF system that models the material. Since the tire exhibits viscoelastic behavior under dynamic loading, this method may be more appropriate, especially in the case of experimental limitations that may prevent the collection of data at particular natural frequencies.

### 7.1.2 Tire Testing for Measuring Stiffness and Damping Properties

A set of experiments for measuring the $k$ and $c$ of the friction test tires was designed. Generally, this type of experimentation requires quasi-static measurements to evaluate the stiffness properties and dynamic measurements to evaluate the damping properties. The ASTM E524 tire used in the LWST was selected to be tested in the first phase of the test program based on the suitability of the LWST test data toward fulfilling the research objectives. Smithers Scientific Services, Inc. (SSS), an independent tire testing company based in Akron, Ohio, developed the experimental setup required for the experiments, and implemented the tests according to the specifications.

The experimental procedure required variation of the most influential parameters on the stiffness and damping properties of the selected tire. As a result, tire inflation pressure and normal load were set to five different levels when determining the test matrices. The original test plan included quasi-static experiments for stiffness measurements along the three axes and separate dynamic experiments to estimate the three damping coefficients. However, due to the excessively-populated test matrices, the quasi-static experiments were omitted from the test plan, and the dynamic data were used to estimate the stiffness parameter as well.

In the dynamic tests, a sinusoidal excitation with linearly varying frequency was applied to the tire at each pressure and normal load. The excitation was supplied as a displacement input to a contact surface created by pasting a textured paper onto a metal plate. The friction between the textured paper and the tire was sufficient to avoid gross slip in the contact area under the tested conditions. Figure 7.2 shows the experimental setup developed by SSS for longitudinal, lateral and vertical damping tests of the ASTM E524 tire.

The standard inflation pressure and normal load for LWST testing are 24 psi and 1085 lb. Considering the fact that the inflation pressure is likely to increase during LWST testing, 5 pressure values 23 psi to 27 psi were selected with 1 psi increments. Inflation pressure was measured with an accuracy of ±0.05 psi. Normal load on the tire can vary around the standard value based on the response of the trailer suspension system to road profile variations. Therefore, two normal loads below and above the standard 1085 lb were selected for testing. The values for the normal load were 800, 1000, 1085, 1200, and 1400 lb, with a ±1 lb accuracy.

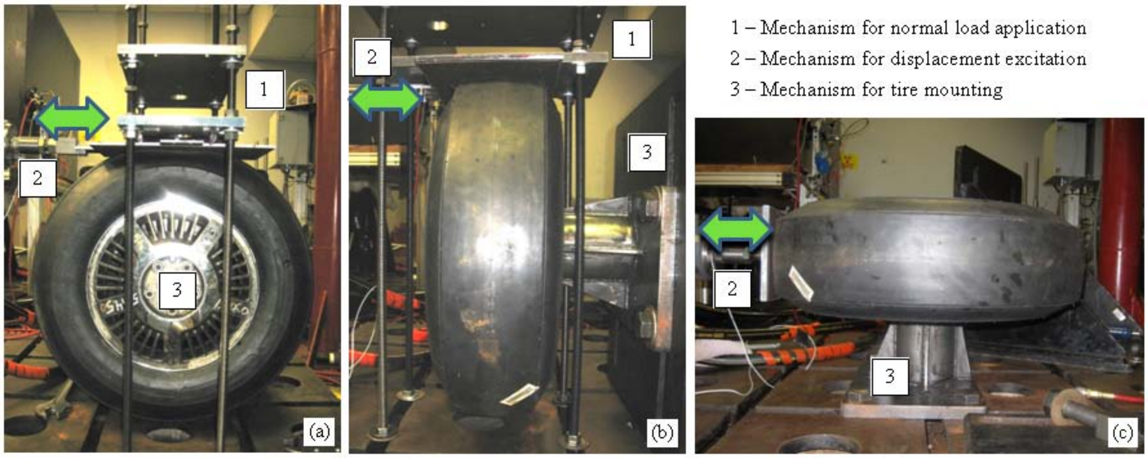

Figure 7.2: Experimental set up to measure the (a) longitudinal, (b) lateral and (c) vertical tire properties of the ASTM E524 tire

Since most of the PFMDs only involve longitudinal tire dynamics, properties in that direction were the main focus in these experiments. As a result, the longitudinal tests were carried out at all 5 inflation pressures and the lateral tests were only performed at 24, 25, and 26 psi. In both lateral and longitudinal tests, the effect of the normal load variation was only studied at the standard inflation pressure. For the tests carried out at other inflation pressures, the normal load was maintained at the standard-specified 1085 lb. For all of the vertical tests, initial static load before the excitation were kept at 1085 lb, and data was collected at the 5 inflation pressure values. Table 7.1 presents the details of the test matrices. The ranges shown in Table 7.1 for the frequency and amplitude of the sinusoidal displacement excitation resulted from restrictions in controlling the excitation. The available amplitude of vibrations was inversely proportional to the frequency in an approximately linear manner. Although the frequency dependence of amplitude was not a part of the experimental design, it enabled important observations to be made on the effect of excitation frequency and amplitude on the stiffness and damping properties of the tire.

Table 7.1: Test variables for the tire parameter measurement experiments

| Test Type | Step | Frequency Range (Hz) | Amplitude Range (mm) | Inflation Pressure (psi) | Normal Load* |
|---|---|---|---|---|---|
| Longitudinal | 1 | 0.5 - 36 | 5.1 – 0.4 | 24 | $L_1$, $L_2$, $L_3$, $L_4$, $L_5$ |
| | 2 | | | 25 | $L_3$ |
| | 3 | | | 26 | $L_3$ |
| | 4 | | | 27 | $L_3$ |
| | 5 | | | 28 | $L_3$ |
| Lateral | 1 | 0.5 - 24 | 2.5 – 1.3 | 24 | $L_1$, $L_2$, $L_3$, $L_4$, $L_5$ |
| | 2 | | | 25 | $L_3$ |
| | 3 | | | 26 | $L_3$ |
| Vertical | | | | | Initial Normal Load |
| | 1 | 0.5 - 24 | 12.7 – 1.5 | 24 | $L_3$ |
| | 2 | | | 25 | $L_3$ |
| | 3 | | | 26 | $L_3$ |
| | 4 | | | 27 | $L_3$ |
| | 5 | | | 28 | $L_3$ |

*Normal load values: $L_1$ = 800, $L_2$ = 1000, $L_3$ = 1085, $L_4$ = 1200, and $L_5$ = 1400 lb

Due to limitations in the capabilities of the experimental setup, the frequency ranges for the tests were implemented in steps. Table 7.2 shows the details of the frequency steps for the three test types and the corresponding ranges for the amplitudes.

Table 7.2: Details of the stepwise frequency sweeps

| Frequency Range (Hz) | Lateral Amplitude inch (mm) | Vertical Amplitude inch (mm) | Longitudinal Amplitude inch (mm) |
|---|---|---|---|
| 0.5 – 8 | 0.1 (2.55) | 0.5 (12.7) | 0.2 (5.1) |
| 6 – 16 | 0.1 – 0.09 (2.55 – 2.30) | 0.1 – 0.09 (2.55 – 2.30) | 0.1 – 0.09 (2.55 – 2.30) |
| 14 – 24 | 0.08 – 0.05 (2.00 – 1.3) | 0.08 – 0.06 (2.00 – 1.50) | 0.08 – 0.06 (2.00 – 1.50) |
| 22 – 30 | na | na | 0.04 – 0.03 (1.00 – 0.76) |
| 28 – 36 | na | na | 0.02 – 0.015 (0.51 – 0.38) |

### 7.1.3 Estimation of LuGre Tire Parameters from Dynamic Tire Test Data

Initially, it was attempted to estimate the $k$ and $c$ parameters using the frequency response method described in section 7.1.1. Figure 7.2 shows the frequency response obtained from the lateral test at a normal load of 800 lb and an inflation pressure of 24 psi. The following calculation employs the method described in section 7.1.1 to calculate the $\sigma_{0y}$ and $\sigma_{1y}$ parameters.

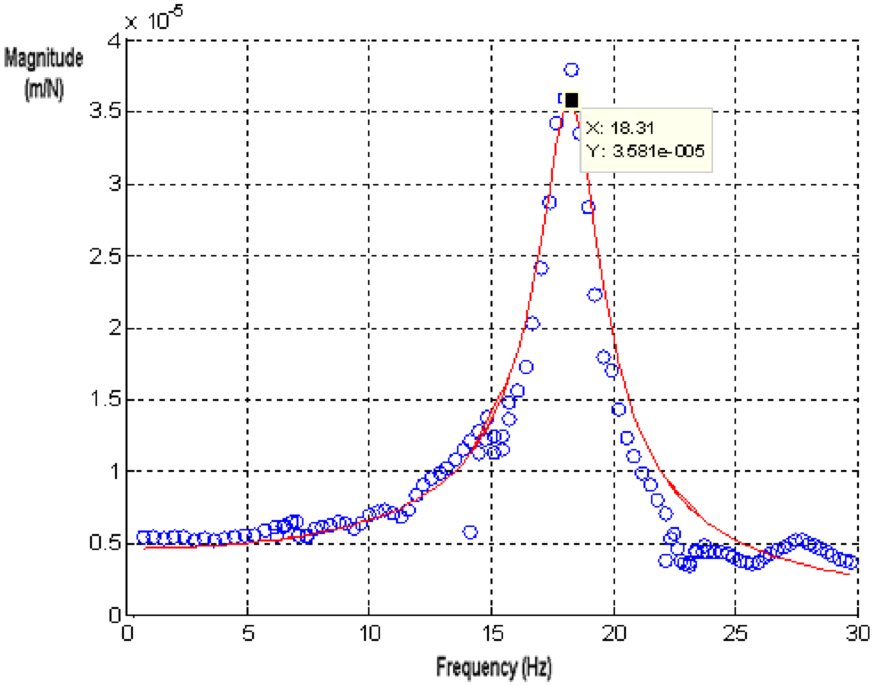

Figure 7.3: Lateral frequency response at normal load = 800 lb and inflation pressure = 24 psi

Eq. (35) was fitted to the data shown in Figure 7.3 to obtain $k_y$ = 2.14 x $10^5$ N/m, $\zeta_y$ = 0.065 and $\omega_n$ = 18.3 Hz. Then, using Eq. (36), $c$ = 1.52 x $10^3$ Ns/m was obtained. Therefore, with $F_n$ = 800 lbf = 3559 N, according to Eq. (34a) and Eq. (34b), $\sigma_{0y}$ = 60 $m^{-1}$ and $\sigma_{1y}$ = 0.427 $sm^{-1}$, respectively. Figure 7.4 shows example frequency responses from all three test types.

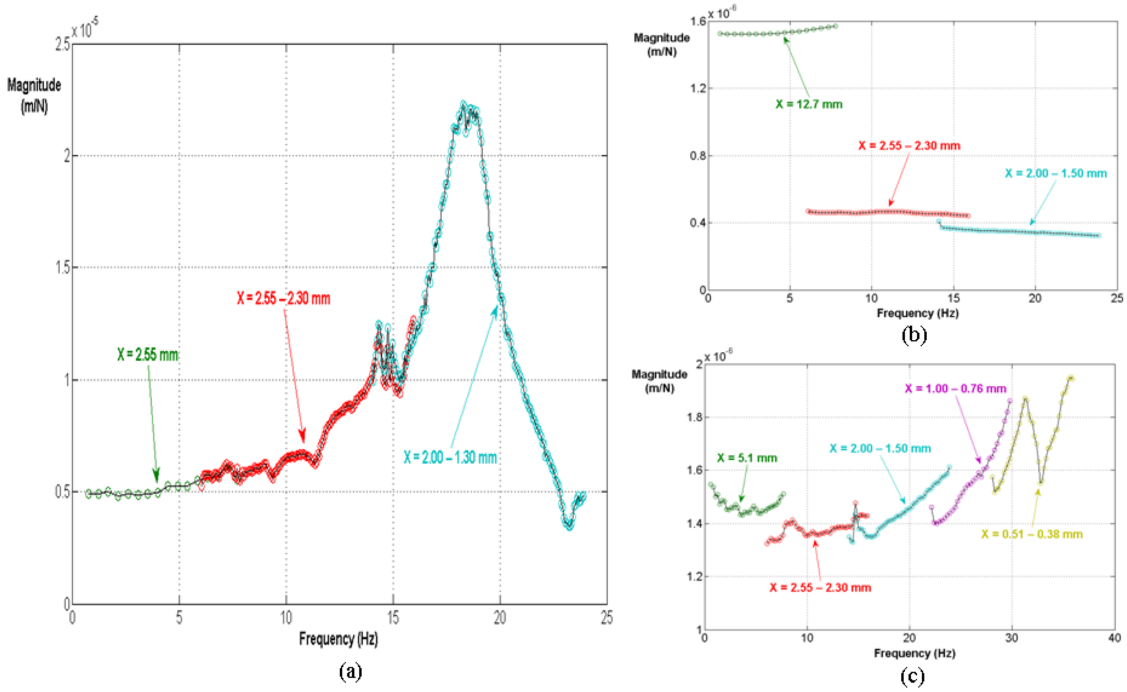

Figure 7.4: Frequency responses at normal load = 1085 lb and inflation pressure = 26 psi (frequency steps are color coded and corresponding amplitude ranges are shown); (a) lateral test, (b) vertical test, and (c) longitudinal test

As can be seen from Figure 7.4, the frequency responses have discontinuities in the cases of the longitudinal and vertical tests. However, the peaks in the frequency response could be identified in the lateral and longitudinal tests. As a result of the inherent limitation of the experimental setup, these observations (Figure 7.4) were common for all of the tests carried out in the experimental program. Therefore, the frequency response method was not used to derive the tire parameters from the experimental data.

The hysteresis loop method explained in section 7.1.1, is not affected by the aforementioned limitation of the test procedure. Therefore, it was used to derive the tire parameters of the LuGre model using the test data.

Figure 7.5 shows example hysteresis loops obtained from the experimental data collected in the longitudinal and vertical directions at different frequencies. According to Figure 7.5, the hysteresis loops are not perfectly elliptical, which shows that the tire does not exhibit linear viscoelastic behavior (Lazan, 1968). Therefore, when using the hysteresis loop method described in section 7.1.1 to estimate the tire parameters, a linear elastic approximation must be made. It is evident from the shapes of the example hysteresis loops shown in Figure 7.5 that this assumption is reasonable.

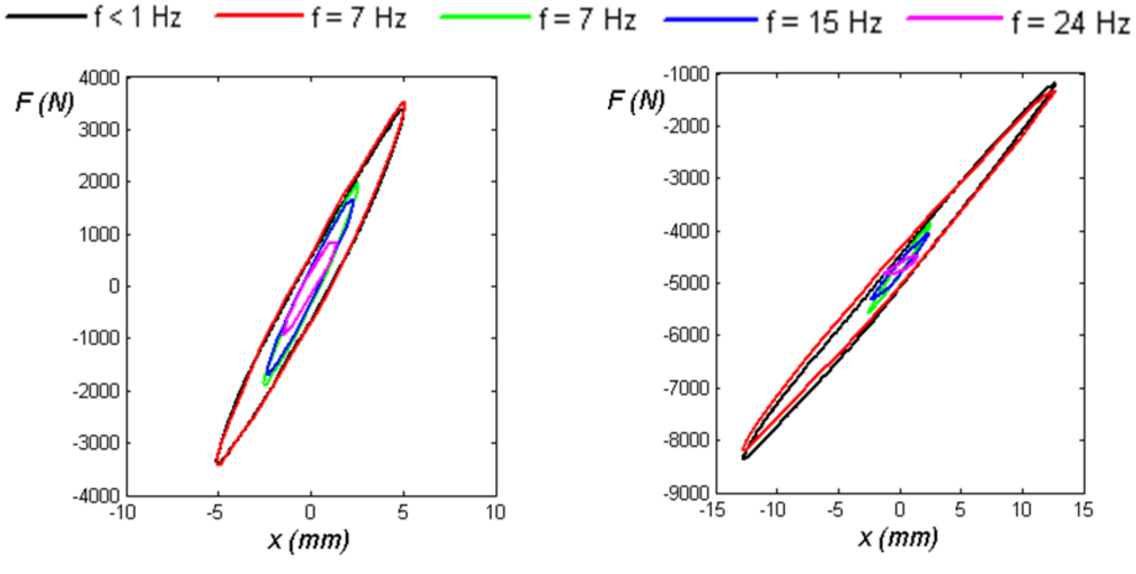

(a) (b)

Figure 7.5: Example hysteresis loops from (a) longitudinal and (b) vertical tests at different frequencies

With the linear viscoelastic assumption for the tire behavior during the tests, the parameter estimation may be carried out following two different approaches. These are both based on the calculation of the area of the hysteresis loop, which is equal to the damping energy loss during the loading cycle. The first method to calculate the area of the hysteresis loop is spline-interpolating the available data points on the hysteresis loop and numerically integrating for the area. The second approach is to fit the equation for an inclined ellipse to the available data points on the hysteresis loop and to calculate the area of that ellipse using the major and minor axis lengths. The equation for an inclined ellipse can be given as shown in Eq. (43). The symbols in Eq. (43) are explained in Figure 7.6.

$$\left(\frac{cos^2\alpha}{a^2}+\frac{sin^2\alpha}{b^2}\right)(x-X_c)^2-2\cos\alpha\sin\alpha\left(\frac{1}{a^2}-\frac{1}{b^2}\right)(x-X_c)(y-Y_c)+\left(\frac{sin^2\alpha}{a^2}+\frac{cos^2\alpha}{b^2}\right)(y-Y_c)^2=1 \qquad (43)$$

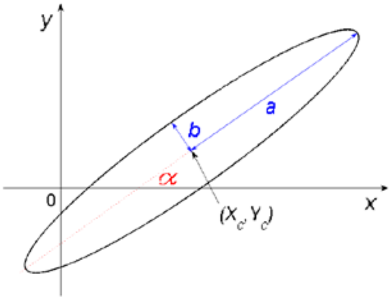

Figure 7.6: Symbolic notations for Eq. (43)

Figure 7.7 shows a comparison of the two methods explained above for calculating the area of an experimental hysteresis loop obtained in the longitudinal tire dynamic test.

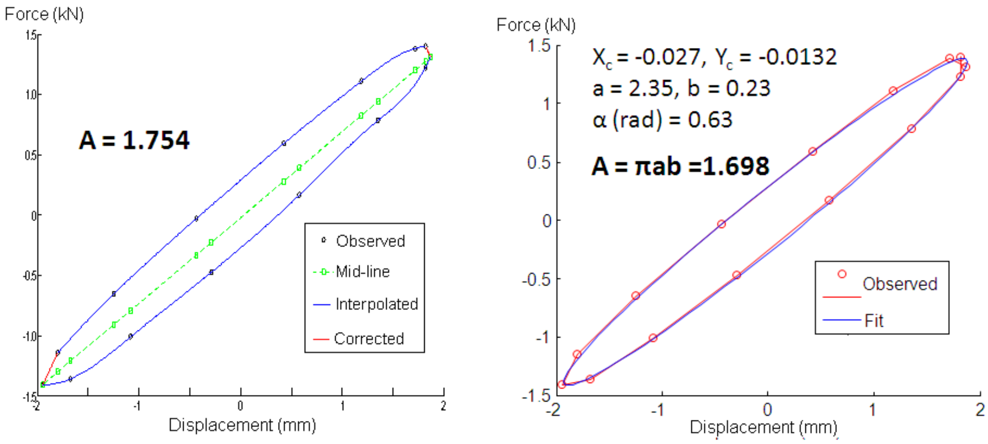

(a) (b)

Figure 7.7: Comparison of (a) Numerical method and (b) Curve-fitting method for calculating area of the hysteresis loop at normal load = 1085 lb, inflation pressure = 24 psi and frequency of excitation = 15 Hz

Table 7.3 shows the steps involved in calculating the LuGre tire parameters using the two methods shown in Figure 7.7. According to Table 7.3, the two methods used for the calculation of the area of the hysteresis loop give results with an acceptable precision. The computational procedures for the two methods were tested using data points on perfect inclined ellipses as well.

Table 7.3: Comparison of the results from the numerical and curve-fitting methods used to calculate the area of experimental hysteresis loops (normal load = 1085 lb, inflation pressure = 24 psi and frequency of excitation = 15 Hz)

| Method for area calculation | $D$ (Nm) | $U$ (Nm) | $\eta$ | $c$ (Ns.m$^{-1}$) | $\sigma_0$ (m$^{-1}$) | $\sigma_1$ (s.m$^{-1}$) |
|---|---|---|---|---|---|---|
| Numerical | 1.754 | 1.297 | 0.215 | 1629 | 147.8 | 0.338 |
| Curve-fitting | 1.698 | 1.300 | 0.208 | 1582 | 148.6 | 0.328 |

When the number of data points on the hysteresis loop is minimal and the shape of the loop deviates from an elliptical shape, the spline interpolation used in the numerical integration method for calculating the area of the hysteresis loop introduces unwanted curvatures between measured data points. This is evident in Figure 7.7. However, the numerical method is efficient, and it is helpful in automating the analysis of large numbers of hysteresis loops. On the other hand, the curve-fitting method can be considerably time-consuming. However, it preserves the basis of the assumption of linear viscoelastic behavior, since a perfect ellipse is fit to the measured data. Therefore, the curve-fitting method was used to analyze the limited number of longitudinal hysteresis loops considered in this study. Since the PFMD analyses considered in this dissertation include longitudinal tire dynamics, properties in the longitudinal direction were analyzed in detail to determine their variations at different operational conditions of the ASTM E524 tire.

### 7.1.4 Longitudinal LuGre Parameters for ASTM E524 Tire

Hysteresis loops observed in the longitudinal tire dynamic tests performed at different normal loads, inflation pressures, excitation frequencies and excitation amplitudes were analyzed using the curve-fitting method to obtain the $\sigma_0$ and $\sigma_1$ parameters in the longitudinal direction. As explained in section 7.1.2, the frequency and amplitude of excitation added another dimension to the test matrix, introduced by an inherent limitation of the test mechanism. However, it is worthwhile to have that information since it can be used to apply the LuGre tire model more effectively.

Table 7.4 shows the variation of $\sigma_0$ and $\sigma_1$ parameters with the normal load on the E524 tire at the standard inflation pressure of 24 psi, an excitation frequency of 7 Hz and amplitude of 5 mm. Figure 7.8 is a plot of $\sigma_0$ and $\sigma_1$ data shown in Table 7.4 and similar data for a frequency of 15 Hz and amplitude of 2 mm.

Table 7.4: Variation of LuGre tire parameters with normal load

| Load (lb) | $D$ (J) | $U$ (J) | $\eta$ | $c$ (Ns/m) | $\sigma_0$ (/m) | $\sigma_1$ (s/m) |
|---|---|---|---|---|---|---|
| 800 | 10.31 | 8.42 | 0.195 | 2876 | 182.4 | 0.808 |
| 1000 | 10.30 | 8.40 | 0.195 | 2881 | 145.9 | 0.648 |
| 1085 | 10.52 | 8.54 | 0.196 | 2974 | 138.3 | 0.616 |
| 1200 | 10.24 | 8.69 | 0.187 | 2475 | 124.3 | 0.464 |
| 1400 | 9.69 | 8.34 | 0.185 | 2731 | 104.3 | 0.439 |

Table 7.5 shows the variation of $\sigma_0$ and $\sigma_1$ parameters with the inflation pressure of the E524 tire at the standard normal load of 1085 lb, an excitation frequency of 7 Hz

and amplitude 5 mm. Figure 7.9 is a plot of $\sigma_0$ and $\sigma_1$ data shown in Table 7.5, and similar data for frequencies of 15, 23 Hz and amplitude of 2 mm.

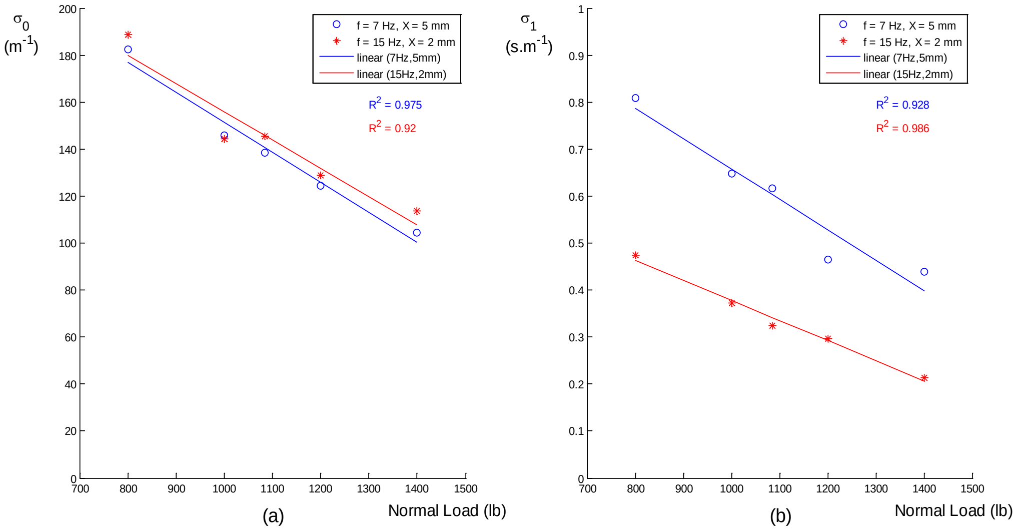

(a)

(b)

Figure 7.8: Dependence of LuGre tire parameters on the normal load (a) $\sigma_0$ and (b) $\sigma_1$

Table 7.5: Variation of LuGre tire parameters with inflation pressure

| Pressure (psi) | $D$ (J) | $U$ (J) | $\eta$ | $c$ (Ns/m) | $\sigma_0$ (1/m) | $\sigma_1$ (s/m) |
|---|---|---|---|---|---|---|
| 23 | 10.12 | 7.94 | 0.203 | 2856 | 128.4 | 0.592 |
| 24 | 10.44 | 8.24 | 0.202 | 2987 | 135.0 | 0.619 |
| 25 | 10.16 | 8.08 | 0.200 | 2921 | 133.0 | 0.605 |
| 26 | 10.21 | 8.11 | 0.200 | 2994 | 136.2 | 0.620 |
| 27 | 10.13 | 8.18 | 0.197 | 2990 | 138.3 | 0.620 |

Table 7.6 shows the variation of $\sigma_0$ and $\sigma_1$ parameters with the frequency and amplitude of the excitation at the standard normal load and inflation pressure. Since a study of the effects of amplitude and excitation frequency on the LuGre tire parameters was not on the original agenda, the data are scattered due to a lack of measurements. Therefore, studying the isolated effect of the frequency or amplitude is not straightforward. It is more suitable to handle this situation by studying the combined

effects of the two variables. This requires obtaining the 3D behavior of each LuGre parameter considering frequency and amplitude as independent variables. Such 3D surfaces were developed for $\sigma_0$ and $\sigma_1$ using scattered data interpolation. Figure 7.10 and Figure 7.11 show the variation of $\sigma_0$ and $\sigma_1$ versus excitation frequency and amplitude, respectively.

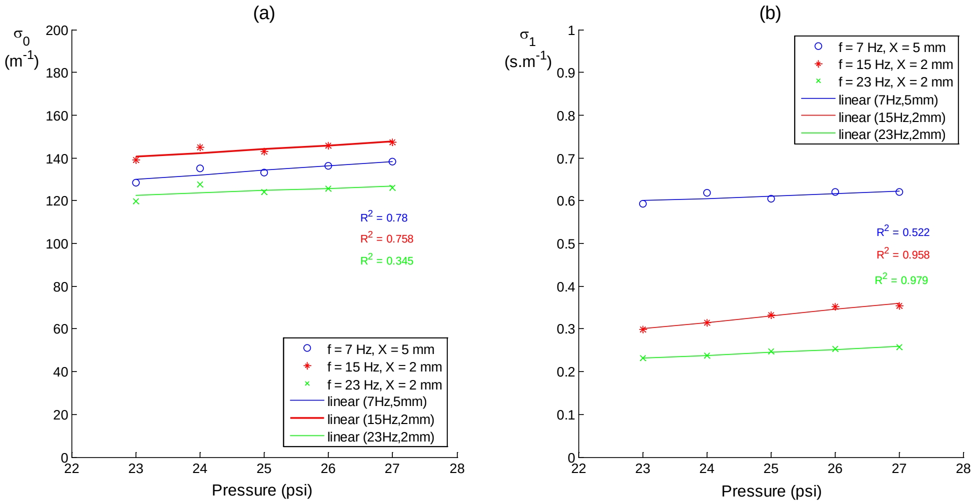

Figure 7.9: Dependence of LuGre tire parameters on inflation pressure (a) $\sigma_0$ and (b) $\sigma_1$

When the interpolated data for the surfaces shown in the Figures 7.10 and 7.11 are available, projection of the 3D surface data of any parameter on the x-z plane illustrates the variation of that parameter with respect to the frequency at different amplitudes (Figure 7.12). Similarly, projection of the 3D surface data of a parameter on the y-z plane illustrates the variation of the parameter with respect to amplitude at different frequencies (Figure 7.13).

Table 7.6: Variation of $\sigma_0$ and $\sigma_1$ with frequency and amplitude of excitation

| Frequency (Hz) | Amplitude (mm) | $D$ (J) | $U$ (J) | $\eta$ | $c$ (Ns/m) | $\sigma_0$ (1/m) | $\sigma_1$ (s/m) |
|---|---|---|---|---|---|---|---|
| 0.75 | 0.005 | 9.98 | 8.35 | 0.190 | 25777 | 132.3 | 5.341 |
| 8 | 0.005 | 12.22 | 7.98 | 0.244 | 3095 | 132.3 | 0.641 |
| 7 | 0.005 | 10.45 | 8.24 | 0.202 | 2988 | 134.9 | 0.619 |
| 7 | 0.0025 | 2.70 | 2.30 | 0.187 | 3124 | 152.2 | 0.647 |
| 6 | 0.0026 | 2.95 | 2.41 | 0.195 | 3758 | 150.3 | 0.779 |
| 16 | 0.0023 | 2.61 | 2.15 | 0.193 | 1330 | 143.8 | 0.275 |
| 15 | 0.0023 | 2.58 | 2.01 | 0.204 | 1515 | 144.9 | 0.314 |
| 15 | 0.0019 | 1.76 | 1.40 | 0.201 | 1535 | 149.5 | 0.318 |
| 14 | 0.0021 | 2.23 | 1.75 | 0.202 | 1669 | 150.4 | 0.346 |
| 24 | 0.0015 | 1.19 | 0.69 | 0.274 | 1086 | 124.1 | 0.225 |
| 23 | 0.0015 | 1.28 | 0.76 | 0.269 | 1144 | 127.5 | 0.237 |
| 23 | 0.0009 | 0.53 | 0.34 | 0.250 | 1169 | 139.9 | 0.242 |

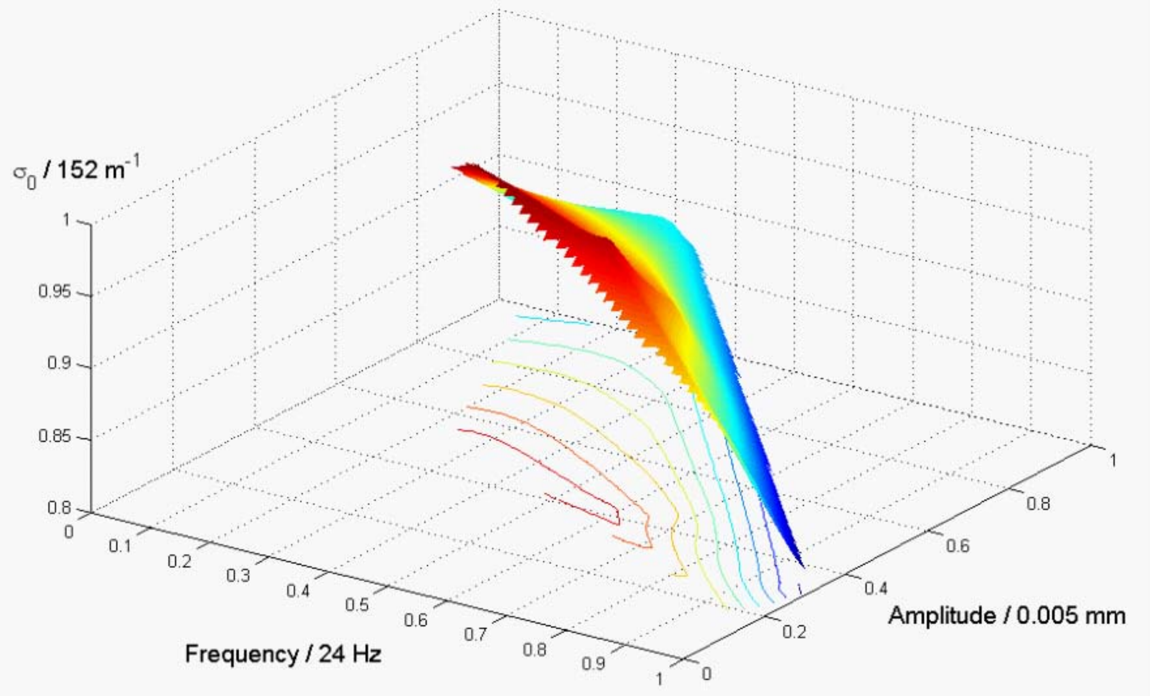

Figure 7.10: Variation of $\sigma_0$ vs. frequency and amplitude at the standard normal load and inflation pressure

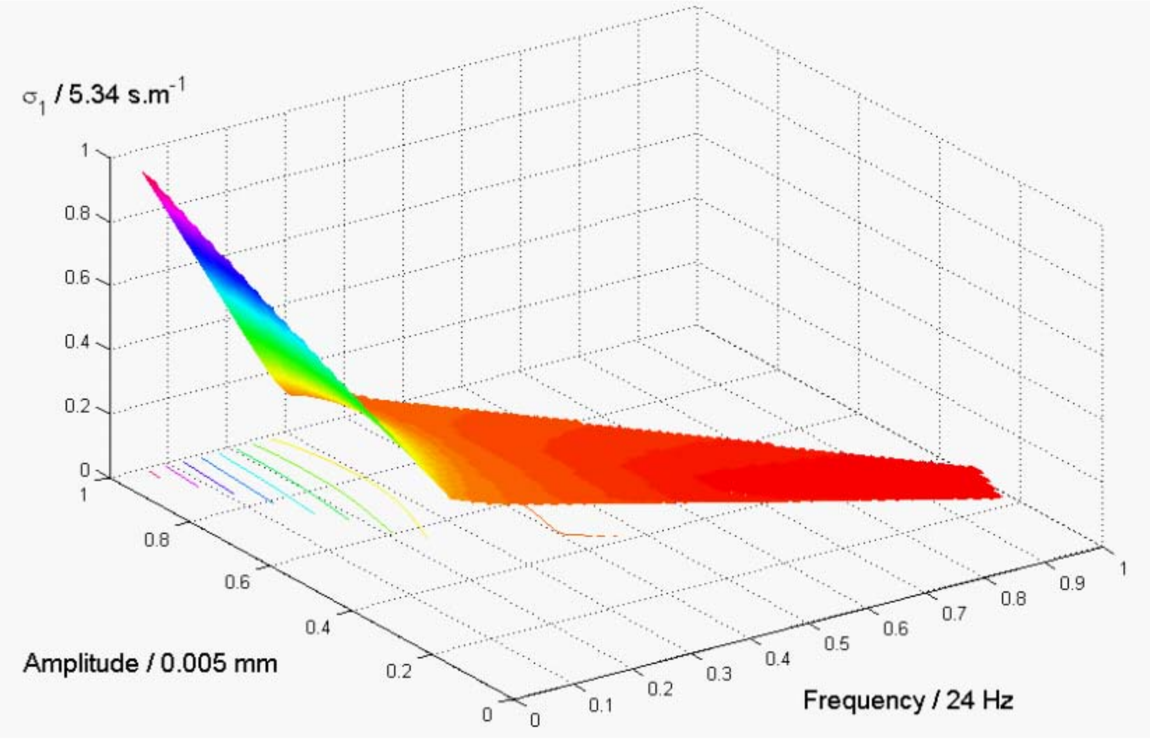

Figure 7.11: Variation of $\sigma_1$ vs. frequency and amplitude at the standard normal load and inflation pressure

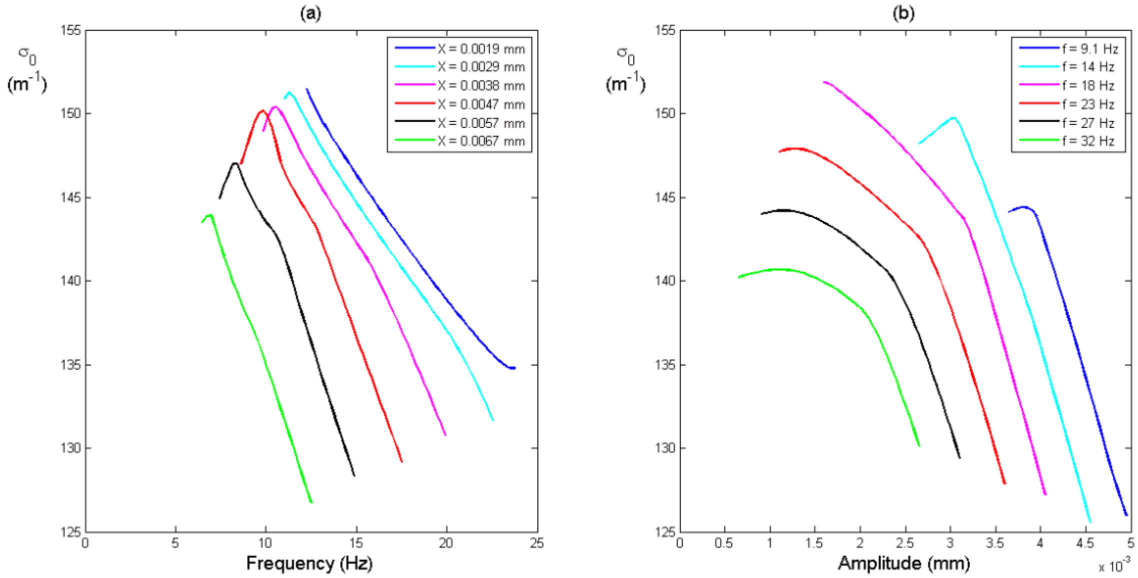

Figure 7.12: (a) Effect of excitation frequency on $\sigma_0$ at different amplitudes and, (b) Effect of excitation amplitude on $\sigma_0$ at different frequencies

According to the interpolated results shown in Figure 7.12, the $\sigma_0$ parameter has decreased significantly with increased excitation frequency and amplitude. Figure 7.13

shows that $\sigma_1$ parameter also decreases significantly with excitation amplitude. However, $\sigma_1$ has a relatively less significant dependence on the excitation frequency.

One of the main objectives of testing the ASTM E524 tire for its stiffness and damping properties and deriving the $\sigma_0$ and $\sigma_1$ parameters was to verify that these parameters have the expected physical significance for this specific application. It is clear from the results presented in the section 7.1 that the $\sigma_0$ and $\sigma_1$ parameters are of the same order of magnitude as those values obtained by empirical data fitting methods, both in this research (chapter 5) and past literature (Canudas-de-Wit et al, 2003).

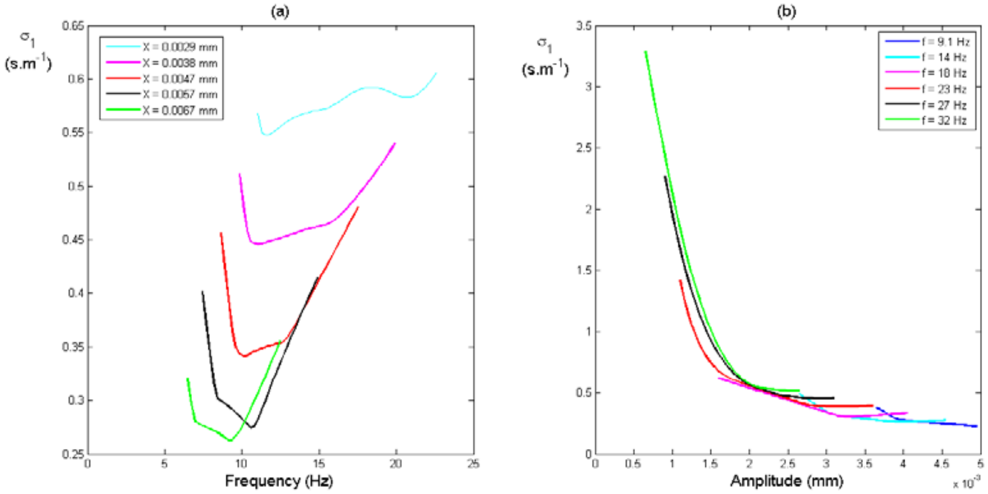

Figure 7.13: (a) Effect of excitation frequency on $\sigma_1$ at different amplitudes and, (b) Effect of excitation amplitude on $\sigma_1$ at different frequencies

## 7.2 Modeling the Effect of Water Film Thickness on Tire/Pavement Friction Using the LuGre Tire Model

In the sensitivity analysis presented in chapter 6, $v_s$ was identified as the major parameter in the LuGre model that represents the effects of water on tire/pavement friction. Furthermore, $v_s$ is a lubrication dependent parameter in the original LuGre model developed for sliding friction (Canudas-de-Wit et al, 1995).

Figure 7.14 is the variation of tire/pavement friction versus the $v_s$ parameter predicted by the LuGre model (Figure 6.2). According to Figure 7.14, tire/pavement friction increases with $v_s$ for all slip values. Based on this observation and the fact that $v_s$ represents the effect of water on tire/pavement friction (section 6.3), $v_s$ can be expected to decrease with increased amounts of water.

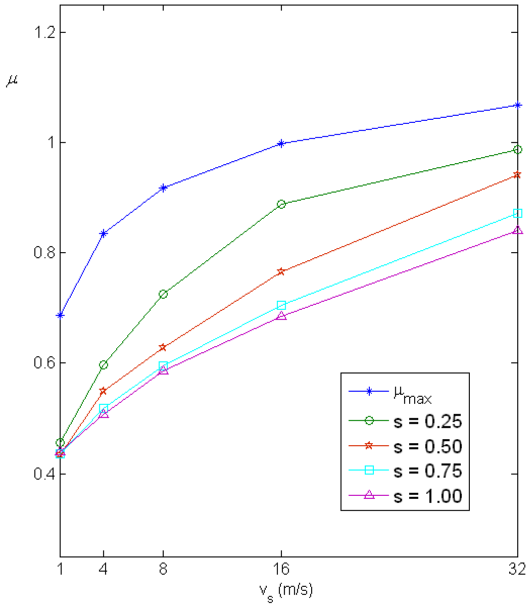

Figure 7.14: Variation of tire/pavement friction with $v_s$ parameter at different slip values

### 7.2.1 Experimental Methodology for Calibrating the $v_s$ Parameter

It is expected that $v_s$ should decrease with increased water amounts on the pavement. The goal of this study was to validate this argument using field experiments and previous research results. The objective of the experimental program was to quantify the effect of nominal water film thickness ($T_n$) on tire friction for different pavements, using the $v_s$ parameter.

The main requirement of the experiments was the ability to vary the $T_n$ value on the tested pavements. Several attempts were made to achieve different pavement water film thicknesses using irrigation systems set up on the pavement. Creating a water puddle and using a sprinkler system on the tested pavement Section were two alternatives that were initially considered. The main advantage of water supply systems external to the PFMDs, is that they can be used for testing with multiple PFMDs for each water film thickness. Furthermore, the water conditions created by external systems are closer to real-world rain conditions. However, several serious drawbacks were experienced in using both types of external water supply systems. The water film thickness on the pavement had to be measured manually to an accuracy of 0.1 mm (0.004 inches) or better (Moore, 1967). With currently available pavement water film measurement methods, there is a significant trade-off between the accuracy and the cost. Another unavoidable disadvantage in using most PFMDs with this type of a water supply system is the disturbance of water on the pavement by the front tires of the devices. This results in a water film thickness different from the measured one, and the differences are difficult to quantify. There is also a similar but less significant disturbance effect from wind. Moreover, external water supply systems are less portable, which limits the ability to test on different pavement Sections unless they are built reasonably close to each other. Due to the disadvantages explained above, irrigation-based water supply systems were not used for the experiments performed in the study presented in this section.

Since the main objective was to quantify the effect of water film thickness on pavement friction and to model it using the $v_s$ parameter in the LuGre model, testing with multiple PFMDs was not a priority. Therefore, it was decided to modify the in-built water supply system of the PFMD most suitable for these tests to provide a range of $T_n$ values. Due to its reliability, availability, and more importantly the detailed nature of the data that facilitates effective calibration of the LuGre model, the LWST was used for the experimental program.

The effect of water on tire/pavement friction is dependent on the amount of water, tire tread pattern, pavement texture, travelling speed, and tire slip. Quantifying the effect of water using the $v_s$ parameter of the LuGre tire model was the priority of this study. In achieving that, the ASTM E524 standard smooth test tire (ASTM E524, 2008) was used on two test Sections representing asphalt and concrete pavements. The dependence of the water effects on tire tread pattern and pavement texture was not a priority in this part of the study.

### 7.2.2 LWST with Variable Water Film Thickness

There are several manufacturers of LWST who build their devices according to the standard specifications (ASTM E274, 2006). Test tire type, normal load on the test tire and the constant $T_n$ to be provided at the contact interface at any test speed are universal specifications for LWSTs. There are many features that are customized differently by manufacturers as well as the users, such as the water tank volume, left-tire or both-tires testing, and water flow data monitoring and recording. For this work it was necessary to have a variable water film thickness. This was done by adjusting the water flow rate through the nozzle. There is no standard for testing of this type of variable $T_n$, and currently no LWST manufacturer provides this function as an option.

The LWST used for this work has left-tire testing only. In the standard test (ASTM E274) it uses a gear pump connected to the driveshaft of the test truck, which provides the standard 0.556 mm $T_n$ at any test speed. No water flow monitoring or recording facility was provided in the original setup. Since the gear pump cannot be used to obtain a variable $T_n$ at any speed, an external water pump was used for this work.

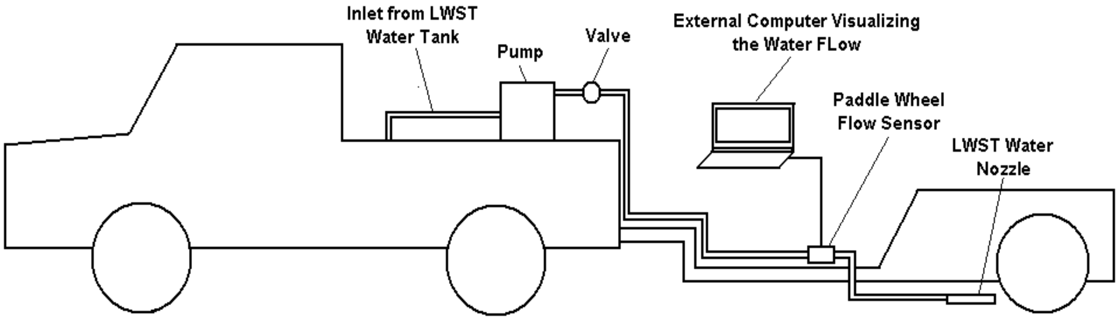

Figure 7.15: Modified water supply system for the LWST

The pump was mounted on top of the water tank of the LWST as shown in Figure 7.15. A set of valves and the throttle of the water pump's engine were used to vary the water flow. A paddle wheel flow sensor installed close to the nozzle was connected to a separate computer to set up a flow data acquisition (DAQ) system independent of the computer system of the LWST. Figure 7.16 shows a screen-print when the DAQ system visualized the effects of a small push on the paddle wheel that turned the wheel until it was stopped by internal friction. This open-loop water flow control system was used to provide pre-determined water flow rates from the nozzle to obtain the required $T_n$ values at any test speed. The water flow from the original gear pump was redirected back into the tank, keeping the LWST test control system running under the same standard conditions.

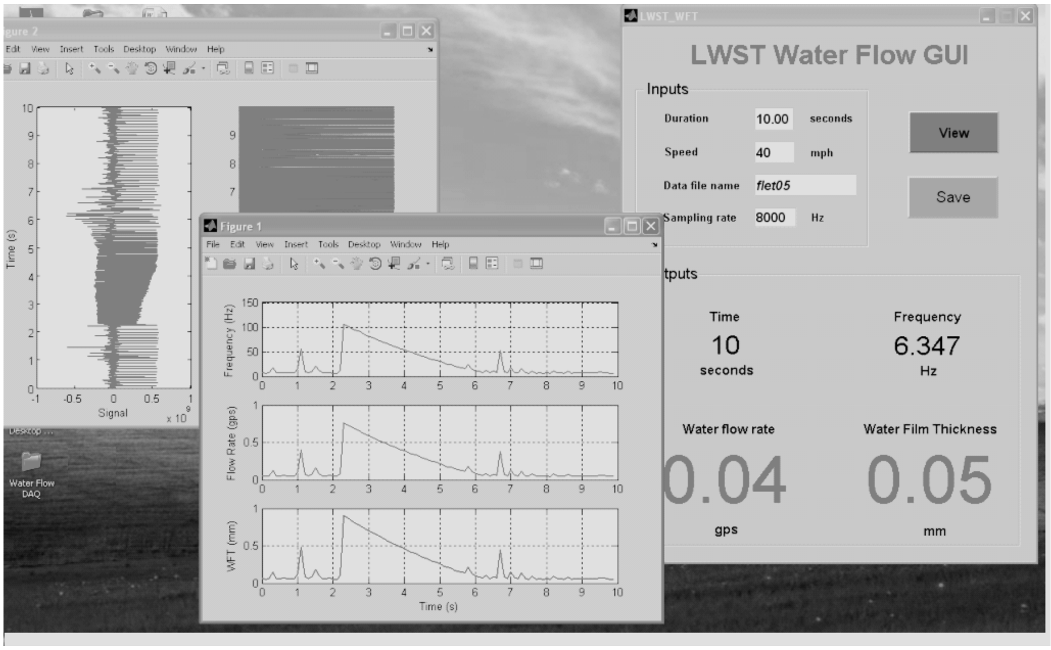

LWST Water Flow GUI

Inputs

Duration 10.00 seconds

Speed 40 mph

Data file name flet05

Sampling rate 8000 Hz

Outputs

Time 10 seconds

Frequency 6.347 Hz

Water flow rate 0.04 gps

Water Film Thickness 0.05 mm

Figure 7.16: Water flow data acquisition

Table 7.7: Data collected on Fletcher pavement Section

| **Speed (km/h)** | **$T_n$ (mm)** | **$T_n$ % standard deviation** | **$\mu_{peak}$** | **$\mu_{lock}$** |
|---|---|---|---|---|
| 48.3 | Dry | - | 0.95 | 0.95 |
| 48.9 | 0.219 | 1.73 | 0.64 | 0.43 |
| 48.4 | 0.503 | 5.10 | 0.56 | 0.39 |
| 48.5 | 0.923 | 2.28 | 0.60 | 0.40 |
| 64.4 | Dry | - | 0.95 | 0.95 |
| 64.3 | 0.214 | 2.73 | 0.60 | 0.40 |
| 64.4 | 0.522 | 5.06 | 0.49 | 0.36 |
| 64.6 | 0.894 | 2.19 | 0.43 | 0.30 |
| 80.5 | Dry | - | 0.95 | 0.95 |
| 81.1 | 0.215 | 2.50 | 0.61 | 0.39 |
| 81.4 | 0.535 | 5.06 | 0.49 | 0.32 |
| 80.7 | 0.895 | 2.12 | 0.38 | 0.30 |
| 96.6 | Dry | - | 0.95 | 0.95 |
| 97.3 | 0.219 | 2.00 | 0.57 | 0.38 |
| 96.5 | 0.555 | 4.45 | 0.38 | 0.28 |
| 96.2 | 0.835 | 2.40 | 0.32 | 0.22 |

### 7.2.3 Summary of Measured Data for Calibrating the $v_s$ Parameter

The modified LWST was used to collect friction data on two pavements (asphalt DGFC – Dense Grade Friction Course and PCC – Portland Cement Concrete) at 4 different speeds (48, 64, 80 and 96 km/h) and under 4 different water conditions (0.90, 0.55, 0.20 mm and dry). The tested pavement Sections are located in Tampa, Florida in close proximity to the University of South Florida's Tampa Campus. The asphalt pavement Section of the west-bound Fletcher Avenue between 56th and 50th streets had been newly paved with a DGFC. The longitudinally grooved concrete pavement Section on south-bound I-275 between Bearss and Fletcher Avenues had been worn considerably on the test wheel path. Table 7.7 contains the average data collected on the Fletcher Section including the $T_n$ values used in the tests.

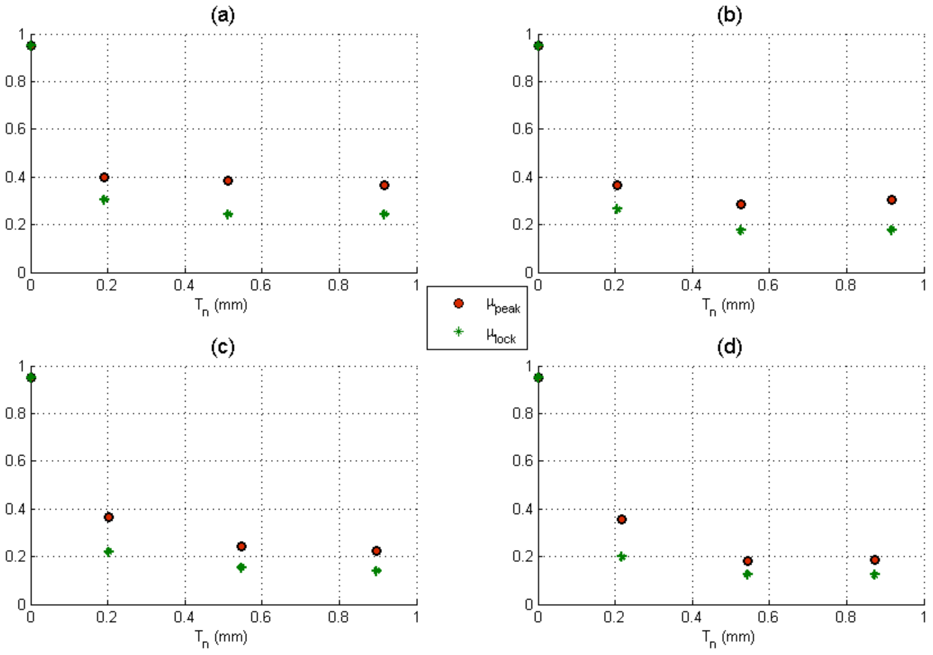

Figure 7.17: Variation of $\mu$ with $T_n$ on I-275 pavement Section at different speeds; (a) 48 km/h, (b) 64 km/h, (c) 80 km/h and (d) 96 km/h

Figures 7.17 and 7.18 show the effect of $T_n$ on friction measurements at different speeds and the effect of speed on friction measured at different $T_n$ values respectively, on the I-275 Section. Figure 7.18 shows a sample plot of the $T_n$ variation provided by the DAQ software during a test. The original gear pump system of the LWST was used to obtain the standard $T_n$ value of 0.55 mm. This was helpful in verifying the accuracy of the flow DAQ system which was calibrated prior to testing.

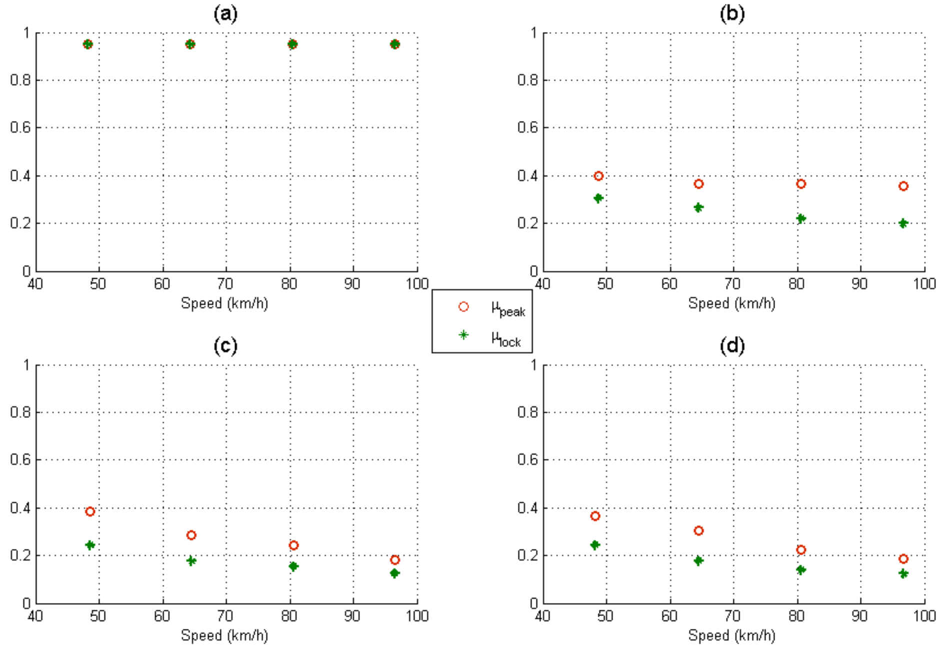

Figure 7.18: Variation of $\mu$ with speed on I-275 pavement Section at different $T_n$ values; (a) Dry, (b) 0.20 mm, (c) 0.55 mm and (d) 0.90 mm

A static $\mu$ value was measured on each surface under both dry and wet conditions by slowly dragging the LWST test tire from a completely stationary position until it started sliding. A sufficient amount of water was applied to create the wet pavement condition. The exact amount of water is immaterial as long as the tire is stationary or moved very slowly, because there is an adequate time for the tire to squeeze out any excessive water and to establish full contact with the pavement. The maximum $\mu$ value during a test, which is attained just before the tire starts moving (the static $\mu$), and the minimum value to which it drops after the sliding motion starts were also recorded. After reaching the minimum value, $\mu$ starts increasing again due to the activation of the stick-slip phenomenon. Table 7.8 shows the average results of these measurements.

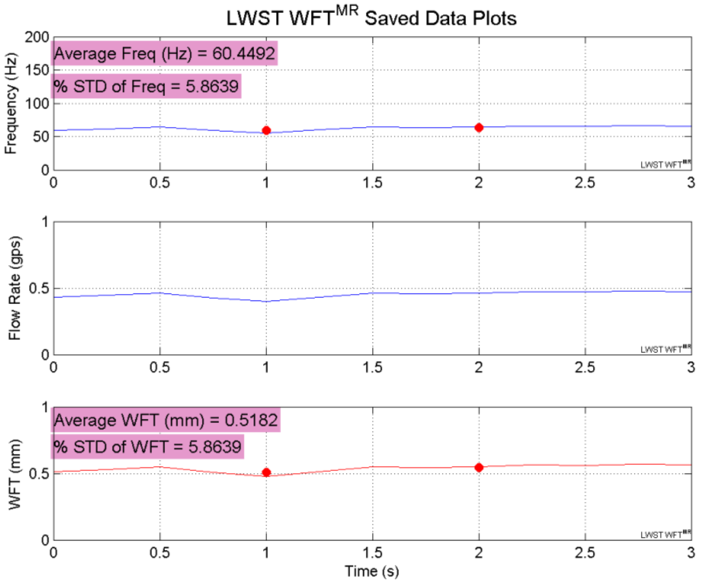

Figure 7.19: Typical variation of water supply during a test

Table 7.8: Results of the static LWST tests on the two pavement Sections

| Pavement Type | Condition | $\mu_{max}$ | $\mu_{min}$ |
|---|---|---|---|
| Fletcher Avenue (asphalt DGFC) | Dry | 1 | 0.65 |
| | Wet | 0.9 | 0.65 |
| I-275 (concrete) | Dry | 1.1 | 0.55 |
| | Wet | 0.9 | 0.45 |

### 7.2.4 Validation of $v_s$ Parameter for Modeling Water Effects

Measured individual data sets that represent the average measured tire/pavement friction behavior were selected for each $T_n$, speed, and pavement Section combination. For each pavement, the LuGre model equations (Eqs. 26) were fitted separately for each $T_n$ by optimizing the model parameters using the selected data sets at the four tested speeds. The *lsqcurvefit* function available in MATLAB was used in the optimization program. Theoretical and physical intuition gained from previous work (Rajapakshe et al, 2010 and Seneviratne et al, 2009) and past literature (Deur, 2001 and Canudas-de-Wit et al, 2003) was used to impose some of the required parameter constraints to achieve a realistic optimization.

The maximum measured values for static $\mu$ (Table 7.8) were used in the model equations for the $\mu_s$ parameter. The parameter $\mu_c$ that has been identified as a constant for a given pavement surface (Rajapakshe et al, 2010), was determined by optimization. The optimized $\mu_c$ values at different $T_n$ values on the same pavement were closely comparable, as expected, and hence a constant $\mu_c$ value that best optimizes the final calibration was picked for each surface under wet conditions. For dry conditions, $\mu_c$ was separately optimized for the two surfaces.

The dependence of longitudinal tire stiffness $\sigma_0$ on the longitudinal displacement amplitude of the tire (Rajapakshe et al, 2010) was taken into account to obtain values for the $\sigma_0$ parameter to achieve realistic optimization with acceptable accuracies. The friction forces experienced on the smooth concrete pavement on I-275 were significantly lower than those on the newly paved asphalt pavement on Fletcher Avenue with a DGFC. Furthermore, the normal load variation was relatively insignificant on both tested pavements. Therefore, it is reasonable to reach the generalized conclusion that the longitudinal displacement amplitude of the tire is significantly lower for the concrete pavement. $\sigma_0$ values determined with this assumption and previously derived $\sigma_0$ vs. amplitude relationships were kept constant in the final optimization of the parameter $v_s$ (Rajapakshe et al, 2010).

Table 7.9 presents the LuGre model parameters determined as explained above for the two pavement Sections. Parameters $\alpha$, $\sigma_2$ and $K_0$ were kept constant at 1, 0.001 s/m and 2, respectively, complying with previous research practices (Seneviratne et al, 2009, Rajapakshe et al, 2010b, Deur, 2001 and Deur et al, 2003). The error in calibrating the model and predicting the $\mu$ values with the calibrated model are also tabulated for each $T_n$. Each calibration was carried out using data collected at 48, 64 and 96 km/h and then the calibrated model equations were used to predict $\mu$ vs. $s$ at 80 km/h.

Table 7.9: Estimated LuGre model parameters for measured data

| Pavement | $T_n$ (mm) | $\mu_c$ | $\mu_s$ | $v_s$ (m/s) | $\sigma_0$ (1/m) | Calibration RMS $\mu$ Error | Prediction RMS $\mu$ Error |
|---|---|---|---|---|---|---|---|
| Fletcher (asphalt DGFC) | 0.90 | 0.24 | 0.90 | 6.92 | 100 | 0.059 | 0.056 |
| | 0.55 | 0.24 | 0.90 | 7.93 | 120 | 0.072 | 0.077 |
| | 0.20 | 0.24 | 0.90 | 11.96 | 160 | 0.066 | 0.064 |
| | Dry | 0.67 | 1.00 | 36 | 200 | 0.113 | 0.103 |
| I-275 (concrete) | 0.90 | 0.18 | 0.90 | 2.63 | 60 | 0.057 | 0.068 |
| | 0.55 | 0.18 | 0.90 | 2.68 | 65 | 0.067 | 0.051 |
| | 0.20 | 0.18 | 0.90 | 5.03 | 90 | 0.063 | 0.046 |
| | Dry | 0.55 | 1.10 | 37 | 200 | 0.074 | 0.069 |

Figure 7.20 shows the quality of calibration of the model equations and the resulting predictions on the asphalt pavement Section of Fletcher Avenue at the $T_n$ value of 0.2 mm. The plots generated for other $T_n$ values on the same pavement and on the other tested pavement were similar to those in Figure 7.9 with the calibration and prediction accuracies resembling those in Table 7.9. On both surfaces, the deviations were comparatively higher for the dry tests as one can see from the calibration and prediction error values.

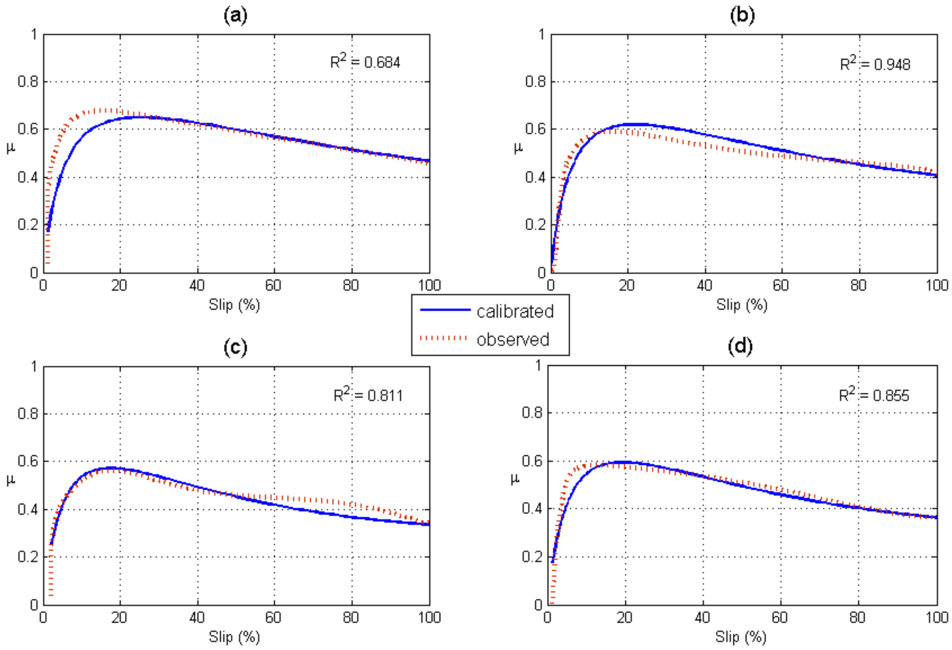

Figure 7.20: Quality of model calibration and predictions on Fletcher pavement Section

There are several significant observations that can be made using the results presented in this section. According to Table 7.9, value of the $v_s$ parameter has decreased with increased $T_n$. Figure 7.20 illustrates how $v_s$ varies with $T_n$ on the two tested pavements. It can be observed that $v_s$ has followed the originally expected behavior based on the sensitivity analysis (Figure 7.13). This is a promising outcome that reinforces the applicability of the LuGre model for tire/pavement friction testing, especially in the harmonization of PFMDs. With the previously identified physical significance of its other parameters and the added capability of modeling the effect of water through the $v_s$ parameter as revealed in this work, the LuGre model can be of enhanced utility for the applications for which it is meant to be used.

It can be seen from Figure 7.21 that the values of $v_s$ for the same $T_n$ are significantly different for the two pavements tested. This is due to the dependence of water effects on tire/pavement friction on the texture of pavements the study of which was not a priority at this stage of the research. It is possible to fit an empirical equation to quantify the $v_s$ vs. $T_n$ relationship. However, based on the observed results, two different parameter sets can be expected for the fitted equation representing the two surfaces. Hence, such an exercise will have only a limited applicability in explaining the general behavior of tire/pavement friction as well as the physical significance of the model. Therefore, it was not pursued in the study performed here and a more detailed experimental and analytical research program is underway to extend this work to achieve the above objective.

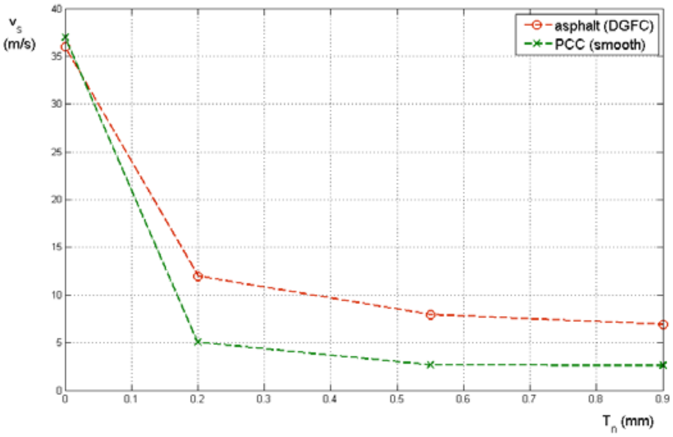

Figure 7.21: Variation of parameter $v_s$ with $T_n$ on the two pavements

In the original LuGre model, developed analytically for general sliding friction (Canudas-de-Wit et al, 1995), $\mu_c$ is physically interpreted as the Coulomb or sliding friction coefficient. It can be seen that the optimized values for $\mu_c$ under dry conditions are almost identical to the minimum friction values obtained in the static friction tests ($\mu_{min}$ in Table 7.8) on both pavements. This can be considered as strong evidence of the physical significance of the LuGre tire model parameters. However, under wet conditions, the $\mu_c$ and the $\mu_{min}$ measured in the static LWST tests are significantly different, which suggests that the original physical interpretation of $\mu_c$ is no longer directly applicable under wet conditions or simply that the experimental procedure followed to obtain $\mu_{min}$ under wet conditions needs further refinement.

The major outcomes of the work presented in section 7.2 with respect to the evaluation of tire/pavement friction can be highlighted as follows.

(i) Experimental validation of the applicability of the parameter $v_s$ in the LuGre tire model for modeling the effect of water film thickness on tire/pavement friction

(ii) Facilitation of calibrating the LuGre tire model according to the physical meanings of Coulomb friction ($\mu_c$) and static friction ($\mu_s$) parameters evaluated by a static version of the LWST test

(iii) Modification of the LWST for friction testing with a variable nominal water film thickness

The above outcomes are quite significant in developing an analytically based modeling procedure for tire/pavement friction testing applications.

# CHAPTER 8

# DEVELOPMENT OF A SEMI-EMPIRICAL METHOD FOR PFMD HARMONIZATION

As explained in section 6.2, a physically intuitive standardization of pavement friction testing can be achieved in three different ways based on the LuGre model. The model can be used to,

(i) extract device-independent pavement friction parameters ($\mu_c$ and $\mu_s$) using regular measurement data obtained from PFMDs

(ii) revise or replace the model used in the current standard procedure for harmonizing PFMD measurements

(iii) provide guidelines to harmonize the PFMDs by making physical adjustments to the measurement mechanisms of some of the devices

In the first approach, appropriately calibrated LuGre model equations for a particular PFMD can be used to derive accurate estimates for $\mu_c$ and $\mu_s$ using fitting of data. When all the PFMDs use the same rubber compound in their friction sensing elements (tires in CFME and rubber pads in DFT), the above parameters are independent of the measuring device and hence represent the basic frictional properties of pavements. Therefore, they can be used as the fundamental parameters for comparing friction levels of different pavements as described in section 5.3.2 of this dissertation with derived $\mu_c$ and $\mu_s$ parameters using LWST data (Rajapakshe et al, 2010). Since the RFT data does not characterize the variation of $\mu$ in the entire range of slip, it is not sufficient to derive the $\mu_c$ and $\mu_s$ parameters (section 5.4). However, according to the results presented in section 8.1, $\mu_c$ and $\mu_s$ parameters derived using LWST data can be used to predict the RFT friction measurement to an acceptable accuracy. Capturing the unavoidable slip variation around 0.13 during the RFT test could increase the potential of directly extracting $\mu_c$ and $\mu_s$ parameters. This is a topic for future research. However, inability to characterize $\mu$ in the entire slip range is inherent to the design of the test mechanism and hence the effectiveness of such an excersice is doubtful. The potential to use $\mu_c$ and $\mu_s$ parameters to represent the basic frictional properties governed by texture was exposed further in the latter part of section 7.2, by identifying a simple quasi-static test method that can be used to directly measure the two parameters. It should be noted that the information provided by the $\mu_c$ and $\mu_s$ parameters for a particular pavement does not include the effects of water, tire properties, etc., and hence cannot be applied directly to predict $\bar{\mu}$ experienced by a tire under different conditions on the pavement. However, the LuGre model equations can be used with appropriate values for the other model parameters to transform $\mu_c$ and $\mu_s$ to a $\bar{\mu}$ that represents the available friction conditions on the pavement (Figures 5.4, 5.5 and 7.20). Furthermore, when the LuGre model equations are applied for aircraft and vehicular tire dynamics, this approach can be extremely reliable and quite useful in practical applications. Regular calibration of the LuGre model equations for a given PFMD is essential in this type of method.

The second approach, which involves revising or replacing the current standardization procedure, requires an approach similar to the one explained above. However, in this approach LuGre model equations for different PFMDs are used to predict the response of a standard reference device (e.g. LWST). This enables transforming measurements from different PFMDs to a common standard scale which is the main objective of the currently used PFMD measurement harmonization (ASTM E1960, 2007).

The third standardization approach based on making physical adjustments to the PFMDs can be helpful in modifying the existing PFMDs and regulating the ones introduced in the future. It even allows continuation of the currently adopted harmonization procedure with an enhanced consistency, due to the compatibility among different PFMDs after appropriate modifications. To achieve this, a suitable PFMD that provides consistent measurements must be chosen as a reference device. The LuGre characteristic plots in Figure 6.2 can be used to facilitate this decision. Based on the results presented in chapter 6, the LWST possesses many advantages as a potential reference device. Therefore, a demonstrative harmonization of an RFT to an LWST is presented in section 8.1. Finally, encouraging results of a reasonably successful attempt to practically implement this type of a harmonization are presented in section 8.2.

## 8.1 A Potential Physical Harmonization Method for LWST and RFT

A physical harmonization of the two PFMDs requires the adjustment of the device-dependent LuGre parameters ($\sigma_0$, $\sigma_1$, $v_s$, $K_0$ and $L$) of the devices, so that the devices provide identical friction measurements under similar testing conditions. In the illustrative harmonization shown in Figures 8.1, 8.2 and 8.3, the parameters $\sigma_0$ and $L$ of the RFT were adjusted to alter its $\mu$ vs. $s$ curves toward overlapping with corresponding curves given by the LWST. This was achieved by increasing the $\sigma_0$ of the RFT from 220 to 300 m$^{-1}$ and increasing its footprint length, $L$, from 0.10 to 0.13 m (Table 6.2). These adjustments were determined by studying the trends exhibited by the characteristic plots for the RFT (Figure B.3 (a) and (g)). The friction measurements and the parameters $\mu_c$ and $\mu_s$ for the three runway pavement Sections used in the analysis are given in Table 6.1.

According to Figures 8.1, 8.2 and 8.3, the harmonization achieved by adjusting the $\sigma_0$ and $L$ parameters of the RFT is highly encouraging. Significant deviations are only seen at the following conditions.

(i) 48 and 96 km/h speeds on Wallops B pavement (Figures 8.1 (a) and 8.1 (d) respectively), where the experimentally observed average RFT $\mu$ values are considerably lower than the LuGre model predicted ones and,

(ii) 48 and 80 km/h speeds on Wallops G pavement (Figures 8.3 (a) and 8.3 (c) respectively), where the experimentally observed LWST peak $\mu$ values are considerably lower than the LuGre model predicted ones.

In general, however, adjustments to the RFT parameters have altered its predicted $\mu$ vs. $s$ curves to match those from the LWST. Although the data provided by the RFT is not sufficient to derive $\mu_c$ and $\mu_s$ parameters (section 5.4), these results show that the RFT measurement at $s$ = 0.13 can be predicted to an acceptable accuracy with the $\mu_c$ and $\mu_s$ parameters derived using LWST data.

Table 8.1 shows the reduction in the error between the LWST and the RFT after this demonstrative harmonization. The minimum reduction in the error achieved by the harmonization is nearly 10% and in some cases the reduction is as much as 36%. Reduction in $\mu$ measurement error of this caliber can save many lives at the tire/pavement operational level and millions of dollars at the pavement management level.

Table 8.1: Reduced error between the RFT and LWST after the harmonization

| Runway Section | $v$ (km h$^{-1}$) | Avg. RFT measured $\mu$ ($s$ = 0.13) | Adj. RFT $\mu$ | Pred. LWST $\mu$ at $s$ = 0.13 | % error between RFT $\mu$ and LWST $\mu$ at $s$ = 0.13 after adjustments | Reduction in % error between RFT $\mu$ and LWST $\mu$ |
|---|---|---|---|---|---|---|
| B | 48 | 0.60 | 0.95 | 0.97 | 2.06 | 36.08 |
|  | 64 | 0.73 | 0.92 | 0.94 | 2.13 | 20.21 |
|  | 80 | 0.66 | 0.88 | 0.90 | 2.22 | 24.44 |
|  | 96 | 0.58 | 0.85 | 0.87 | 2.30 | 31.03 |
| C | 48 | 0.71 | 0.86 | 0.88 | 2.27 | 17.05 |
|  | 64 | 0.73 | 0.83 | 0.85 | 2.35 | 11.76 |
|  | 80 | 0.66 | 0.8 | 0.82 | 2.44 | 17.07 |
|  | 96 | 0.62 | 0.78 | 0.79 | 1.27 | 20.25 |
| G | 48 | 0.80 | 0.97 | 1.00 | 3.00 | 17.00 |
|  | 64 | 0.85 | 0.94 | 0.96 | 2.08 | 9.38 |
|  | 80 | 0.81 | 0.91 | 0.93 | 2.15 | 10.75 |
|  | 96 | 0.73 | 0.87 | 0.89 | 2.25 | 15.73 |

Although, a particular combination was selected for the two parameters $\sigma_0$ and $L$ in the demonstration shown in this section, other combinations can also be found by changing one parameter and adjusting the other parameter to compensate for the resulting effects. Therefore, in practical applications, a suitable combination can be selected for the two parameters to satisfy any other constraints. The required physical modifications to the RFT would include increasing the diameter of the RFT tire to increase the footprint length ($L$) and increasing the tire's standard inflation pressure or modifying its structure to increase the longitudinal lumped stiffness ($\sigma_0$). However, increasing the inflation pressure of a tire decreases its footprint length. Therefore, an adjustment in the vertical load on the test tire may be required to obtain a suitable combination for the two parameters. The magnitudes of the physical modifications required to achieve the required parameter adjustments can be determined by suitable modeling or experimentation. Longitudinal lumped damping $\sigma_1$, can also be changed as a result of changing the test tire characteristics. However, that change does not affect the measurements significantly because of the lower sensitivity of the output $\bar{\mu}$ to the $\sigma_1$ parameter (Figure 6.2 (b)).

## 8.2 Practical Validation of LuGre Model-Based Harmonization between LWST and RFT

The best interpretation for the word ‘harmonization’ in the context of this research was found in *www.businessdictionary.com* (Businessdirectory.com, 2011). It defines harmonization as “Adjustment of differences and inconsistencies among different measurements, methods, procedures, schedules, specifications, or systems to make them uniform or mutually compatible”. According to the above definition, either the measurements of the systems or the systems themselves may be adjusted. The current IFI method for pavement friction harmonizes the measurements from different PFMDs. However, harmonizing the devices themselves sho be more long-lasting and dependable, and more importantly the results would not be limited to a representative data set. A reliable harmonization approach that can accommodate different measurement mechanisms is required. The results presented in this dissertation show that the LuGre tire model can be used to develop such a harmonization method.

In Figure 3.1, the harmonization method envisioned between the LWST and RFT is illustrated. At the RFT’s typical slip ratio of 0.13, there is a significant difference between the measurements of the two devices. A successful harmonization has to either shift the $\mu$ vs. $s$ curve of the RFT towards that of the LWST or vice-versa. The knowledge gained from the LuGre model can be used to determine which physical properties of the tires used in these devices should be adjusted to achieve this purpose. According to the results presented in the chapters 5, 6 and 7, the LWST satisfies the requirements of a reference device for harmonization. However, due to the difficulty in making modifications to the RFT, the properties of the LWST were adjusted in the experimental harmonization presented in this section. Ability to adjust the inflation pressure as well as the normal load of the LWST with relative ease was the reason for this selection. According to Figure 3.1 the LWST $\mu$ vs. $s$ curve should be shifted down by a successful harmonization. It should be noted that the decision to adjust the LWST does not imply that the RFT is superior to the LWST or otherwise.

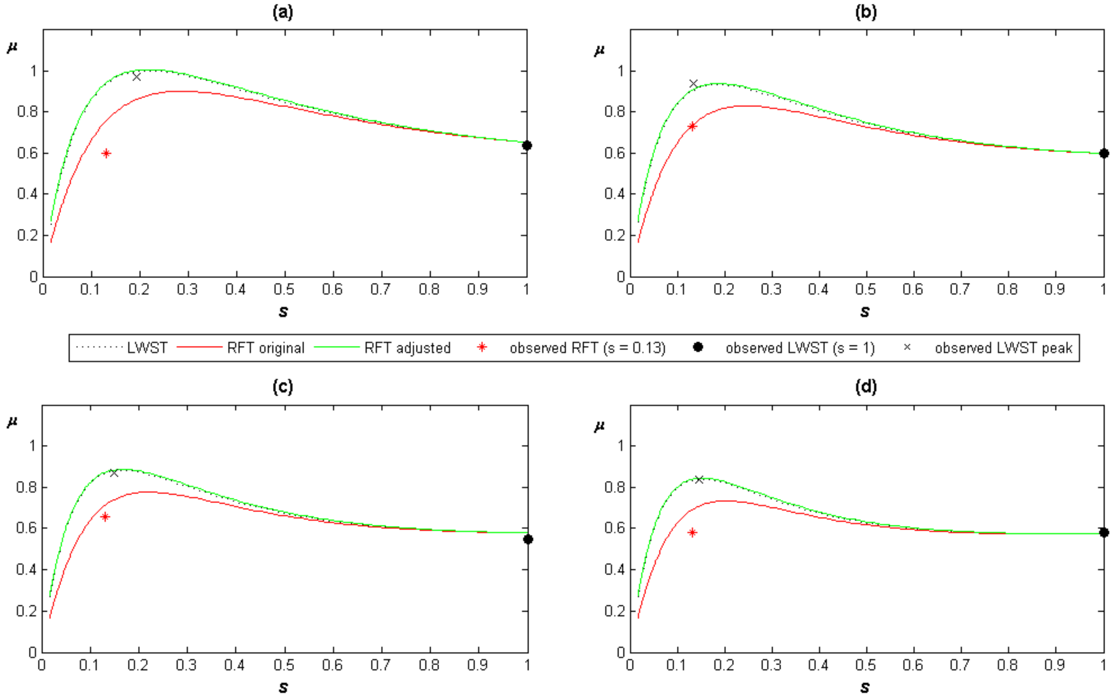

Figure 8.1: Quality of harmonization shown with data on Wallops B pavement at different speeds, (a) 48 km/h, (b) 64 km/h, (c) 80 km/h, (d) 96 km/h

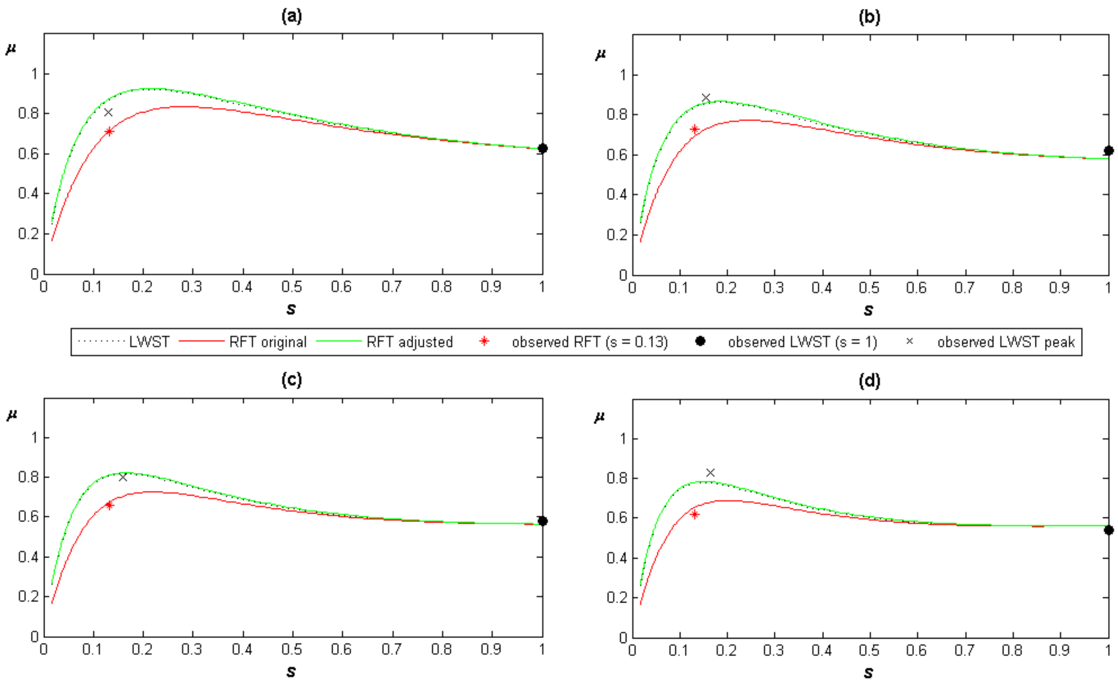

Figure 8.2: Quality of harmonization shown with data on Wallops C pavement at different speeds, (a) 48 km/h, (b) 64 km/h, (c) 80 km/h, (d) 96 km/h

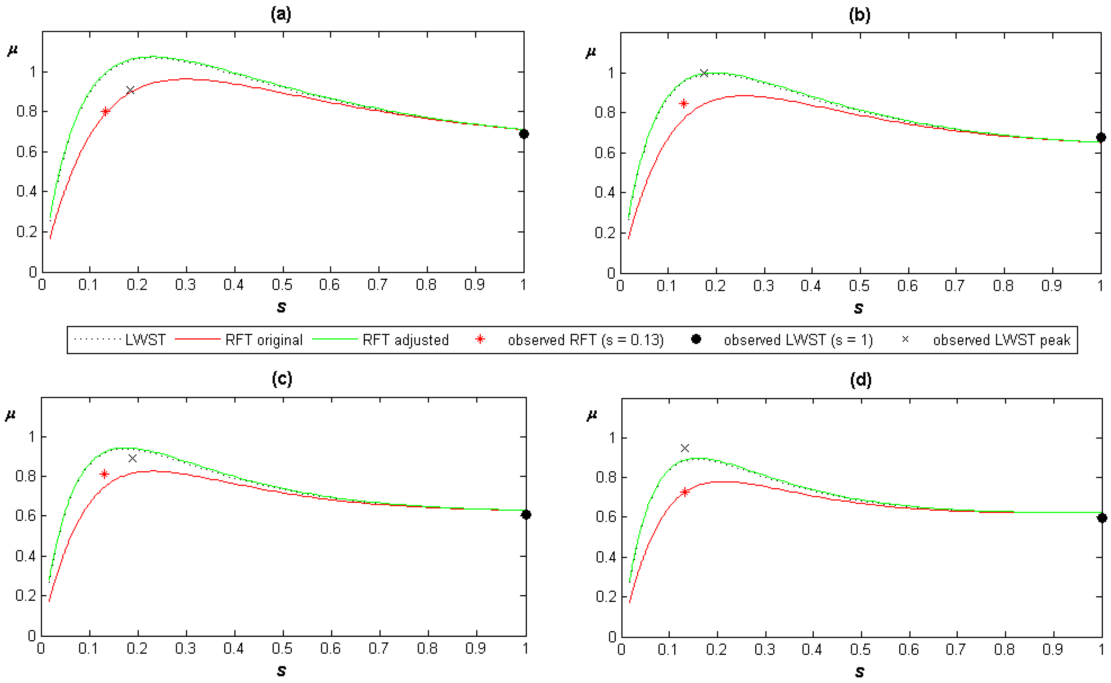

Figure 8.3: Quality of harmonization shown with data on Wallops G pavement at different speeds, (a) 48 km/h, (b) 64 km/h, (c) 80 km/h, (d) 96 km/h

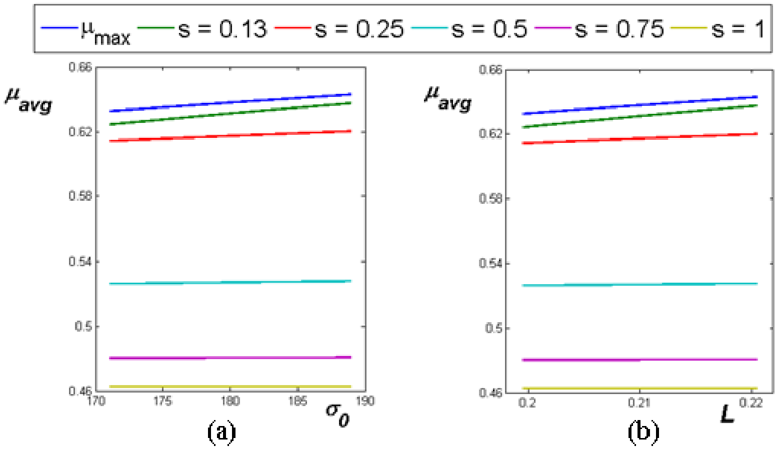

Figure 8.4: Variation of LWST measured $\mu$ with $\sigma_0$ and $L$

Figure 8.4 shows some important results found by the local sensitivity analysis of the LuGre model equations for a LWST (Figure 6.5). According to Figure 8.4, to decrease the measured friction, tire stiffness, which is quantified by the $\sigma_0$ parameter, and footprint length ($L$) have to be decreased. If the inflation pressure is decreased to decrease the stiffness of the tire, it increases the footprint length. The most practically feasible way to compensate that is to decrease the normal load on the test tire. In practicality, the weight of the LWST trailer can be adjusted.

Adjustments were made to the LWST as follows to decrease its measured friction. The inflation pressure was lowered to 19 psi from 24 psi to compensate for the resulting increase in the footprint length. The normal load was decreased to 750 lbs by removing the weights from the trailer without affecting its symmetry and leveling. After these adjustments, regular friction tests were carried out using the adjusted LWST on the same pavement Section on Fowler Avenue, Tampa, Florida described in section 5.3.1. These tests were followed by the RFT tests, and the LWST test without any adjustments made in the device. The results of these experiments are shown in Figure 8.5. The details of the results are presented in Table 8.2 in terms of the percentage reduction in the percentage error between the LWST $\mu$ measured at $s = 0.13$ and the RFT measured $\mu$.

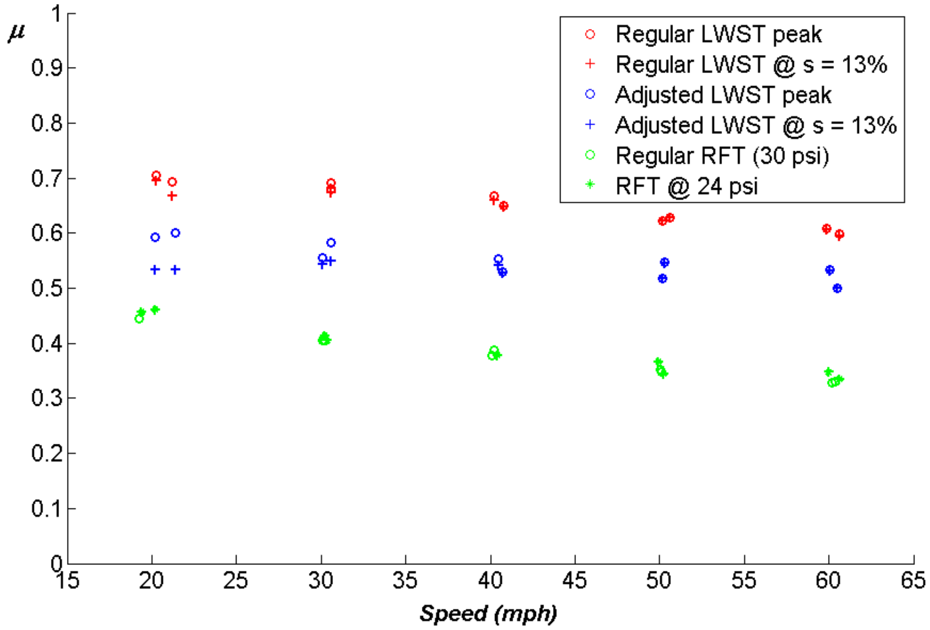

Figure 8.5: Harmonization achieved between the LWST and RFT

Table 8.2: Reduction in the error between LWST and RFT measured $\mu$ after modifying the LWST

| Regular LWST | | RFT | | Modified LWST | | Existing % $\mu$ Error | % $\mu$ Error after Harmonization | % Reduction in % $\mu$ Error |
|---|---|---|---|---|---|---|---|---|
| $v$ (mph) | $\mu$ at $s$ = 13% | $v$ (mph) | $\mu$ ($s \approx$ 13% | $v$ (mph) | $\mu$ at $s$ = 13% | | | |
| 20.3 | 0.696 | 19.2 | 0.444 | 20.2 | 0.534 | 56.82 | 20.26 | 64.34 |
| 30.6 | 0.674 | 30.1 | 0.406 | 30.1 | 0.543 | 66.20 | 33.85 | 48.87 |
| 30.6 | 0.682 | 30.2 | 0.405 | 30.6 | 0.549 | 68.46 | 35.66 | 47.91 |
| 40.2 | 0.660 | 40.1 | 0.377 | 40.5 | 0.541 | 75.10 | 43.50 | 42.08 |
| 40.8 | 0.647 | 40.2 | 0.387 | 40.7 | 0.528 | 67.12 | 36.39 | 45.79 |
| 50.2 | 0.622 | 50.0 | 0.352 | 50.2 | 0.517 | 76.87 | 47.03 | 38.83 |
| 50.6 | 0.628 | 50.1 | 0.348 | 50.3 | 0.545 | 80.51 | 56.67 | 29.61 |
| 59.8 | 0.607 | 60.2 | 0.329 | 60.0 | 0.531 | 84.51 | 61.48 | 27.25 |
| 60.6 | 0.594 | 60.3 | 0.329 | 60.5 | 0.500 | 80.28 | 51.74 | 35.54 |

According to the experimental results presented in Figure 8.5 and Table 8.2, the attempt to adjust the LWST measured friction has been successful. According to Table

8.1, the average percentage reduction in the percentage error between the measured $\mu$ of the LWST and the RFT is 42%. Complete harmonization could not be achieved due to the limited capability to adjust the properties of the measurement mechanisms of the devices. However, the results show that the method developed in this research is useful in identifying and quantifying practically feasible physical adjustments that can be introduced to PFMDs in order to bring them to a more dependable and robust harmonization.

To further evaluate the harmonization method presented in this dissertation, an extensive and controlled harmonization experiment that includes different PFMDs and pavement types such as those used in the PIARC experiment (Wambold et al, 1994) should be performed. The experiment should necessarily include different types of pavement and PFMDs with different measurement mechanisms. The first step is to carry out the standard friction measurements required to perform the currently used IFI based harmonization (sections 2.1 and 5.3.1). Then, predetermined modifications should be introduced to the measurement mechanisms of other devices based on a selected consistent and reliable PFMD designated as the reference device. The methods developed in this dissertation research using the LuGre tire model can be invaluable in determining the required modifications. As the next step, the same friction experiments carried out in the first step should be repeated with the modified PFMDs. As the final step, the data should be analyzed and the harmonization achieved by the two methods should be compared in terms of accuracy, reliability and feasibility. An extensive harmonization exercise of this caliber requires the involvement of relevant authorities, PFMD manufacturers and the end users.

# CHAPTER 9

# CONCLUSION

The research for this dissertation was carried out under a project funded by NASA entitled “Runway Characterization and Friction Measuring Device Calibration for Improving Safety of Aircraft Ground Operations”. Two main objectives of the project were (i) Comparative study of existing PFMDs and (ii) State-of-the-art research in runway friction characterization. The research carried out under this dissertation was designed to directly address these objectives.

## 9.1 Research Achievements

Prior research (Seneviratne et al 2009) identified the LuGre friction model as a potential tool to solve the problems in pavement friction measurement. Research carried out under this dissertation has certainly advanced the original application of the model toward the development of a physically meaningful harmonization method for PFMDs. The research tasks accomplished under this dissertation are as follows.

(i) Development of computational methods for the analysis of PFMD data using the tire/pavement friction models considered in the research program

(ii) Validation of the LuGre model to characterize PFMD measurements

(iii) Confirming the superiority of the LuGre model over the model used in the current PFMD standardization method

(iv) A detailed literature study on the development and applications of the LuGre model

(v) Ranking the LuGre model parameters according to their contribution toward tire/pavement friction force development and identifying the effects of variations in those parameters on tire/pavement friction using sensitivity analysis

(vi) Validating the physical significance of LuGre model parameters using specially developed methods based on experiments

(vii) Development and validation of a practical method to calibrate the LuGre tire model to represent the effect of the amount of water at the tire/pavement interface on friction

(viii) Development and experimental validation of a harmonization method for two widely used PFMDs: LWST and RFT

## 9.2 Scholarly Publications and Technical Presentations

The following are publications and presentations made in professional meetings and conferences on this research.

(i) M.P.N. Rajapakshe, M. Gunaratne, A.K. Kaw, “Evaluation of LuGre Tire Friction Model with Measured Data on Multiple Pavement Surfaces”, Tire Science and Technology, 38(3) pp. 213-227, 2010

(ii) M.P.N. Rajapakshe and M. Gunaratne, “Applicability of the LuGre Friction Model for Calibration of Multiple CFMEs”, Meeting of the ASTM Committee E17 on Vehicle – Pavement Systems, Miami, FL, 2008

(iii) M.P.N. Rajapakshe and M. Gunaratne, "Parameter Estimation and Evaluation of LuGre Tire Friction Model Using Data Collected on Multiple Pavement Surfaces", 28th Annual Meeting and Conference on Tire Science and Technology, Akron, OH, 2009

(iv) M.P.N. Rajapakshe, M. Gunaratne, A.K. Kaw, J. Andrasik, K. McGinnis and J. McIntyre, "Derivation of LuGre Tire Parameters Using Laboratory Tests", 29th Annual Meeting and Conference on Tire Science and Technology, Akron, OH, 2010

(v) M.P.N. Rajapakshe and M. Gunaratne, "A Practical Method for Improving Continuous Friction Measurement Equipment Harmonization using Physical Adjustments to the Measuring Mechanisms", 18th Annual Friction Workshop, University Park, PA, 2011

(vi) M.P.N. Rajapakshe, M. Gunaratne, A.K. Kaw, "Development of a Semi-Empirical Method to Facilitate the Standardization of Tire/Pavement Friction Measurement Devices", submitted to the ASTM Journal of Testing and Evaluation

(vii) M.P.N. Rajapakshe, J.R. Metz, J. Smith and M. Gunaratne, "Capturing the Effect of Water Film Thickness on Tire/Pavement Friction Measurements using the LuGre Tire Model", under preparation for submission

## 9.3 Future Work

Although most of the objectives of this dissertation research were achieved, there are opportunities for improvement and continuation of this work. Improvement of the computational and experimental methods used in this research will enhance the applicability and accuracy of the results. The new method introduced in this research for harmonizing PFMDs needs to be further validated prior to implementing it into the standards. Independent research for validating this method is greatly appreciated and encouraged by the author.

The author’s future research goals on this research problem include

(i) Further validation of the developed harmonization method Using multiple PFMDs on different types of pavements
(ii) Development of an FEA-based method to estimate LuGre tire parameters
(iii) Providing analytical explanations to some of the experimental observations
(iv) Improving the LuGre model of expand its versatility
(v) Developing easy-to-use model parameter computation procedures for practical applications of the model

The theoritical contribution from this research is limited since the underlying model for the work was previously developed (Canudas-de-Wit et al, 1995, Canudas-de-Wit et al, 2003 and Deur et al, 2001). It had also just been introduced to the tire/pavement friction research area through an effort (Seneviratne et al, 2009) in which the author also played a major role. However, engineering is about how effectively and efficiently theory can be applied for the advancement of technology. In other words, engineering provides the link between the theoretical realm and the real world. It is in this respect that this dissertation should receive its merit, as it has vividly illustrated an approach through which theory can be applied to practical and efficient solution of real world problems and the improvement of safety standards as envisioned in the original objectives of the research.

# LIST OF REFERENCES

AGRAWAL S.K., MEYER W.E. and HENRY J. J., 1977. *Measurement of Hydroplaning Potential*. PTI 7701, University Park, PA, USA, Pennsylvania Transportation Institute.

ANDRESEN A. and WAMBOLD, J.C., 1999. *Friction Fundamentals, Concepts and Methodology*. TP 13837E. Transport Canada.

ARMSTRONG-HELOUVRY B., 1991. *Control of Machines with Friction*. Boston: Kluwer Academic Publishers.

ARMSTRONG-HÉLOUVRY B., DUPONT P., and CANUDAS-DE-WIT C., 1994. A Survey of Models, Analysis Tools and Compensation Methods for the Control of Machines with Friction. *Automatica,* 30(7), pp. 1083-1138.

ASTM STANDARD E1170 - 97, 2007. *Standard Practices for Simulating Vehicular Response to Longitudinal Profiles of Traveled Surfaces*. West Conshohocken, PA, 2007: ASTM International.

ASTM STANDARD E1337 - 90, 2008. *Standard Test Method for Determining Longitudinal Peak Braking Coefficient of Paved Surfaces Using Standard Reference Test Tire*. West Conshohocken, PA, 2008: ASTM International.

ASTM STANDARD E1551 - 08, 2008. *Standard Specification for Special Purpose, Smooth–Tread Tire, Operated on Fixed Braking Slip Continuous Friction Measuring Equipment*. West Conshohocken, PA, 2008: ASTM International.

ASTM STANDARD E1845 - 09, 2009. *Standard Practice for Calculating Pavement Macrotexture Mean Profile Depth*. West Conshohocken, PA, 2009: ASTM International.

ASTM STANDARD E1859 - 97, 2006. *Standard Test Method for Friction Coefficient Measurements Between Tire and Pavement Using a Variable Slip Technique.* West Conshohocken, PA, 2006: ASTM International.

ASTM STANDARD E1890 - 01, 2001. *Standard Guide for Validating New Area Reference Skid Measurement Systems and Equipment.* West Conshohocken, PA, 2006: ASTM International.

ASTM STANDARD E1911 - 09AE1, 2009. *Standard Test Method for Measuring Paved Surface Frictional Properties Using the Dynamic Friction Tester.* West Conshohocken, PA, 2009: ASTM International.

ASTM STANDARD E1960 - 07, 2007. *Standard Practice for Calculating International Friction Index of a Pavement Surface.* West Conshohocken, PA, 2007: ASTM International.

ASTM STANDARD E2157 - 09, 2009. *Standard Test Method for Measuring Pavement Macrotexture Properties Using the Circular Track Meter.* West Conshohocken, PA, 2009: ASTM International.

ASTM STANDARD E2340 - 06, 2006. *Standard Test Method for Measuring the Skid Resistance of Pavements and Other Trafficked Surfaces Using a Continuous Reading, Fixed-Slip Technique.* West Conshohocken, PA, 2006: ASTM International.

ASTM STANDARD E2341 / E2341M - 05, 2009. *Standard Test Method for Determining the Stopping Distance Number by Initial Speed and Stopping Distance at Traffic Incident Sites.* West Conshohocken, PA, 2009: ASTM International.

ASTM STANDARD E2666 - 09, 2009. *Standard Practice for Correlations of Mu Values of Continuous Friction Measurement Equipment to Determine Maintenance Levels for Use at Airports.* West Conshohocken, PA, 2009: ASTM International.

ASTM STANDARD E274 - 06, 2006. *Standard Test Method for Skid Resistance of Paved Surfaces Using a Full-Scale Tire.* West Conshohocken, PA, 2006: ASTM International.

ASTM STANDARD E303 - 93, 2008. *Standard Test Method for Measuring Surface Frictional Properties Using the British Pendulum Tester.* West Conshohocken, PA, 2008: ASTM International.

ASTM STANDARD E445 / E445M - 88, 2008. *Standard Test Method for Stopping Distance on Paved Surfaces Using a Passenger Vehicle Equipped With Full-Scale Tires.* West Conshohocken, PA, 2008: ASTM International.

ASTM STANDARD E501 - 08, 2008. *Standard Specification for Standard Rib Tire for Pavement Skid-Resistance Tests.* West Conshohocken, PA, 2008: ASTM International.

ASTM STANDARD E524 - 08, 2008. *Standard Specification for Standard Smooth Tire for Pavement Skid-Resistance Tests.* West Conshohocken, PA, 2008: ASTM International.

ASTM STANDARD E867 - 06, 2006. *Standard Terminology Relating to Vehicle-Pavement Systems.* West Conshohocken, PA, 2006: ASTM International.

ASTM STANDARD F538 - 09, 2009. *Standard Terminology Relating to the Characteristics and Performance of Tires.* West Conshohocken, PA, 2009: ASTM International.

ASTROM K. J., and CANUDAS-DE-WIT C., 2008. Revisiting the LuGre Friction Model. *Control Systems Magazine, IEEE,* 28(6), pp. 101-114.

BARAHANOV N. and ORTEGA R., 2000. Necessary and sufficient conditions for passivity of the LuGre friction model. *Automatic Control, IEEE Transactions on,* 45(4), pp. 830-832.

BOZDOG D., and OLSSON W.W., 2005. An Advanced Shell Theory Based Tire Model. *Tire Science and Technology,* 33(4), pp. 227-238.

BUSINESSDIRECTORY.COM, 2011. Definition of ‘Harmonization’, *http://www.businessdictionary.com/definition/harmonization.html*, August 2011.

CANUDAS-DE-WIT C. and TSIOTRAS P., 1999. Dynamic Tire Friction Models for Vehicle Traction Control, *Proceedings of tbe 38th Conference on Decision & Control* 1999, pp. 3746-3751.

CANUDAS-DE-WIT C., 1999. Control of Friction-Driven Systems, *Proceedings of the European Control Conference* 1999.

CANUDAS-DE-WIT C., OLSSON H., ASTROM K.J. and LISCHINSKY P., 1995. A New Model for Control of Systems with Friction. *IEEE Transactions on Automatic Control,* 40(3), pp. 419-425.

CANUDAS-DE-WIT C., TSIOTRAS P., VELENIS E., BASSET M. and GISSINGER G., 2003. Dynamic Friction Models for Road/Tire Longitudinal Interaction. *Vehicle System Dynamics,* 39(3), pp. 189-226.

CARLSON C. R. and GERDES J. C., 2005. Consistent Nonlinear Estimation of Longitudinal Tire Stiffness and Effective Radius. *IEEE Transactions on Control Systems Technology,* 13(6), pp. 1010-1020.

CHO J.R., LEE H.W. and YOO W.S., 2007. A wet-road braking distance estimate utilizing the hydroplaning analysis of patterned tire. *International Journal for Numerical Methods in Engineering,* 69(7), pp. 1423-1445.

CHO J.R., LEE H.W., SOHN J.S., KIM G.J. and WOO J.S., 2006. Numerical investigation of hydroplaning characteristics of three-dimensional patterned tire. *European Journal of Mechanics - A/Solids,* 25(6), pp. 914-926.

CLAEYS X., YI J., ALVAREZ L., HOROWITZ R. and CANUDAS-DE-WIT C., 2001. A Dynamic Tire/Road Friction Model for 3D Vehicle Control and Simulation, I*ntelligent Transportation Systems,* 08/25/2001 - 08/29/2001 2001, pp. 483-488.

CLAEYS X., YI J., ALVAREZ L., HOROWITZ R., CANUDAS-DE-WIT C. and RICHARD L., 2001. Tire friction modeling under wet road conditions, June 2001, pp. 1794-1799.

CLARK S. K., 1981. *Mechanics of Pneumatic Tires.* Washington D.C.: US Department of Transportation.

CLOVER C. L. and BERNARD J. E., 1998. Longitudinal Tire Dynamics. *Vehicle System Dynamics,* 29(4), pp. 231-260.

COOKE J.C., 1969. *A Model for the Aquaplaning of Tyres on Wet Runways.* C. P. No. 1078. London: Her Majesty's Stationary Office.

DAHL P., 1968. *A Solid Friction Model.* TOR-0158H3107–18I-1. California: The Aerospace Corporation.

DE ROSA R., DI STAZIO F., GIORDANO D., RUSSO M. and TERZO M., 2008. ThermoTyre: Tyre Temperature Distribution During Handling Maneuvers. *Vehicle System Dynamics*, 46(9), pp. 831-844.

DEUR J., 2001. Modeling and Analysis of Longitudinal Tire Dynamics Based on the LuGre Friction Model, *Proceedings of 3rd IFAC Workshop Advances in Automotive Control* 2001, pp. 91-96.

DEUR J., 2002. A Brush-Type Dynamic Tire Friction Model for Non-Uniform Normal Pressure Distribution, *Proceedings of 15th Triennial IFAC World Congress* 2002, IFAC.

DEUR J., ASGARI J. and HROVAT D., 2004. A 3D Brush-type Dynamic Tire Friction Model. *Vehicle System Dynamics*, 42(3), pp. 133-173.

DEUR J., IVANOVIĆ V., TROUBLIS M., MIANO C., HROVAT D. and ASGARI J., 2005. Extensions of the LuGre Tyre Friction Model Related to Variable Slip Speed along the Contact Patch Length. *Vehicle System Dynamics,* 43, pp. 508-524.

DEUR J., KRANJˇCEVI´C N., HOFMANN, O., ASGARI, J. and HROVAT, D., 2009. Analysis of Lateral Tyre Friction Dynamics. *Vehicle System Dynamics,* 47(7), pp. 831-850.

DEUR, J., ASGARI, J. and HROVAT, D., 2003. Comments on the Paper "Dynamic Friction Models for Road/Tire Longitudinal Interaction", by Canudas-de-Wit et al, VSD 39(3), pp: 189-226. *Vehicle System Dynamics: International Journal of Vehicle Mechanics and Mobility,* 40(5), pp. 373 AB.

DREHER R. C. and HORNE W.B., 1963. *Phenomena of pneumatic tire hydroplaning.* NASA-TN-D-2056. Langley Research Center: NTRS.

FEIGHAN K., 2006. Pavement Skid Resistance Management. In: FWA T.F., *Handbook of Highway Engineering*. Taylor and Francis, pp. 21-1-21-30.

FERRETTI G., MAGNANI G., and ROCCO P., 2004. Model-Based Friction Compensation. *Advances in Control of Articulated and Mobile Robots,* 10(1), pp. 87-100.

FREIDOVICH L., ROBERTSSON A., SHIRIAEV A. and JOHANSSON R., 2010. LuGre-Model-Based Friction Compensation. *Control Systems Technology, IEEE Transactions on,* 18(1), pp. 194-200.

GENGENBACH W., 1968. Experimentelle Untersuchung von Reifen auf nasser Fahrbahn (Experimental Investigation of Tires on Wet Pavements). *Automobiltechnische Zeitschr (Automotive Technology Magazine),* 70, pp. 83-89, 288-293, 310-316.

HAESSIG D. A. and FRIEDLAND B., 1991. On the Modeling and Simulation of Friction. *ASME Journal of Dynamic Syastems, Measurement and Controls,* 113(3), pp. 354-362.

HENRY J. J., 1978. The Relationship between Texture and Pavement Friction. *Tire Science and Technology,* 6(4), pp. 215-232.

HESS D. P., and SOOM A., 1990. Friction at a Lubricated Line Contact Operating at Oscillating Sliding Velocities. *ASME Journal of Tribology,* 112, pp. 147-152.

HUEBNER R.S., REED J.R. and HENRY J.J., 1986. Criteria for Predicting Hydroplaning Potential. *Journal of Transportation Engineering,* 112(5), pp. 549-553.

INMAN D. J., 2006. *Vibration with Control.* West Sussex, England, John Wiley and Sons, Ltd.

JIUHONG R., FUGUANG Y., XUYUN Q. and YIBIN L., 2008. Wheel Independent-Drive Control Based on Dynamic Tire LuGre Friction Model, *Control Conference, 2008. CCC 2008. 27th Chinese* 2008, pp. 441-445.

KARNOPP D., 1985. Computer Simulation of Slip-Stick Friction in Mechanical Dynamic Systems. *ASME Journal of Dynamic Syastems, Measurement and Controls,* 107(1), pp. 100-103.

KELLY R., 2004. Enhancement to the LuGre Model for Global Description of Friction Phenomena. *Latin American Applied Research,* 34(3), pp. 173-177.

KELLY R., LLAMAS J., and CAMPA R., 2000. A Measurement Procedure for Viscous and Coulomb Friction. *IEEE Transactions on Instrumentation and Measurement,* 49(4), pp. 857-861.

LACOMBE J., 2000. Tire Model for Simulations of Vehicle Motion on High and Low Friction Road Surfaces, *Proceedings of the 32nd Conference on Winter Simulation* 2000, pp. 1025-1034.

LAZAN B.J., 1968. *Damping of Materials and Members in Structural Mechanics,* London, England, Pergamon Press Inc.

LIU D.P., 2006. Parameter Identification for LuGre Friction Model Using Genetic Algorithms, *Machine Learning and Cybernetics, 2006 International Conference on* 2006, pp. 3419-3422.

MATHEWS P., 2005. *Design of Experiments with MINITAB*, Milwaukee, USA, American Society for Quality.

MOORE D. F., 1975. *The Friction of Pneumatic Tyres.* Elsevier Scientific Publishing Company.

MOTULSKY H. J., and RANSNAS L. A., 1987. Fitting Curves to Data Using Nonlinear Regression: A Practical and Nonmathematical Review. *The Journal of the Federation of American Society for Experimental Biology,* 1(1), pp. 365-374.

OLSSON H., 1996. *Control Systems with Friction*, Department of Automatic Control, Lund Institute of Technology.

OLSSON H., ASTROM K.J., CANUDAS-DE-WIT C., GAFVERT M. and LISCHINSKY P., 1998. Friction Models and Friction Compensation. *Europian Journal of Control,* 4(3), pp. 176-195.

PACEJKA H.B. and SHARP R.S., 1991. Shear Force Development by Pneumatic Tyres in Steady State Conditions: A Review of Modeling Aspects. *Vehicle System Dynamics,* 20(3 and 4), pp. 121-175.

PADTHE A. K., OH J.H. and BERNSTEIN D. S., 2006. On the LuGre Model and Friction-Induced Hysteresis, *American Control Conference*, June 14-16, 2006 2006, pp. 3247-3252.

PERSSON B. N. J. and TOSATTI E., 2000. Qualitative Theory of Rubber Friction and Wear. *Journal of Chemical Physics,* 112(4), pp. 2021-2029.

PERSSON B. N. J., 1998. On the Theory of Rubber Friction. *Surface Science,* 401(3), pp. 445-454.

PERSSON B. N. J., 2001. Theory of Rubber Friction and Contact Mechanics. *Journal of Chemical Physics,* 115(8), pp. 3840-3861.

POTTINGER M. G., 1992. The Three-Dimensional Contact Patch Stress Field of Solid and Pneumatic Tires. *Tire Science and Technology,* **20**(1), pp. 3-32.

RADO Z., 1994. *A Study of Road Surface Texture and its Relationship to Friction,* Penn State University.

RAJAPAKSHE M. P. N., and GUNARATNE M., 2011. A Practical Method for Improving Continuous Friction Measurement Equipment Harmonization Using Physical Adjustments to the Measuring Mechanisms, *18th Annual Friction Workshop,* University Park, Pennsylvania, USA, l2011.

RAJAPAKSHE M. P. N., GUNARATNE M. and KAW A. K., 2010. Evaluation of LuGre Tire Friction Model with Measured Data on Multiple Pavement Surfaces. *Tire Science and Technology,* 38(3), pp. 213-227.

RANGANATHAN A., 2005. Preventing wet runway accidents. *The Hindu*.

SAITO K., HORIGUCHI T., KASAHARA A., ABE H. and HENRY J., 1996. Development of a Portable Tester for Measuring Skid Resistance and Its Speed Dependency on Pavement Surfaces. *Transportation Research Record: Journal of the Transportation Research Board,* 1536(1), pp. 45-51.

SALTELLI, A., CHAN, K. and SCOTT, M., 2000. *Sensitivity Analysis,* New York, USA, Wiley.

SCHALLAMACH A., 1952. The Load Dependence of Rubber Friction, 1952, pp. 657-661.

SENEVIRATNE H. N., RAJAPAKSHE M. P. N. and GUNARATNE M., 2009. Field Calibration of an Analytical Model for Pavement Friction Testing Applications. *Journal of Testing and Evaluation,* 37(1), pp. 21-30.

TAN D., WANG Y. and ZHANG L., 2007. Research on the Parameter Identification of LuGre Tire Model Based on Genetic Algorithms, *International Conference on Intelligent Systems and Knowledge Engineering*, October 15-16,2007 2007.

TSIOTRAS P., VELENIS E. and SORINE M., 2004. A LuGre Tire Friction Model with Exact Aggregate Dynamics. *Vehicle System Dynamics,* 42(3), pp. 195-210.

VAN ES, G. W. H., 2001. *Hydroplaning of modern aircraft tires.* NLR-TP-2001-242. Amsterdam, Netherlands, Nationaal Lucht-en Ruimtevaartlaboratorium (NLR).

WAMBOLD J. C. and HENRY J. J., 1994. International PIARC Experiment to Compare and Harmonize Texture and Skid Resistance Measurement. *Nordic Road and Transport Research,* 6(2), pp. 28-31.

WIKIPEDIA CONTRIBUTORS, 2011, List of accidents and incidents involving commercial aircraft, Homepage of Wikipedia, The Free Encyclopedia: *http://en.wikipedia.org/wiki/List_of_accidents_and_incidents_involving_commercial_aircraft*, August, 2011.

YAGER T. J., WAMBOLD J. C., HENRY J. J., ANDRESEN A. and BASTIAN M., 2002. Joint Winter Runway Friction Program Accomplishments, *Pavement Evaluation 2002 Conference* 2002.

YI J., ALVAREZ L., CLAEYS X. and HOROWITZ R. 2003. Emergency Braking Control with an Observer-based Dynamic Tire/Road Friction Model and Wheel Angular Velocity Measurement. *Vehicle System Dynamics,* 39(2), pp. 81-97.

YI J., SURYANARAYANAN S., HOWELL A., HOROWITZ R., TOMIZUKA M. and HEDRICK K., 2002. *Development and Implementation of a Vehicle-Centered Fault Diagnostic and Management System for the Extended PATH-AHS Architecture: Part II.* University of California, Berkeley.

ZEGELAAR, P.W.A., 1998. *The Dynamic Response of Tyres to Brake Torque Variations and Road Unevennesses,* Delft University of Technology.

# APPENDICES

# Appendix A: Pictures of the PFMDs Used in the Research

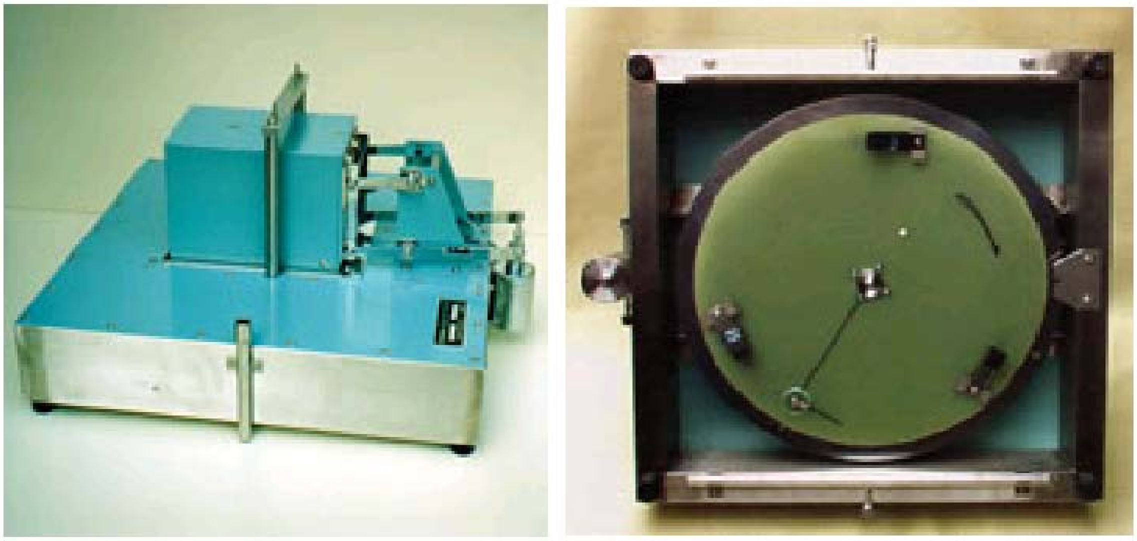

Figure A.1: Dynamic Friction Tester (DFT)

Figure A.2: Locked Wheel Skid Tester (LWST)

Figure A.3: Runway Friction Tester (RFT)

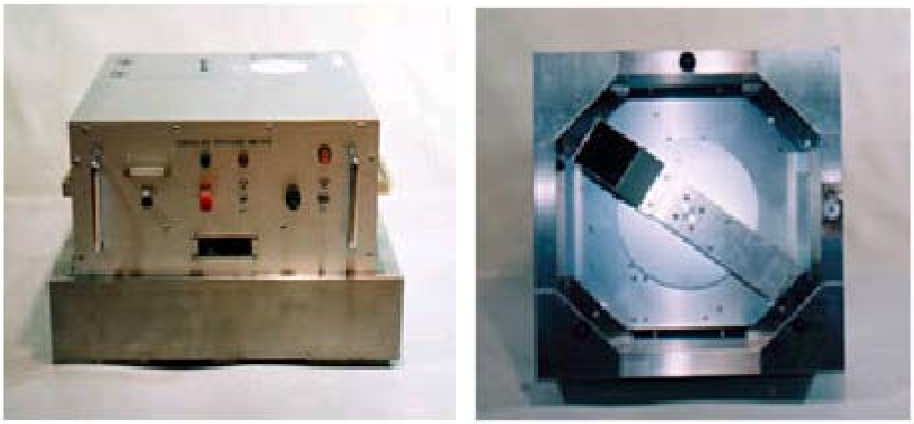

Figure A.4: Circular Track Meter (CTM)

## Appendix B: Local Sensitivity Analysis of LuGre Model for RFT

The uncertainty and local sensitivity analyses performed for the LWST as described in Chapter 6 was carried out for the RFT and the results are presented here.

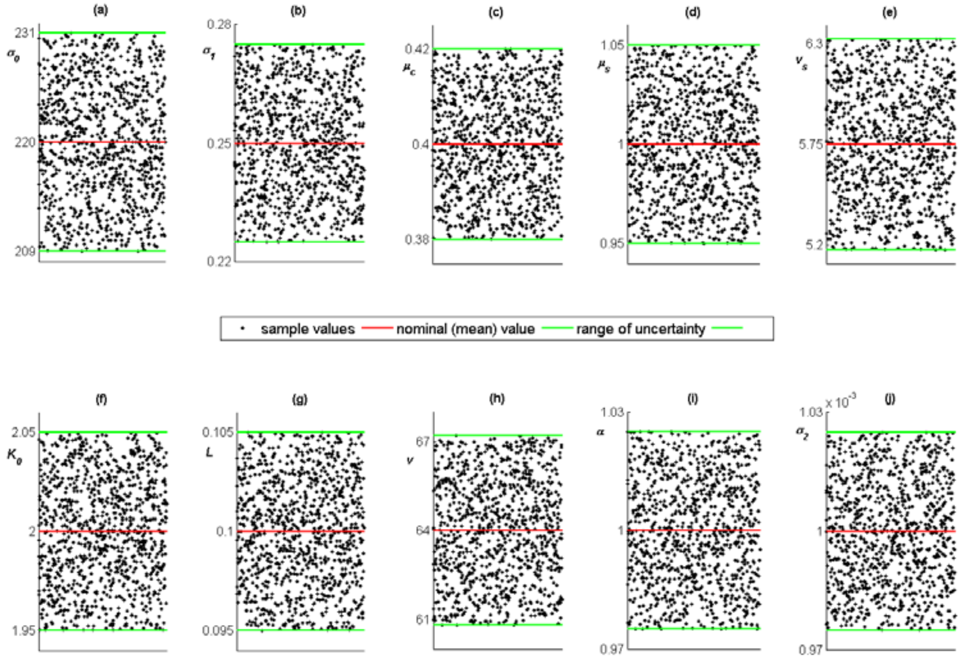

Figure B.1: Nominal values and the sample values of the parameters for the uncertainty analysis representing RFT testing

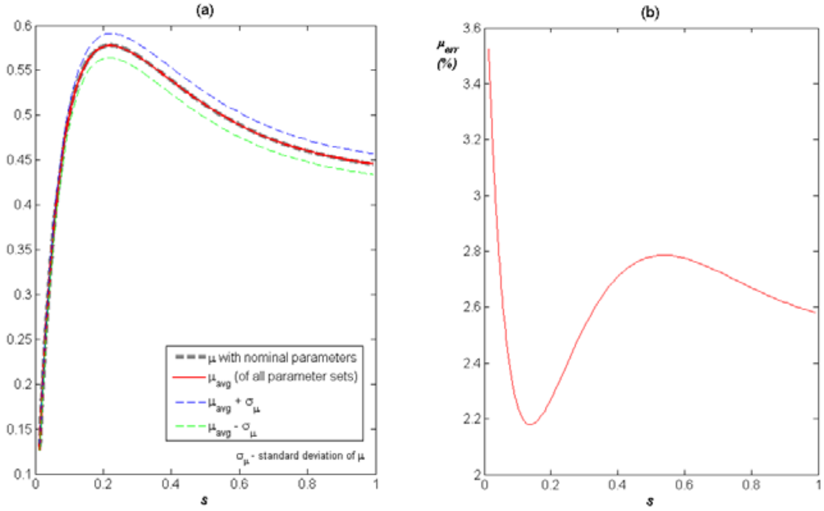

Figure B.2: Uncertainty in the model output due to uncertainty of the parameters for RFT testing; (a) quality of the uncertainty analysis, (b) % standard deviation from the actual value due to the uncertainty introduced to the input parameters

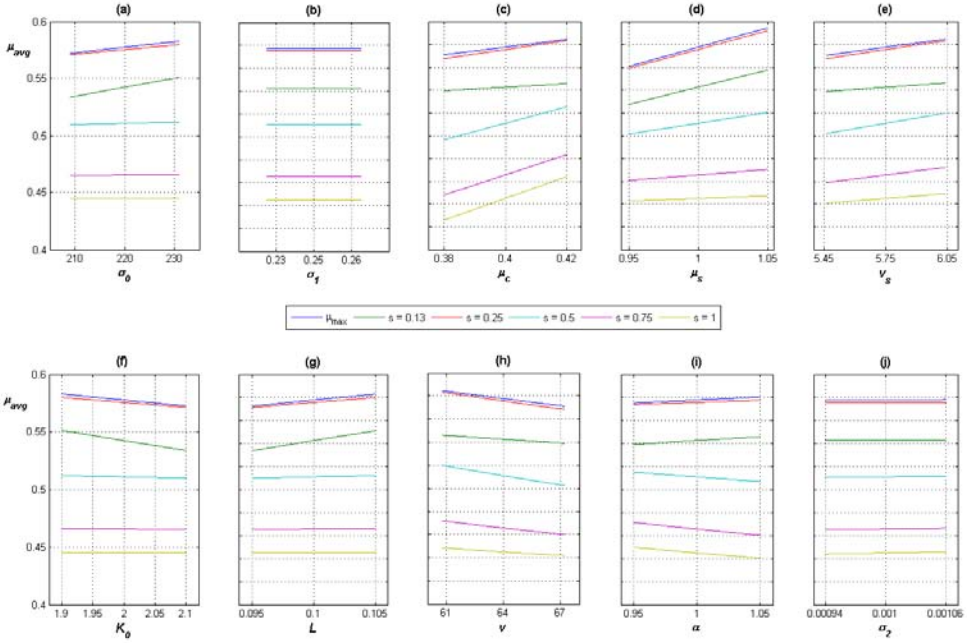

Figure B.3: Local sensitivity of the LuGre model output at a nominal set of parameters representing RFT testing

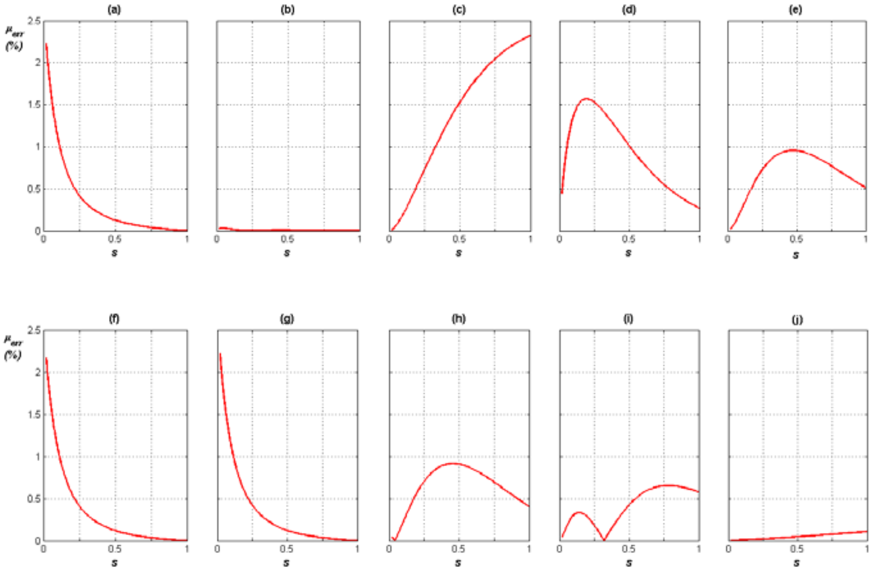

Figure B.4: Standard deviation of the output $\mu$ as a percentage of its nominal value vs. slip ratio for ±5% local variation in the nominal parameter values for (a) $\sigma_0$, (b) $\sigma_1$, (c) $\mu_c$, (d) $\mu_s$, (e) $v_s$, (f) $K_0$, (g) $L$, (h) $v$, (i) $\alpha$, (j) $\sigma_2$ representing RFT testing

# ABOUT THE AUTHOR

Madhura P.N. Rajapakshe obtained his B.Sc. degree in Mechanical Engineering in the year 2006 from the University of Peradeniya, Sri Lanka. He started his graduate studies in the year 2007 at the University of South Florida, Tampa, Florida, and obtained a Master of Engineering Degree from the Department of Civil and Environmental Engineering in 2008.